PhD degree in Systems Medicine (Curriculum in Molecular Oncology)

European School of Molecular Medicine (SEMM),

University of Milan and University of Naples "Federico II"

Settore disciplinare: MED/04

LSD1-directed therapy hinders glioblastoma by deregulating ATF4-dependent integrated stress response

Stefania Faletti

European Institute of Oncology

Tutor: Prof. Saverio Minucci
University of Milan – European Institute of Oncology

Co-Tutor: Prof. Giuliana Pelicci
European Institute of Oncology

PhD Coordinator: Prof. Giuseppe Viale

Anno accademico 2019-2020

b

Table of contents

List of abbreviations

AOs	Amino Oxidases
AAR	Amino Acid Response
ac	acetylation
ACK	Ammonium-Chloride-Potassium
AML	Acute Myeoid Leukemia
AOL	Amine Oxidase-like catalytic domain
APL	Acute promyelocytic leukemia
ATAC-RSB	ATAC Resuspension Buffer
ATAC-seq	Assay for Transposase Accessible Chromatin
AUC	Area Under the Curve
BBB	Brain Blood Barrier
BSA	Bovine Serum Albumine
CE	Clonal Evolution
CETSA	Cellular Thermal Shift Assay
CEUS	Contrast-Enhanced Ultrasound
CGH	Comparative Genomic Analyses
ChIP-qPCR	Chromatin Immunoprecipitation quantitative polymerase chain reaction
ChIP-seq	Chromatin Immunoprecipitation sequencing
CL	Classical
CNA	Copy Number Alteration
CNS	Central Nervous System
CRISPR	Clustered Regularly Interspaced Short Palindromic Repeats
CSC	Cancer Stem Cell
Ct	Threshold cycle
DEGs	Differentially expressed genes
DN-LSD1	N-terminal truncated LSD1
DTT	Dithiothreitol
EC50	Effective Concentration 50
EDTA	Ethylenediaminetetraacetic Acid
EGTA	Ethylene glycol bis (2-aminoethyl ether) tetraacetic acid
ENCODE	Encyclopedia of DNA Elements
ER	Endoplasmatic Reticulum
FDA	Food and Drug Administration
G-CIMP	Glioma CpG Island Methylator Phenotype
GBM	Glioblastoma
GBM TIC	Glioblastoma Tumor Initianting Cell
GSC	Glioblastoma Stem Cell
GSEA	Gene Set Enrichment Analysis
H3	Histone H3
H3K27	Histone H3 Lysine 27
H3K36	Histone H3 Lysine 36
H3K4	Histone H3 Lysine 4
H3K79	Histone H3 Lysine 79
H3K9	Histone H3 Lysine 9
H4K20	Histone H4 Lysin 20
HDAC	Histone De Acetylase
Hepes	hydroxyethylpiperazine ethane sulfonic acid

hESC	human Embryionic Stem Cell
HisOH	L-Histidinol
HK	House Keeping gene
hPTM	histone Post Translational Modification
HRP	Horse Radish Peroxidase
IEO	Istituto Europeo di Oncoologia
IF	Immunofluorescence
IHC	Immunohistochemistry
IPA	Ingenuity Pathway Analysis
ISR	Integrated Stress Response
ISRIB	Integrated Stres Response Inhibitor
KD	Knock down
KDM	Lysine demethylase
KO	Knock out
LOH	Loss of Heterozygosis
LSD1i	LSD1 inhibitor
me1	monomethylation
me2	dimethylation
me3	trimetylation
MEDS	Mosaic End double-stranded oligonucleotides
MES	Mesenchimal
MMP	Matrix Metallo-Proteinase
MRI	Magnetic Resonance Imaging
mRNA	messenger RNA
MS	Mass Spectrometry
N	Neural
NEB	Nuclear Extraction Buffer
NGS	Next Generation Sequencing
NOD/SCID	Non-Obese Diabetic/Severe Combined immunodeficiency
NOS	Not Otherwise Specified
NPC	Neral progenitor cell
NSC	Neural Stem cell
OPC	Oligodendrocytes Progenitor Cell
PBS	Phopshate-Buffered Saline
PCR	Polymerase Chain Reaction
PCV	Procarbazine, Lomustin and Vincristine
PDX	Patient Derived Xenograft
PIC	Proteinase Inhibitor Cocktail
PLA	Proximity Ligation Assay
PLT	Platelets
PMSF	Phenylmethylsulfonyl fluoride
PN	Proneural
PVDF	polyvinylidene fluoride
RA	Retinoic Acid
RBC	Red Bloot Cells
RIN	RNA integrity number
RIPA	Radioimmunoprecipitation assay buffer
RNA-seq	RNA sequencing
RPKM	Rads Per Kilobase Milion

RT-qPCR	Quantitative reverse transcription PCR
RTK	Receptor Tyrosin Kinase
SAM-dependent MTases	S-adenosilmethionine dependent methyltransferases
SCC	Squamous Cell Carcinoma
SCLC	Small Cell Lung Cancer
SDS	Sodium Dodecyl Sulphate
SDS-PAGE	Sodium Dodecyl Sulphate - Polyacrylamide Gel Electrophoresis
shRNA	short hairpin RNA
SVZ	Subventricular Zone
TBS	Tris-buffered saline
TCGA	The Cancer Genome Atlas
TCP	Tranylcypromine
TE	Tris-EDTA
TIC	Tumor Initiating Cell
TMZ	Temozolomide
TSS	Transcription Start Site
TTfields	Tumor Treating Fields
UCSC	University of California Santa Cruz
UPR	Unfolded Protein Response
WB	Western Plot
WBC	White Blood Cells
WHO	Whorld Health Organisation
XIC	Extracted Ion Chromatograms

Figure and Table Index

1. ABSTRACT

Despite all the progresses in medicine, glioblastoma (GBM) remains one of the most devastating human cancers. The amelioration of the standard of care for GBM patients has been significantly delayed by GBM impressive inter- and intra-tumoral heterogeneity, further amplified by its hierarchical organization, as well as its invasive behavior, the high resistance to a multitude of therapeutic approaches and the presence of the blood-brain barrier. Hence, new therapeutic strategies aimed to defeat such a terrible disease are urgently needed.

An important breakthrough in the fight against GBM may be represented by the eradication of the GBM tumor initiating cells (TICs) compartment, responsible of GBM heterogeneity and of tumor relapse after treatments withdrawal. The key of GBM TIC resistance to standard therapies lays its foundation in the plasticity and dynamicity of GBM TIC epigenetic landscape, hence encouraging the development of novel epigenetic targeted therapies. Several studies have revealed that Lysine-specific histone demethylase 1A (LSD1), besides being a key player in stemness maintenance, has also a fundamental pro-oncogenic role in either hematological or solid malignancies. I have exploited patient-derived TICs and xenograft orthotopic models to demonstrate that LSD1 is a putative druggable target in GBM. LSD1 pharmacological inhibition by means of the novel, selective, orally bioavailable and brain penetrant inhibitor DDP_38003 effectively impairs growth, viability, stem-like traits and tumorigenic potential of GBM TICs. Remarkably, I have assessed the effectiveness of LSD1i administration in different patient-derived GBM TICs and xenograft models, irrespectively of their mutational profiles. By applying RNA-sequencing technology, I have identified LSD1 as a regulator of the Integrated Stress Response (ISR), an adaptive pathway activated in response to different stresses unavoidably encountered by tumor cells due to their explosive growth, such as accumulation of unfolded proteins or nutrient shortage. Specifically, LSD1 targeting causes an aberrant ISR activation and prevents GBM TICs from mounting a positive adaptive response to stress and restore homeostasis, irrespective of the stress inducer used to trigger the ISR. The maladaptive effects of unabated and over-lasting ISR lead to increased cell-death, thus endangering the preservation of the GBM TIC pool. Our analysis revealed that LSD1 regulates the expression of Activating Transcription Factor 4 (ATF4),

which is considered the hub of the ISR, through a non-canonical mechanism. Indeed, LSD1 targeting did not alter the activation of ATF4 upstream regulators. Instead, LSD1 binds ATF4 promoter and directly regulates its transcriptional activity. Hence, our findings point to LSD1 as a novel regulator of ATF4. Lastly, through a combination of ChIP-sequencing analysis and rescue-experiments, we demonstrated that LSD1 regulates the ATF4-dependent ISR independently by its demethylase activity, thus shedding light on the importance of LSD1 scaffolding functions in GBM TICs.

Overall, the data presented in this thesis support the hypothesis that LSD1-targeting therapy is likely a promising strategy to hinder GBM by counteracting the ATF4-mediated adaptation to stress.

The demonstration of the effectiveness of the LSD1-directed therapy in different patient-derived samples, independently of their heterogeneous molecular landscape, place a strong rationale toward the rapid clinical translation of this approach for GBM treatment, alone or in combination with other treatments.

2. INTRODUCTION

2.1 Gliomas

Gliomas are primitive central nervous system (CNS) tumors belonging to the class of neuroepithelial malignacies and are the most common primary intracranial cancers, representing about 30% of all primary brain tumors in adults, and about 75-80% of the malignant ones. Gliomas comprise a various group of heterogenous neoplasms, primarly occurring in the brain and arising from cells glial tissue.

Before 2016, the classification of the CNS tumors formulated by the World Health Organization was based solely by histopathology, regardless of the several genomic alterations present in gliomas[1].

According to morphological similarities between tumor cells and normal glial cells, cytoarchitecture and immune-histological marker profile, gliomas were divided into three main categories: astrocytomas (related to astrocytes), oligodendrogliomas (related to oligodendrocytes) and oligoastrocytomas (related to a mixture of these two cell types). For each of these types of gliomas, there are neoplasms that span a broad spectrum of biologic aggressiveness[2]. The majority of gliomas are represented by astrocytomas, whose ability to infiltrate the brain parenchima identifies them as circumscribed (as pylocitic astrocytoma and sub-ependymal astrocytoma) or diffuse (as diffuse astrocytoma, anaplastic astrocytoma and glioblastoma)[2].

Furthermore, a grading system was created as a scale of malignancy. Four grades (I, II, III, and IV) distinguish astrocytomas, while oligodendrogliomas and oligoastrocytomas are classified in two grades (II and III). Lower grade astrocytomas (grade I tumors as pylocitic astrocytoma and sub-ependymal astrocytoma – grade II tumors as diffuse astrocytoma) are well differentiated, have increased cell density and some cellular anomalies or atypias, but in general they resemble the non-neoplastic tissue. These gliomas are biologically indolent. Tumors of higher grade (grade III tumors, as anaplastic astrocytoma) are anaplastic with nuclear atypia, increased vessels and cell density and elevated mitotic activity. The grade IV astrocytoma, also known as glioblastoma, exhibits the additional presence of microvascular proliferation, necrosis and diffuse infiltration throughout the brain parenchyma, which denote the fully malignant state.

Despite being the most common primary intracranial neoplasms, gliomas have a relatively rare incidence, that is disproportionate to their high grade of mortality and morbidity. Globally, every year, ~100,000 people worldwide are diagnosed with gliomas, but its incidence rate is variable by histological type, age at diagnosis, gender, race and geographic location[3].

In general, malignant gliomas are 40% more common in men than women, with the exception of pilocytic astrocytoma, and the incidence is 2-3 times higher in white than in black people. Individuals of all ages can be afflicted but they are most common among elderly adults with a peak around 50-55 years. Although, this is strongly dependent by the tumor type. The peak age of onset is 35 to 44 years for oligodendroglioma and oligoastrocytomas[4], while the median age of patients at the time of diagnosis is 64 years in the case of GBM[2].

2.2 Glioblastoma

Glioblastoma (GBM) is the most aggressive diffuse glioma and represents about 60-70% of this enormous social burden[2]. As its moniker implies, GBM is "multiforme". Macroscopically, the tumor is dotted with necrotic and hemorrhagic area. Microscopically, heterogeneous cell populations with high degree of cellular pleomorphism and nuclear atypia and numerous giant cells coexist with area of high cellular uniformity. Other GBM histological features are hyper-cellularity with mitotic figures, microvascular proliferation due to endothelial cell hyperplasia and hypertrophy, vessel thrombosis and necrosis. The tumoral mass in composed not only by tumor cells, but also by endothelial cells, activated microglia and non-tumoral brain parenchymal cells wrapped by highly infiltrating tumoral offshoots. Glioma infiltration pattern is defined as secondary structures of Scherer, in which glioma cells, migrated through the brain parenchima, collect below the pial margin, surround vessels and neurons and migrate through the white matter. This peculiar behavior results in the spread of individual tumor cells over long distances, giving origin to both multifocal lesions and recurrences localized far away from the primary tumor.

GBM were divided into two main subtypes on the basis of clinical presentation and biological features[5]. Primary GBMs occur *de novo* with no antecedent lower grade pathology, typically in patients older than 50 years of age. On the contrary, secondary GBMs are quite rare and are manifested in younger patients as low grade or anaplastic astrocytomas that transform over a period of 5-10 years into GBM. Despite their distinct

clinical course and genetic background, primary and secondary GBMs are morphologically indistinguishable and respond similarly to conventional therapy[6].

2.3 Genetic abnormalities in GBM

Numerous molecular abnormalities are linked to the pathogenesis of different glioma variants. The comparative genomic analyses (CGH) and the large-scale integrated genomic analyses[7,8] have resulted in more comprehensive analyses of the molecular aberrations underlying gliomagenesis. TCGA has so far accumulated expression, copy number alterations and sequencing data from hundreds of histologically confirmed GBMs and has comprehensively catalogued the genomic anomalies associated with GBM. Furthermore, the biological relevance of many of these molecular abnormalities to the process of gliomagenesis has been confirmed by mouse modeling studies[9]. Genetic alterations characteristic of astrocytic glioma lead to aberrant activation of key signaling pathways, mainly involved in mitogenic signaling and cell cycle control.

2.3.1 Growth factor pathways

Alterations of the receptor tyrosine kinases (RTKs) and their associated downstream pathways occur in a large percentage of diffuse gliomas and appear to be critical to oncogenesis in these tumors. Genomic amplification and activating mutations in the EGFR locus occur in 57.4% of primary GBM patients compared to 8% of secondary GBM and represent the most prevalent RTK-associated molecular abnormality in malignant glioma[10]. About half of the tumors with EGFR amplification express a constitutively auto-phosphorylated variant of EGFR, known as EGFRvIII, that lacks the extracellular ligand-binding domain (exon 2 through 7), and results constitutively active[11]. EGFRvIII pro-tumorigenic properties span from growth sustainment to the promotion of invasion and angiogenesis[12,13].

Enhanced PDGF signaling, either through receptor (PDGFRA) amplification/mutation or through ligand over-expression has been found to be a common feature of low grade glioma along with a significant subset of GBMs[14]. Although activating mutations in PDGFRA are uncommon[15], frequent co-expression of both the receptor and its ligand, most commonly PDGFB, indicates the potential for autocrine or paracrine loops boosting

oncogenic signaling through the PDGF network. Moreover, many studies points to PDGFR alterations as actual driver mutations sustaining glioblastoma genesis in rodents[16].

Hepatocyte growth factor (HGF) and its RTK MET (also known as HGFR) appear to operate in a smaller subset of GBMs[17]. MET alterations sustain GBM cell cycle progression, proliferation and angiogenesis[18,19], while contributing to chemo-radio resistance[18,20].
Also the RTK ligand insulin-like growth factor 2 (IGF2) plays a pivotal role in GBM pathogenesis, sustaining the growth rate of GBM cell by the activation of the insulin-like growth factor receptor 1 and phosphoinositide-3-kinase regulatory subunit 3 (PIK3R3), a regulatory subunit of phosphoinositide 3-kinase that shows genomic gains in some highly proliferative GBM cases. It has been demonstrated that IGF2 can substitute for EGF to allow GBM cell growth *in vitro* and that alterations of the axis IGF2-PIK3R3 allow high-grade glioma growth in absence of EGFR amplification or mutations[21].

Common signal transduction pathways activated by growth factors are the mitogen-activated protein kinase (MAPK) pathway and the PI3K-Akt-mTOR pathways, which are respectively involved in proliferation and cell cycle progression, and in the inhibition of apoptosis and cellular proliferation[22,23]. Further dysregulation of the downstream PI3K-Akt-mTOR and Ras-MAPK signaling pathways also exists in the majority of malignant gliomas [24]. Mutations in the catalytic or regulatory domain of PI3K that are hypothesized to lead to its constitutive activation occur in 15% of GBMs[7,10], sustaining their growth, migration and invasion[25]. Notably, PTEN and neurofibromin 1 (NF1), important negative regulators of the PI3K-AKT-mTOR and Ras-MAPK networks, respectively, are frequently mutated or deleted in GBM (36% and 18%, respectively), and loss of PTEN at the protein level is found in more than 80% of the cases[7].

2.3.2 Cell cycle regulators

p53 and Rb functions are inhibited by mutations or copy number alterations in at least 87% and 78% of GBM, respectively (Cancer Genome Atlas Research Network 2008). Mutations in the TP53 gene frequently characterize low-grade astrocytomas and the secondary GBMs into which they evolve, while are less predominant in primary GBMs[5]. The Rb tumor suppressor pathway has been shown to be defective in 43% of secondary

and 14% of primary GBMs, either by inactivating mutations or by methylation of its promoter region[5].

Rb functions can be also made defective by amplification of its negative regulators cyclin-dependent kinase 4 (CDK4) and, less frequently, CDK6[26] Analogously, amplification of the p53 antagonists mouse double minute 2 homolog (MDM2) and MDM4 have also been found in distinct subsets of primary TP53-intact GBMs[27].

GBM are often characterized by mutations and/or deletions in the CDKN2A locus that encodes INK4A and ARF, which are two crucial positive regulators of Rb and p53, respectively[28].

2.3.3 Other genetic alterations

Integrated genomic analyses have facilitated the identification and characterization of additional genes involved in glioma pathogenesis. Missense mutations in isocitrate dehydrogenase 1 (IDH1) are found in a significant number of GBMs that tend to occur mostly in younger patients with protracted clinical courses[8]. These point mutations are restricted exclusively to the R132 residue in the active site region of the protein in which they disrupt hydrogen bonding with its substrate[8,29]. Interestingly, a separate group of gliomas harbor mutations in the IDH1 homologue IDH2 at the analogous residue (R172). Further investigations have shown that mutations in IDH1 and IDH2 are present in high proportions of grade II and III astrocytic and oligodendroglial tumours (72–100%) along with secondary GBMs (85%), but are largely absent in primary GBMs (5%)[29]. Furthermore, across all histological types of diffuse glioma, IDH mutations tend to segregate with other low-grade glioma-associated genomic abnormalities, such as TP53 mutations and 1p/19q deletion, and are not associated with anomalies occurring frequently in primary GBM, such as EGFR amplification and chromosome 10 loss[29]. IDH mutational status has also been linked with DNA methylation profiles in diffuse glioma. A TCGA analysis has discovered a small subset of GBM (8.8%), which exhibits a CpG island methylator phenotype (G-CIMP) characterized by stereotyped hypermethylation of CpG islands in over 1,500 loci across the genome[30]. G-CIMP-positive GBMs exhibit increased frequency of characteristic copy number alterations (CNAs) in 8q and 10p and are highly enriched for IDH mutations[31]. By report, approximately 87% of G-CIMP-positive versus 5% of G-CIMP-negative tumors are IDH-mutant.

Lastly, one of the commonest genetic alterations in GBM is represented by loss of heterozygosity (LOH) of chromosome 10 (LOH#10), which implies the deletion of PTEN and other potential onco-suppressor genes. Despite LOH#10 frequency in primary and secondary GBM is quite comparable (47% VS 54%), the majority of primary GBMs loose the entire chromosome, while secondary GBMs tend to retain 10p arm[32].

2.4 Glioma molecular classification

Being based solely on histologic visual criteria, the 2007 WHO classification was prone to subjective inter-observer variations; on top of that, the histological heterogeneity of gliomas further complicated the diagnosis, so that many tumors failed to adhere to one single class[33]. In addition, in many cases the 2007 WHO classification was not reliably associated with tumor aggressiveness, and demonstrated a low prognostic and predictive value, hence raising the necessity to improve the criteria of glioma classification[34]. Over the last decades, research efforts have resulted in a better understanding of the molecular basis of glioma-genesis as well as the genetic alterations commonly identified in diffuse gliomas, leading to the classification of lesions into molecular groups based on multi-gene predictors. Since May 2016, the World Health Organization classification has undergone major restructuring drawing on the last advances in molecular genetics and the development of epigenetic profiles. The updated guidelines now incorporate molecular and histologic criteria, allowing an integrated, and more accurate, diagnosis, where the histopathological name is followed by the genetic features (i.e. Glioblastoma, IDH wild tipe)[35]. The use of molecular criteria provides a better patient prognostication, so that genotype is considered more reliable and informative than histological phenotype in case of incoherent results from histological and molecular profiling[36]. Moreover, the increased predictive power of the molecular classification hopes to provide useful insights to enhance the identification and the development of individualized therapeutic plans[35].

Briefly, starting from 2016, gliomas have been separated in two distinct groups: circumscribed gliomas (WHO grade I) and diffusely infiltrating gliomas (WHO grade II-IV). Circumscribed gliomas do not harbor IDH mutations and are often BRAF-mutated; clinically, they are considered as benign tumors curable by surgical resection.

Surgical resection is instead insufficient alone to treat diffusely infiltrating gliomas. These tumors, already graded using histopathological criteria, have been further stratified into

three diagnostic and prognostic subgroups based on their genomic profile, and in particular IDH, TP53, ATRX and 1p/19q status.

The WHO grade II diffuse astrocytomas and WHO grade III anaplastic astrocytomas are now each divided into IDH-mutant, IDH-wildtype and NOS (i.e., not otherwise specified) categories. When key driver IDH mutation is associated with peculiar TP53 and ATRX gene alterations, grade II-III gliomas are now diagnosed as "Diffuse astrocytoma, IDH mutant". In presence of IDH but absence of ATRX mutations, the codeletion of 1p/19q allows to identify a "Oligodendroglioma, IDH mutant and 1p/19q co-deleted". Finally, a diagnostic designation of "Diffuse astrocytoma, IDH WT" or "Oligodendroglioma, NOS" can be assigned in the very rare cases of IDH-WT grade II-III gliomas (**Fig. 1**)

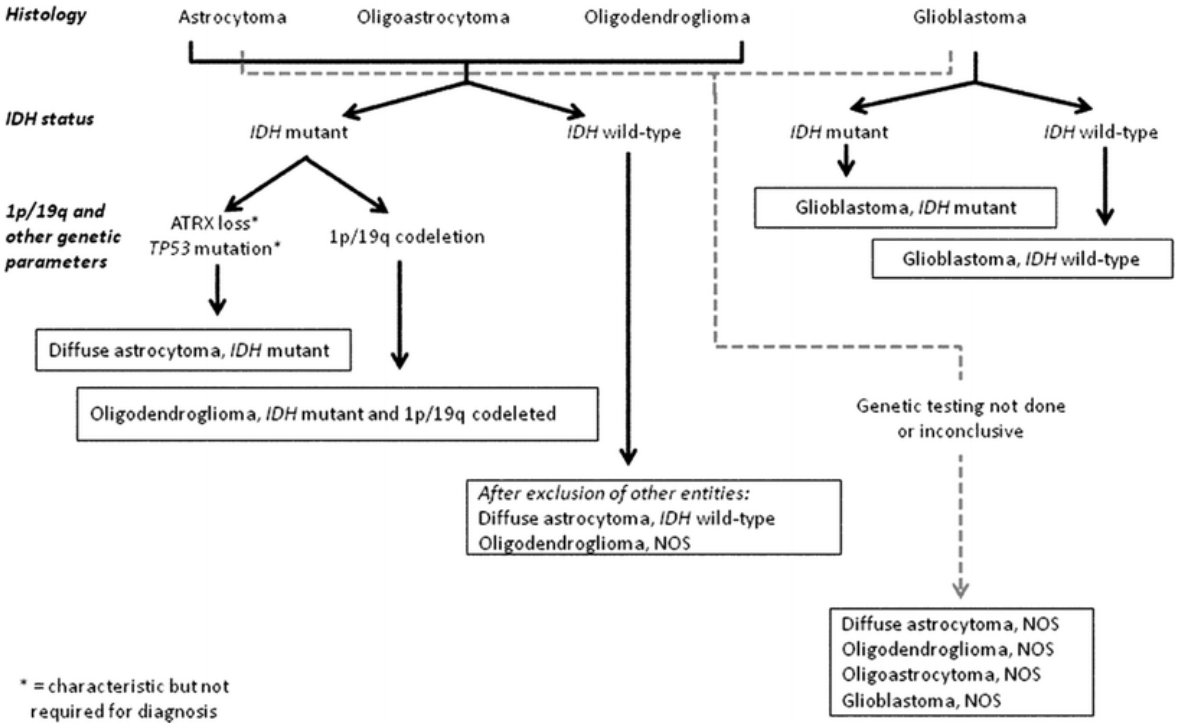

Figure 1. A simplified algorithm for classification of the diffuse gliomas based on histological and genetic features. The diagnostic "flow" does not necessarily proceed from histology first to molecular genetic features next, since molecular signatures can sometimes outweigh histological characteristics in achieving an "integrated" diagnosis[35]

The molecular profiling of gliomas has an enormous importance not only to guide their differential diagnosis, but also in virtue of the prognostic and predictive power of some molecular markers:

Isocitrate dehydrogenase mutations: IDH mutations can occur within either IDH1 (90%) and IDH2 genes (10%). Among IDH1 mutations, R132H is highly recurrent[1]. IDH mutation are involved and responsible of the early stage of glioma-genesis[29] and are found in a small percentage of GBMs (12%) but in about 70% of grade II-III gliomas[37]. IDH mutations behave, above as a diagnostic marker, also as a prognostic factor, conferring a better prognosis regardless of tumor grade and other genomic alterations[29,37].

1p/19q co-deletion: 1p/19q co-deletion, resulting from the unbalanced translocation of chromosomes 1 and 19, is found in up to 90% of oligodendrogliomas[38,39]. Further, 1p/19q co-deletion and ATRX/TP53 mutations are relatively exclusive of one another, supporting the employment of molecular markers to distinguish astrocytomas and oligodendrogliomas. Tumor harboring this alteration show an increase response to alkylating agents and tends to behave in an indolent fashion, so that 1p/19q co-deletion can be considered a favorable prognostic marker[38,39].

O6-methyl-guanine-DNA methyltransferase (MGMT) status: MGMT gene codes for a DNA repair enzyme deputed to the removal of O6 alkyl guanine adducts induced by alkylating chemotherapy. The methylation status of a CpG island located within MGMT promoter regulates its expression levels and thus glioma cell ability to repair such damages. MGMT promoter methylation is found in about 36% of gliomas, especially in anaplastic astrocytomas and GBMs, being less common in lower grade gliomas, and it has been associated with a better response to both alkylating agents and radiotherapy[40,41].

2.5 GBM molecular subgroups

Besides genetic alteration characterization, also gene expression profiling studies have been used to further classify gliomas on the base of their transcriptional signature. Earliest studies identified gene expression differences among morphologically defined gliomas. Differentially expressed genes were found among GBMs and lower grade gliomas[36,42,43], primary and secondary GBMs[43,44] adult and pediatric brain tumors[45] or a variety of morphologically defined glioma subtypes[43]. These studies confirmed that morphological differences among gliomas are reflected at the mRNA level. In some cases, gene expression profiles classify diagnostically challenging malignant gliomas in a manner that better correlates with clinical outcome than standard pathology does[36,42].

Basing on the transcriptional signatures, also GBMs, previously described as primary or secondary, have been divided in molecular subgroups.

Several schemes for classifying GBM subtypes have been proposed in the past several years[46–49]. The first relevant study carried out by Phillips and colleagues divided a cohort of malignant gliomas, comprising both WHO grade III and IV, into three molecular subtypes named Proneural, Proliferative, and Mesenchymal, in recognition of the key features of the molecular signatures associated with each group (**Fig. 2**). The Proneural subtype is defined by genes implicated in neurogenesis and is associated with better outcome than either of the other two subtypes. In contrast, the Proliferative and Mesenchymal gene signatures are respectively defined by proliferation and extracellular matrix/invasion-related genes, and are both associated with poor outcome. Mesenchymal GBMs show also evidence for increased angiogenesis, further worsening the prognosis of these tumors[50].

Prognostic significance of molecular subtypes has been validated in an independent cohort of 184 gliomas of various histological types. Remarkably, nearly all WHO grade III tumors (65 out of 73) felt into the Proneural subgroup, along with a subset of GBMs occurring in younger patients with prolonged disease courses. Moreover, recurrent tumors, although mostly retaining their initial transcriptional sub-classification, seemed to significantly shift their mRNA signatures towards the Mesenchymal profile. Of note, a recent work has identified a set of master regulator transcription factors, the most important of which are the signal transducer and activator of transcription 3 (STAT3) and CCAAT/enhancer-binding protein beta (C/EBP **β**), which seem to mediate the expression of the Mesenchymal phenotype and so enhance GBM aggressiveness[51].

An additional clustering analysis conducted by Verhaak et al. using transcriptional data obtained by the TGCA on 200 primary GBMs has established four distinctive GBM subtypes, namely Proneural, Neural, Classical, and Mesenchymal[48]. Significant similarities, but not entirely overlap, were found between the Mesenchymal and Proneural phenotypes described in Phillips' and Verhaak's works (**Fig. 2**).

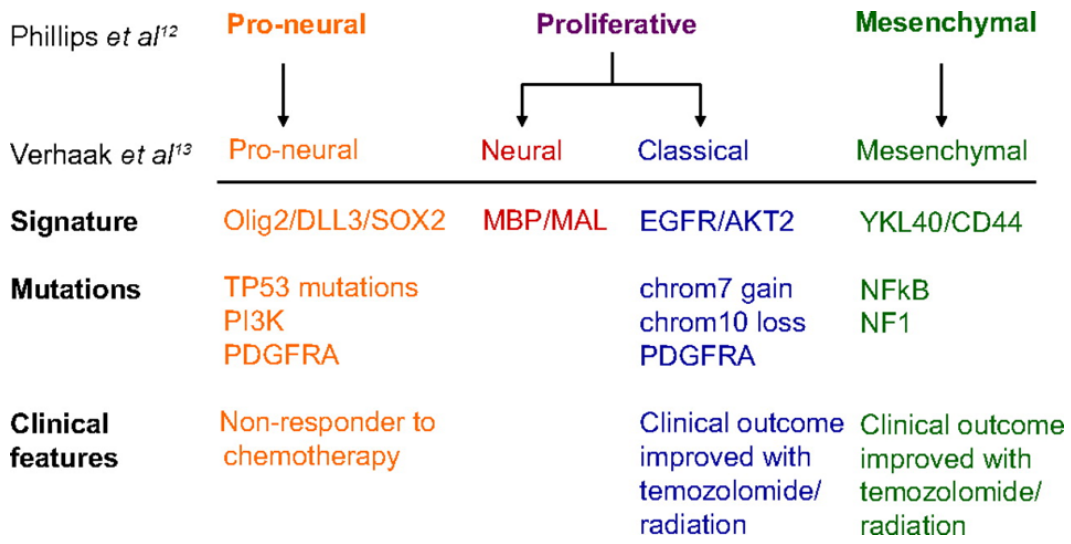

Figure 2. Molecular classification of GBM based on their transcriptional profile[52]

Unlike observed in previous studies, there was no correlation between the TCGA Proneural subtype and a better prognosis in the data-set consisting solely of grade IV astrocytomas, while it has been confirmed in the validation data-sets containing also low-grade gliomas[50,53]. Conversely, re-analysis of the TCGA data using Phillips' molecular subtype designations confirmed a slightly more favorable prognosis of the "Phillips-Proneural" relative to "Phillips-Mesenchymal/Proliferative" GBMs.

Further studies have linked GBM molecular subtypes with either genomic aberration, proteomic profile or epigenetic landscape, as described below:

Recurrent genomic aberrations in each molecular subtype have been identified. The Proneural subtype harbors frequent PDGFRA amplifications and mutations in IDH1, PIK3CA/PIK3R1 and TP53. The Proneural group shows high expression of oligodendrocytic development genes (such as PDGFRA, NKX2-2 and oligodendrocyte transcription factor 2 [OLIG2]) as well as proneural developmental genes like SOX genes, doublecortin (DCX), delta-like 3 (DLL3), aschaete-scute homolog 1 (ASCL1) and transcription factor 4 (TCF4)[48]. The Neuronal subtype is characterized by the expression of neuron markers such as NEFL, GABRA1, SYT1 and SLC12A5. The Classical subtype is characterized by frequent EGFR amplification and EGFRvIII mutations and a distinct lack of TP53 mutations and CDKN2A deletion. The Mesenchymal subtype is typified by deletion of NF1, TP53, and PTEN genes and displayed expression of mesenchymal markers, such as CHIL3 (also known as YKL40) and MET, as described elsewhere[48].

Using a proteomic analysis, three proteomically-defined subclasses of GBM have been identified. These subclasses are characterized by protein- and phosphorylation-level abnormalities in the EGFR, PDGFR, or NF1 pathways and correspond to Classical, Proneural, and Mesenchymal subtypes of GBM, respectively[54].

Analysis of epigenetic changes from TCGA GBMs identified a distinct subset of samples with characteristic promoter methylation alterations, indicating the existence of a G-CIMP phenotype[30]. G-CIMP tumors are mainly secondary or recurrent GBMs and are tightly associated with IDH1 mutations and display distinct copy-number alterations. Patients with G-CIMP positive tumors are younger and survived longer than G-CIMP negative GBM patients. Integration of DNA methylation data with gene expression data showed that G-CIMP positive tumors represent a subset of Proneural tumors. Thus, G-CIMP could be used to further refine the gene expression-defined groups into an additional subtype with clinical implications.

Overall, the growing knowledge accumulated about GBM molecular features, and the prognostic value of molecular classification led to the development of a gene expression profile-based diagnostic test, which is currently under evaluation in two prospective, randomized clinical trials[55]. A 9-gene profile (AQP1, CHI3L1, EMP3, GPNMB, IGFBP2, LGALS3, OLIG2, PDPN, and RTN1) predictive of clinical outcome has been identified for the development of a qRT-PCR assay performed on FFPE samples. On the basis of the logistical difficulties in obtaining fresh frozen tumors for DNA microarray-based assays, such an assay is absolutely critical for successful clinical implementation with FFPE GBMs, which constitute the vast majority of clinical samples.

In summary, molecular sub-typing now has the potential to become a readily implemented clinical test that may guide future treatment decisions.

2.6 Glioblastoma diagnosis

Patients with a malignant glioma may present a variety of symptoms including endocranial hypertension, comitial crisis, headache, confusion and loss of memory, neurological deficits and personality changes. Symptom onset is often tardive and progressive. The diagnosis of malignant gliomas is usually made by magnetic resonance imaging (MRI), computer tomography (CT) or positron emission tomography (PET). The images typically show an enhancing mass surrounded by edema. GBMs frequently have central areas of necrosis and more extensive peritumoral edema than those associated with anaplastic gliomas.

2.7 Glioblastoma prognosis

Despite decades of research and attempt to ameliorate the standard of care, GBM prognosis is poor, with patient median survival ranging from 12-15 months and a 5-year survival rate for patients <5%[6]. GBM treatment is made more challenging by its intrinsic biological features. This tumor is indeed defined by a diffuse invasiveness in the brain normal tissue, making surgical resection poorly effective and, being located beyond the blood brain barrier (BBB), it is protected from the exposure of many systemic chemotherapy[56]. Resistance to conventional therapies if further worsened by a high grade of cellular and molecular heterogeneity, and by a hierarchical organization, with a cellular compartment endowed with stem-cell like features that is responsible of both tumor growth sustainment and therapy resistance. The role of these stem-cell like tumor initiating cells in GBM will be discussed more in details in the next chapters. Lastly, over-expression of proteins involved in DNA repair machinery could dampen the effects of radio- and chemotherapy[57].

Over the last years, many efforts have been focused on increasing our knowledge about gliomas, and in particular on GBM. Recent advances in molecular biology have improved understanding of GBM pathogenesis, and several clinically relevant genetic alterations have been described, by employing a combination of new animal models and large-scale genomic analysis.

International organizations that join institutes around the world, such as the Cancer Genome Atlas (TCGA), were created with the mission of understanding 'the molecular

basis of cancer through the application of genome analysis technologies' and selected GBM as the first cancer type for study, based on its uniformly poor prognosis and limited treatment options. TCGA permitted collection of huge amounts of data on brain tumors and the creation of web-tools freely accessible by the entire scientific community. Sadly, despite some advances in treatment, the overall survival of GBM cases is still not that different than it was several years ago.

2.8 Glioblastoma treatment

The poor prognosis of GBM patients is related not only to the aggressive behavior and the high relapse rate of the tumor, but correlates also with the lack of adequate drug-based treatments able to overwhelm this phenomenon. When feasible, current treatments of newly diagnosed glioblastoma include maximal surgical resection to reduce the tumoral mass (debulking), in the meanwhile providing a more precise histological diagnosis and tumor genotyping. The size and localization of the tumor is important for the possibility to perform optimal surgery. Also due to GBM invasive growth, surgical tumor excision is never totally radical, hence resulting in the increased probability of recurrence[58]. Albeit partial, the surgical elimination of the tumor reduces the symptoms caused by mass effect and provide a survival advantage to the patient[58]. Several aid, such as neuro-navigation techniques, intra-operatorial echography and the employment of tumor-specific dye, as the 5-aminolevulinic acid, are currently used to guide surgeons to distinguish tumor from normal brain, with the final aim to simultaneously maximize surgical resection and reduce iatrogenic neurological damages[59].

Since surgical resection alone is insufficient to eradicate the disease, it must be combined with radio and chemotherapy.

Radiotherapy dosage is set according to a dose-effect relation: as the radiations dose increases, also patient survival is extended, until a maximum dose of 60Gy is reached. However, brain radiotherapy is not devoid of both acute and late side effects due to radio-induced damages to normal brain tissue[60].

On the other hand, many efforts have been focused on the development of an effective chemotherapy regimen against GBM, leading to test the efficacy of nitrosuree (i.e. Carmustine and Lomustine)[61] and of combinatorial treatment of different drugs, as PCV (Procarbazine, Lomustine and Vincristine) [62]. The treatment of glioblastoma have to face

unique challenges, as the presence of the BBB, a highly selective semipermeable barrier preventing both large and small (<400 Da) molecule drug from reaching their targets in the brain[56]. The main issue about chemotherapy is thus the necessity to administer high and toxic dosages of these drugs in order to allow BBB crossing. In the last decades, the cytotoxic alkylating agent Temozolomide has been therefore established as the drug of choice thanks to its oral availability, reduced toxicity and ability to easily cross the BBB. Indeed, nowadays, in the gold standard GBM treatment protocol, surgery is followed by the "Stupp protocol", i.e. radiotherapy plus concomitant and adjuvant Temozolomide administration[63]. For patients with GBM, the median survival from time of diagnosis is about three months without treatment. After treatment with surgery and postoperative temozolomide and radiotherapy, the survival increases up to 14.6 months[6].
Notably, Temozolomide efficacy strictly depends on the methylation of MGMT, whose enzymatic DNA repairing activity abrogates the chemotherapy advantages. Therefore, MGMT promoter methylation serves as predictive marker for the response to Temozolomide[40,41].

In addition to the traditional therapies, the technology improvement led to the employment of Tumor Treating Fields (TTFields), an antimitotic treatment modality that impairs chromosome segregation during mitosis through the application of low intensity alternating electric fields[64]. Such technology was tested in combination with maintenance Temozolomide showing a slightly longer progression-free survival compared to Temozolomide alone[65]. However, despite the FDA approval, TTFields position in the GBM clinical management remains controversial.

Another example of technology transfer is nowadays represented by the possibility to employ therapeutic ultrasound against GBM. Contrast-enhanced ultrasound, also called CEUS, is an ultrasound diagnostic technique that uses gas-filled microbubbles as contrast agent. Gas-filled microbubbles are featured by a high degree of echogenicity, that is the ability of an object to reflect ultrasound waves. Pulsed, focused ultrasound can be used to induce a series of microbubble vibrations, leading to cavitation effects. These mechanical effects can be exploited to temporarily increase BBB permeability in a controlled fashion. Consequently, CEUS is regarded as a promising tool to improve the efficacy of drug delivery to the brain[66].

Lastly, if on one hand the cellular and molecular GBM heterogeneity complicates the establishment of effective therapeutic strategies, on the other the increasing knowledge about genomic alteration sustaining this devastating tumor offers the possibility to design new targeted therapies and to develop new tailored multimodality approaches.
Several approaches have been used to target individual signaling molecules involved in gliomagenesis. Particular interest has been focused on inhibitors of RTKs and their downstream effectors and on inhibitors of angiogenesis.

EGFR is one of the most widely expressed RTK in human gliomas, so several EGFR inhibitors have been developed[67]. Gefitinib (ZD1839, Iressa™)[68,69], Erlotinib (Tarceva®)[70–72] and Afatinib[73] have been investigated in recurrent gliomas with limited activity. Recently, a third-generation EGFR-targeted drug, AZD9291, emerged as a novel and irreversible inhibitor that showed enhanced efficacy against GBM in pre-clinical models[74].
EGFR has been also targeted by monoclonal antibodies (mAb) such as Cetuxibab. After entering in a phase II trial, Cetuximab demonstrated to be well tolerated in patients with recurrent high-grade glioma, but exhibited only limited activity in this patient population[75].
An alternative approach has been developed based on a vaccination strategy against the constitutively activated EGFRvIII[76]. Rindopepimut, a peptide-based vaccine that targets the tumor specific mutated segment of EGFRvIII, has entered with promising results in phase II studies, but the subsequent randomized double blind phase III clinical trial was discontinued in 2016[77].

Given the disappointing clinical results obtained by EGFR inhibitors, additional druggable targets have been selected, including platelet derived growth factor (PDGFR), highly expressed in GBM. Imatinib (Gleevec®) is a small molecule inhibiting PDGFRA, PDGFRB and the RTKs c-Abl and c-KIT. Despite encouraging results obtained in preclinical models, it demonstrated only limited anti-tumor activity in patients with recurrent GBM, both alone and in combination with hydroxyhurea[78].

Many efforts have been also focused to target VEGF signaling pathway, considered as a cornerstone in angiogenesis, one of the main hallmarks of malignant gliomas. VEGF inhibitors-based monotherapies, as Tivozanib and Pazopanib, failed to increase progression free survival of GBM patients[79,80]. More promising results came from a phase

II clinical trial in which Bevacizumab (Avastin®), a humanised anti-VEGF mAb, was combined with Irinotecan[81], and Bevacizumab was subsequently approved by FDA for the treatment of recurrent GBM[82].

However, a meta-analysis of four clinical trials demonstrated that the combination of Bevacizumab and standard chemo-radiotherapy only prolongs progression free survival, without improvement in overall survival, and that there are emerging problems with both developing treatment-resistance and adverse effects associated with anti-VEGF therapy such as disturbance of VEGF-dependent physiological functions and homeostasis in the cardiovascular and renal systems, wound healing and tissue repair[83].

In the last decade, the failure of other novel antiangiogenic therapies, and the high rate of GBM recurrence linked to VEGF-targeted therapies have held back the initial enthusiasm about this therapeutic strategy [84–88].

Because of GBM inter-tumoral heterogeneity, it is naive to believe that there will be one single treatment against GBM; rather, the combination of multiple treatment strategies will have the best effect. Ideally, in the future GBM treatment could be completely tailored to achieve highest possible efficacy depending on the expression/mutation analysis of that particular patient's tumor, according to the precision medicine concept.

2.8. GBM heterogeneity and hierarchical organization

GBM management is further complicated due to a high grade of intra-tumoral heterogeneity. Fidler and colleagues firstly described the concept of intra-tumoral heterogeneity more than 30 years ago, referring to the presence of many cell sub-population within a single tumor in a murine model[89]; nowadays, this concept has been expanded to include all the genetic, epigenetic and molecular differences within individual tumor cells[90].

Whole-exome sequencing analysis of paired primary and recurrent GBMs, revealed that, despite recurrent tumors acquire new mutational patterns, there are also overlapping mutations between the primary and the recurrent GBMs, indicating that therapy-refractory cellular sub-clones gave rise to the relapse. These sub-clones can either be present from the tumor origin, and/or be acquired during tumor evolution, also due to the pression exerted by therapies[91] (**Fig. 3**).

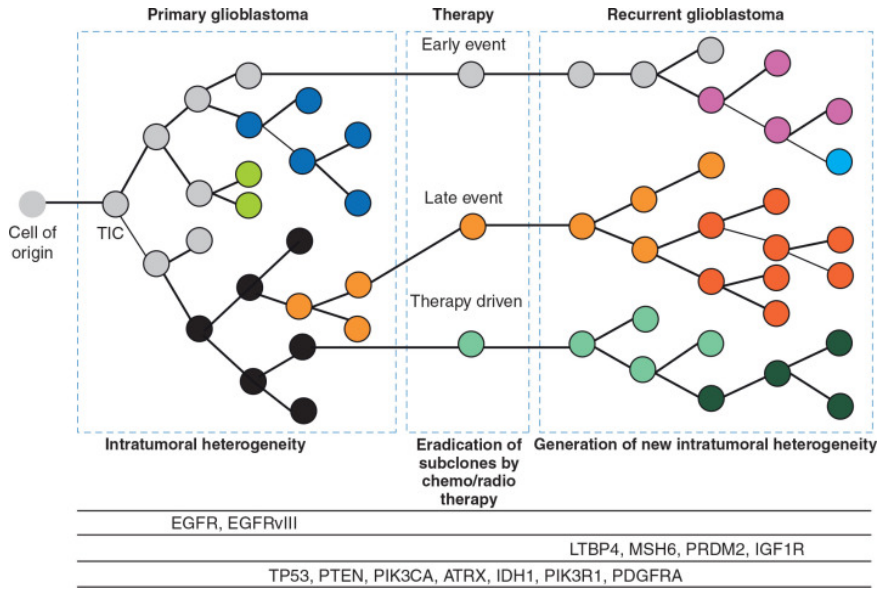

Figure 3. Subclonal populations in primary glioblastoma escape therapy and give rise to treatment-refractory, heterogeneous recurrent glioblastoma. After a normal cell (grey) acquires mutations (black outlined circles), it gives rise to multiple subclonal cell populations that are further selected upon the application of different stresses,including therapy (different colored circles). The administration of therapy for primary glioblastoma, leads to the selection of pre-existing subclonal cell populations or allow the establishment of a new therapy-driven-resistant subclone. These treatment-refractory subclonal populations then seed tumor relapse and lead to the formation of a heterogeneous recurrent glioblastoma that has a distinct clonal composition from primary glioblastoma[91]

Understanding the molecular architecture of these residual or newly acquired populations is critical for the development of successful therapies that take into account the molecular

signatures driving tumor evolution and treatment failure, above changes physiologically acquired by GBM over time (**Fig. 4**).

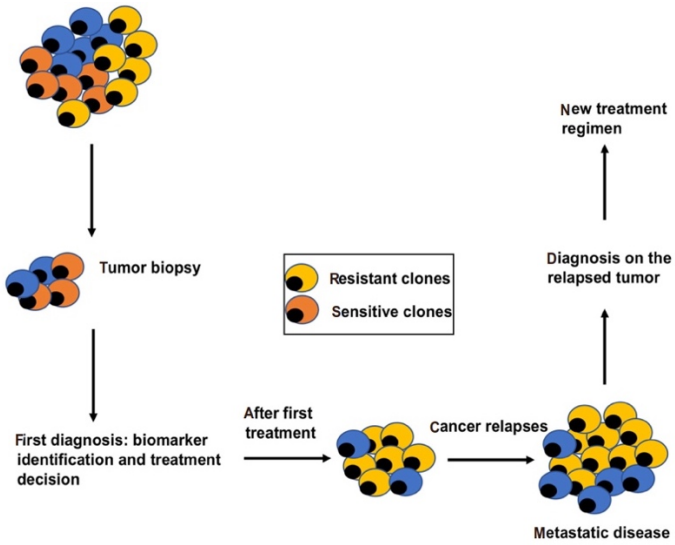

Figure 4. Therapeutic implications of GBM heterogeneity: Initial diagnosis, and subsequent treatment choice, are based on tumor biopsy, which is not representative of the whole, heterogenous GBM. After the first-line treatment, the second-line treatment should be based on a new molecular diagnosis to kill persistant resistant clones[92]

Bulk transcriptome analysis has been successfully employed to classify GBM molecular subtypes and to establish signatures able to predict patient's therapy response and outcome. Although, it becomes clearly ineffective to identify and better characterize rare cell sup-populations whose contribution to the overall tumor gene expression profile is diluted by that of more abundant cell groups. Single cell-sequencing introduction represented a breakthrough in the analysis of intra-tumoral heterogeneity, reaching a resolution that not only allow to discriminate different cell sub-population, but also to gains insights about their genetic, epigenetic and functional profile[92].

In the 2014, Patel and colleagues, by carrying out single-cell RNA-sequencing of 430 cells obtained from five GBMs, demonstrated the existence of high-level cellular variability within the tumor bulk as well as the presence of a wide plethora of stem and more differentiated cells, supporting the idea of a hierarchal organization[93]. Couturier and colleagues confirmed this hypothesis by exploiting single cell analysis aimed to compare the transcriptome profile of GBM cells to the lineage hierarchy of the developing human brain. They demonstrated that GBM recapitulates a normal human neuro developmental hierarchical organization characterized by the presence of three neurodevelopmental lineages deriving from glial progenitor-like cells[94].

Altogether, these data encourage to intensify scientific efforts focusing on the tumor heterogeneity, in terms of genetic, epigenetic and transcriptional landscape, to provide new insights into the GBM complexity in the attempt to develop new targeted therapeutic strategies.

2.9 Tumor initiating cells

Currently, intra-tumoral heterogeneity origin and maintenance are explained by two prevalent models: the stochastic or clonal evolution (CE) model[95,96], and the hierarchy or cancer stem cell (CSCs) model[97,98].

The CE model holds that genetic and epigenetic changes occur over time in individual cancer cells, that are previously biologically equivalent. Such changes may for instance increase tumor aggressiveness, invasiveness, or treatment resistance. Every change conferring a selective advantage will allow individual clones of cancer cells to out-compete with other clones. Indeed, CE can lead to genetic heterogeneity, conferring phenotypic and functional differences among the cancer cells within a single patient[99].

In contrast with the CE model, the CSCs model postulates that the growth and progression of many tumors are driven by a minority subpopulation of cancer cells with stem-like features, known as cancer stem cells (CSCs), or tumor initiating cells (TICs). TICs share important properties with normal tissue stem cells, including self-renewal (by symmetric and asymmetric division) and differentiation capacity, albeit aberrant[100]. This implies that many cancers are hierarchically organized in much at the same manner as normal tissues. Just as normal stem cells differentiate into phenotypically diverse progeny with limited differentiation potential, TICs also differentiate into phenotypically non-tumorigenic cells that compose the bulk of the cells in the tumor. As a result, tumors are composed of a hierarchy of cell types that include highly tumorigenic TICs, intermediate progenitors and terminally differentiated progeny[100].

The first experimental proof identifying cancer stem cell-like cells as cells capable to generate tumor occurred in the late 90s, by Dominique Bonnet and John Disk. They isolated CD34+/CD38- human leukemic cells, a rare susbset of cells comprising 0.01-1% of the total population, and demonstrated their ability to self-renew, differentiate and

proliferate upon xenotransplantation in immunodeficient mice, establishing a hierarchical organization[101]. Therefore, this study provided a breakthrough in cancer knowledge, paving the way for the detection of TICs in many other tumor types, e.g. brain tumor[102,103], breast[104], colorectal[105], and pancreatic cancer[106]

Further in contrast with the CE model, the CSCs model implies that TICs can be identified and purified on the base of their intrinsic properties, and hence pharmacologically targeted. Notably, TICs are not only associated with the tumor formation and its cancerous progression, but they are also responsible for many biological phenomena as plasticity to drug response and recurrence[107]. There is mounting evidence that TICs drive refractoriness to chemotherapeutic agents[108], radio-resistance[57] and relapse in glioma mouse models after TMZ administration[109]. Moreover, they are involved in tumor neo-vascularization[110], invasion processes[111] and metastatization[112].

The concept that cancer growth can be sustained by stem-like cells leads to the necessity of new and more effective antitumor treatments. According to the CSCs model, indeed, therapeutic approaches that do not eradicate the TIC compartment are likely to achieve little success; they might kill the majority of tumor cells and induce temporary regression of gross tumor lesions but fail to prevent disease relapse and metastatic dissemination.

Although the CE and the CSCs model are dissimilar and place differing weight on the importance of stem cells and the microenvironment, they are not mutually exclusive[113]. Indeed, in cancers that follow a CSCs model, TICs can evolve by CE[114] (**Fig. 5**). This hypothesis, known as plasticity model, lays its foundation on the evidences that cancer cells can interconvert between stem cell and differentiated states (**Fig. 5**). Intrinsic or micro-environmental stimuli could influence differentiated tumor cells to reacquire stem cell characteristics[115]. Moreover, if a mutation conferring self-renewal or growth properties advantages occurs, a more dominant TIC clone may emerge among the others.

According to the plasticity model, stemness and tumorigenic properties are not intrinsic properties, but rather a plastic state that most cancer cells can adopt upon reversible state transitions. Thus, the capacity of any tumor cell to reconstitute tumor heterogeneity raises the necessity to develop new therapeutic approaches able to hit the molecular mechanisms supporting cancer cell plasticity.

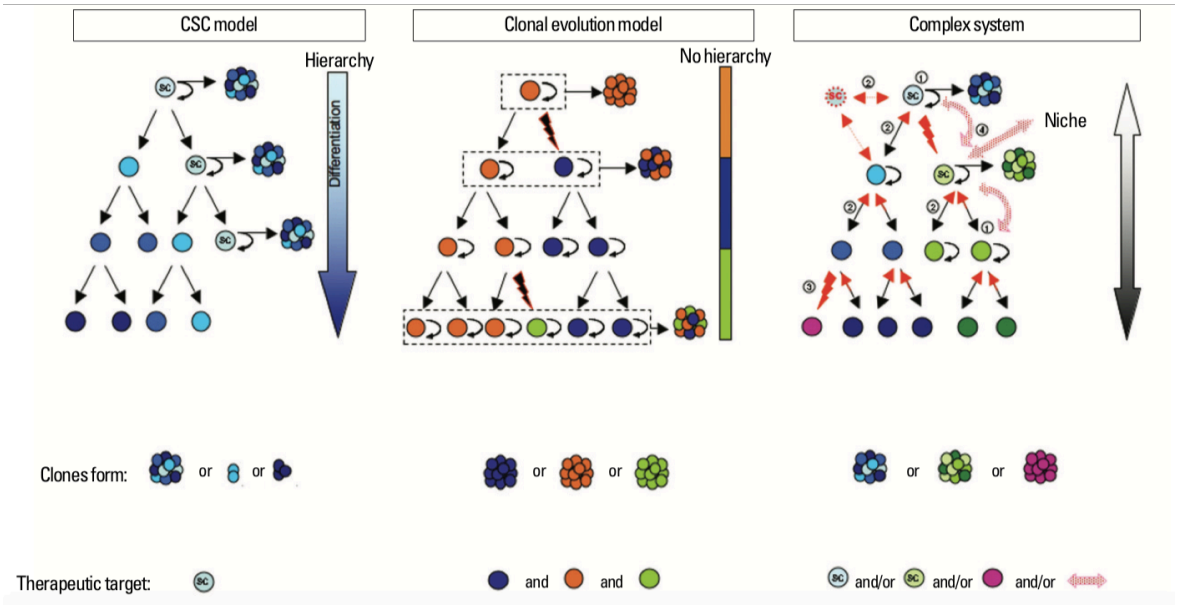

Figure 5. Different models of tumoral heterogeneity. According to the cancer stem cell model (left panel), only a sub-population of stem cell like-cells (SC) subjected to pro-oncogenic alterations can give rise to tumors. This forms a hierarchical lineage system where the primary therapeutic cell target is the Cancerous stem cell (CSC) itself. The clonal evolution model (middle panel) exhibits no lineage hierarchy, and most of the cell subtypes are capable of tumor formation, which makes them all targets of therapeutic interventions. In a complex (also named "plastic") model (right panel), cancer cells can switch between stem cell-like and differentiated state (#2) in response to both genetic and epigenetic changes, so that each tumor cell may produce new tumor cell populations (#3). Further complexity is added by cell-cell and cell-niche interactions (red arrows, #4). While all potential tumor forming cells have to be targeted for successful therapy in this model, the interruption of the cell-cell and cell-niche interactions may also weaken the tumor system as a whole[116].

2.10 Tumor initiating cells in GBM

2.10.1 GBM cells of origin

The origin of GBM-TICs is extremely debated. While some support the central role of normal neural stem cells (NSC), after accumulation of genetic mutations/aberrations, in TIC establishment, other hypotheses suggest a more dynamic process whereby progenitors and more differentiated cells, undergoing de-differentiation in response to microenvironmental stimuli, might acquire stem-like traits, and give rise to cancer[117] (**Fig. 6**).

Currently there are experimental evidences in mouse brain tumors for cell of origin from stem/progenitor cells as well as more differentiated cells [118–120].

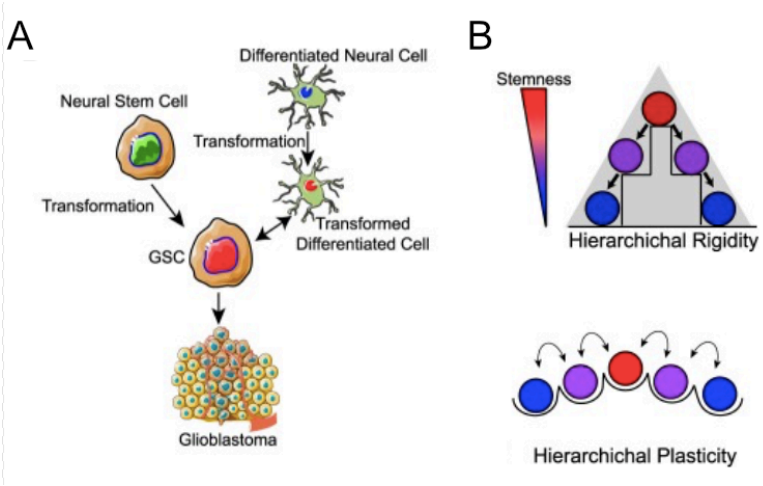

Figure 6. GBM TIC origins. (A) GBM TIC (here indicated as GSCs) may arise from both neural stem cells or transformed astrocytes that gain access to stem-specific transcriptional programs. According to these findings, GBM TIC origin model could adhere to both hierarchical and platicity model as shown in (B). Adapated from Gimple et al., 2019[117]

It is also of relevant note that brain tumors of different phenotypes, in different locations, with different genetic mutations, may have different cell of origin[121]. Identifying the cell of origin of brain tumor may be important for several reasons. The particular cell in which an oncogene is expressed may determine the subsequent phenotype and resulting aggressiveness of the tumor, suggesting that the efficacy of different treatments could depend on the cell of origin of the tumor.

Currently, the two main candidates are oligodendrocytes progenitor cells (OPCs) and NSCs. OPCs represent the largest pool of proliferating cells in human brain, hence increasing the probability to acquire mutations leading to the transformation. On the other hand, evidences supporting the main role of NSCs rely on the fact that knocking-

out of tumor suppressor gene or overexpression of oncogenes trigger NSC capability to generate tumor after xenotransplantation. Moreover, NSCs are reasonable candidates as cell of origin of brain tumor stem cells, because their long existence may subject them more easily to acquisition of multiple gene abnormalities necessary for tumorigenesis[122]. A remote, not impossible scenario might contemplate both hypotheses, but no solid data have been produced, therefore exacerbating the need for further insightful studies. In this regard, since the majority of GBM arises *de novo*, a better understanding of the origin of the TIC compartment will be helpful in the clinical management.

2.10.2 Isolation of GBM TICs

In the context of GBM, TICs are found in specific perivascular niches and present an enhanced proliferative rate compared to the normal NSCs, consistently with their role in tumor evolution[123].

Experimentally, the first human GBM-derived stem cells isolation was described by Ignatova and coworkers, which demonstrate neurosphere-forming capacities in culture as well as neuronal and astroglial markers expression[124]. Afterward, the presence of stem-cell like cells in brain tumors has been demonstrated in several studies[102,103,124,125]. The isolation of brain tumor cells with tumorigenic capacity, tested *in vivo* using the xeno-transplantation assay, was initially reported independently by two groups[103,125]. Although they arrived at similar conclusions, they used different approaches for isolating brain TICs: the cell sorting based on selection for the cell surface marker CD133[103] and the neurosphere assay[125].

The first prospective *in vitro* and *in vivo* identification and characterization of putative TIC from human brain tumors was based on cell sorting for the neural stem cell surface marker CD133[103]. *In vitro*, CD133-positive cells formed clonogenic neurosphere colonies, and could be induced to differentiate into mature neural cell lineages. Moreover, CD133-positive brain tumor cells were highly enriched for tumor initiating activity *in vivo*[103]. Afterwards, several studies have questioned the utility of CD133 in the isolation of GBM TICs. First, CD133 is often undetectable in many fresh GBM specimens and in established glioma cell lines, which nonetheless retain *in vivo* tumorigenic potential[126]. Second, cells with stem cell characteristics and tumorigenic potential have been isolated also from

CD133-negative GBMs[127]. Other cell surface markers have been proved useful, but not decisive, for the isolation of GBM TICs, including CD15, CD44 and Integrin-α6, highlighting the necessity of additional and more specific markers or the use of combinatorial markers[128].

Due to the lack of reliable selective surface markers, the identification and isolation of GBM-TICs rely mainly on functional criteria, such as the ability to self-renew and the tumorigenic *in vivo* potential. The gold standard method is based on serial orthotopic transplantations in mice in order to reproduce the original tumoral morphology and molecular pattern[129]. Alternatively, a good choice is to culture them in selective serum-free medium (**Fig. 7**). The selective conditions in which the neurosphere assays is carried out allow the stem-like cells to continually divide and form multipotent clonal spheres, namely neurospheres, while the more differentiated cells incapable of self-renewal and multipotency die off with serial passages[102]. Notably, on mitogen removal and addition of serum, these cells retain the ability to differentiate into neurons, astrocytes and oligodendrocytes[130] (**Fig. 7**).

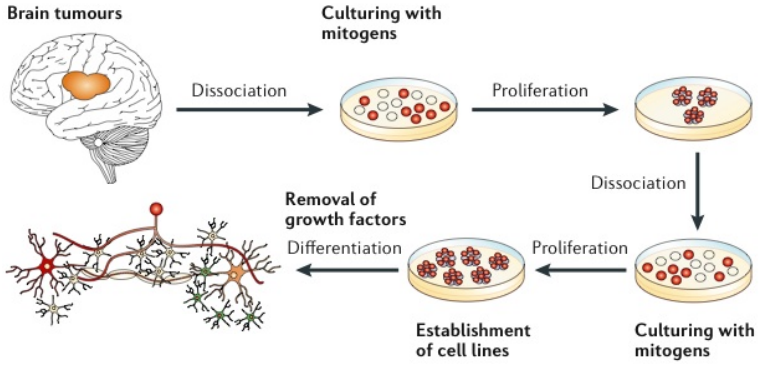

Figure 7. Isolation, perpetuation and differentiation of brain tumor stem cells in culture. The neurosphere assay is a serum-free culture system that allow the isolation of stem cell-like cells from surgical specimen based on their intrinsic properties of exclusive and extensive self-renewal potential[130]

TICs isolated from human GBM mirror the same genotype of the patient's primary tumor[131] and show stable stem cell properties: extensive self-renewal, multipotency and the capacity to initiate new tumors that recapitulate the histological features of the parental tumor after xenotransplantation *in vivo*[125].

The main issue related to this assay is that neurospheres are composed by a heterogeneous cell population that consists of stem cells, together with progenitors and

more differentiated cells, and a true separation of stem and progenitor cells remains problematic[132].

2.10.3 Therapeutic relevance of tumor initiating cells in GBM

A previous study of our group employed an orthotopic *in vivo* limiting dilution assay to calculate the TIC frequency in fresh human GBM specimen and demonstrated that the TIC frequency correlates with both mice survival and with the clinical course of human GBM patients. Patients with low TIC frequency experienced a trend towards a longer progression free survival, further supporting the hypothesis that TICs play a pivotal role during glioma-genesis[133].

From a clinical perspective, the cancer stem cell-like concept has significant implications, as these cells need to be eradicated in order to provide long-term disease control. TICs are thought to be resistant to chemotherapy and targeted therapy through active mechanisms. They often express higher level of drug-resistance proteins such as ATP-binding cassette sub-family G member 2 (ABCG2) and ABCG5 and multidrug resistance protein 1 (MDR1) transporters[134,135]. Human CD133-positive GBM cells are resistant to radiation therapy, retaining a clonogenic and tumorigenic potential, because of a more potent activation of DNA damage checkpoint mechanisms. This repair mechanism can be targeted through pharmacologic inhibition of the checkpoint kinases Chk1 and Chk2, which renders the CD133 GBM cells more radiosensitive[57].

Many different therapeutic approaches have been proposed so far. Calabrese and colleagues showed that targeting angiogenetic processes by treating GBM-bearing mice with Bevacizumab depleted tumor blood vessels and caused a dramatic reduction in the number of GBM stem cells and the growth rate of the tumor[123].

Also pathways regulating neural stem cell proliferation and differentiation might be targeted in brain tumor treatment. BMPs, which normally induce astrocyte differentiation from normal neural precursors, have been shown to promote GBM cell differentiation *in vitro* and *in vivo*, reducing stem cell tumorigenicity and supporting the hypothesis that promotion of tumor stem-cell differentiation may be an important strategy for treatment of brain tumor[136]. A further possibility is to target the process of GBM TICs differentiation into endothelial cells. Indeed, it has been demonstrated that a significant portion (range 20-90%, mean 60.7%) of vascular endothelium has neoplastic origin and that its selective targeting reduces the growth of GBM mouse xenografts[137].

Although many efforts, GBM TICs demonstrated high resistance to a plethora of different therapeutic approaches. Prager and colleagues argued that the key of this resistance lays its foundation in the plasticity and dynamicity of GBM hierarchical organization, in which GBM TICs can occupy a broad spectrum of multipotent microstates[138]. They postulated the so-called "attractor state model", in which GBM TICs have the highest entropy and capacity for adaptation in response to both intrinsic and extrinsic cues, known as "attractor states" (e.g., microenvironmental niches, genetic mutations, therapeutic intervention). In this model, the attractor states drive the formation of heterogenous TIC subpopulation, enhancing the diversity of the overall population. As cell differentiate, instead, they are "drawn down into an energy valley" and must stick to a well-defined and limited transcriptional program, whose vulnerabilities can be identified and exploited to design an effective targeted therapeutic intervention. In contrast, GBM TIC chromatin landscape is characterized by a widespread loss of repressive histone marks and by an aberrant activation of multiple transcription factor networks that results in a greater access to alternative pathway activation in response to both intrinsic and extrinsic stimuli[139]. This permissive epigenetic landscape, together with a mutational landscape that revokes crucial cellular checkpoints, allow continuous transcriptional fluctuations. Thus, GBM TICs can be described as heterogeneous and highly adaptable entities, whose enormous plasticity prime them to elude therapies, by providing a wide range of escape routes in response to various therapeutic approaches[138].

GBM TIC dynamic state is also shaped by extrinsic clues from the tumor micro-environment. Stem cell biology is strongly supported by a specialized microenvironment or stem cell niche. Stem cell niches are complex dynamic entities that actively regulate stem cell function, in particular their self-renewal and fate[140].

The three main GBM microenvironments are the perivascular niche, the hypoxic-necrotic core and the invasive edge, each of them activating different cellular program in GBM TICs and being, in turn, modeled by GBM TIC themselves as a result of a continuous bi-directional crosstalk[141] (**Fig. 8**).

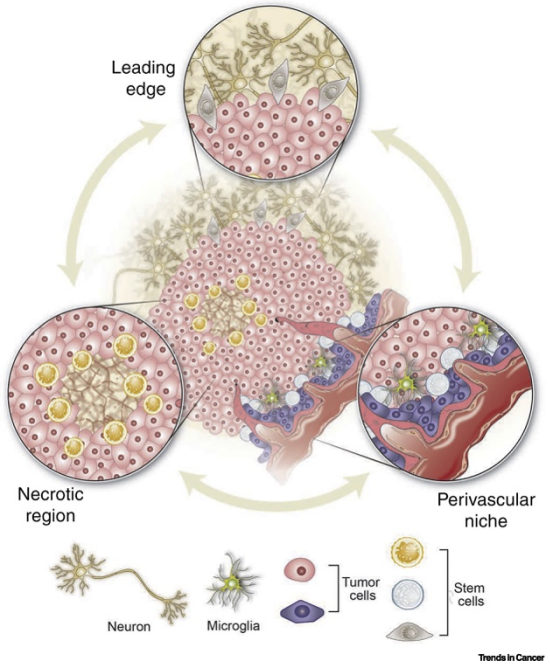

Figure 8. The three main GBM TIC niches. GBM TICs are found in the tumor microenvironment and maintain heterogeneity through unique cell–cell interactions and niche properties throughout the tumor. These niches are not stable and independent, but instead are dynamic drivers of cellular adaptation and resistance that communicate and interconvert as the tumor grows and adapts[138].

Within the perivascular niche, endothelial cells sustain stem cell-like traits maintenance through the induction of NOTCH, sonic hedgehog and nitric oxide pathways[142,143]. In turn, GBM TICs secrete pro-angiogenic factors to stimulate endothelial cell proliferation, migration and survival, and drive blood vessel permeability[144]. The perivascular niche contributes also to induce chemo-radio resistant properties and to promote a migratory/invasive phenotype. CXCL12, a ligand expressed by endothelial cells, positively regulates the expression of matrix metallo-proteinase (MMP), important mediators of invasion[143]. Moreover, TGF-β contributes to both the expression of MMP9[145] and the activation of DNA repair pathways[146]. GBM TICs strongly depend on their niche and on angiogenic processes. Notably, co-transplanting brain tumor stem cells and endothelial cells into immunocompromised mice, the initiation and growth of tumors in the brain were accelerated by the endothelial derived factors. Brain tumor stem cells seem to have potent angiogenic properties and can recruit vessels during tumorigenesis. It was shown that CD133-positive human GBM produced high level of VEGF and formed highly vascular and hemorrhagic tumors in the brains of immunocompromised mice. Furthermore, treating CD133-positive cells with Bevacizumab blocked their ability to induce endothelial cell migration and tube formation in culture, and initiate tumors *in vivo*[110]. Moreover it was observed that GBM TICs directly differentiate into endothelial cells lining tumor vessels[137].

Despite these premises, several anti-angiogenic therapies showed only modest efficacy in clinical trials. In some cases, their failure is related to the ability of GBM to satisfy its need of vascularity circumventing VEGF targeting. In other cases, the hypoxic niche expands and compensate for the destruction of the perivascular niche. Under hypoxic conditions, TICs acquire ability to survive in a nutrient-depleted environment and switch their metabolism toward aerobic glycolis. Furthermore, hypoxia leads to TIC quiescence, allowing them to evade chemo-radio therapies. These effects are mainly mediated by the hypoxia-inducible factor 1 (HIF-1 and HIF-2). HIF-1a promotes also GBM TIC survival and radio-resistance through the induction of ERK and contributes to regenerate the perivascular niche by promoting VEGF expression[147] HIF-2a is instead involved in the activation of stem cell-related signaling pathways mediated by KLF4, SOX2 and OCT4, thus contributing to stemness maintenance[148].

Finally, highly migratory and invasive GBM TICs are enriched in the third niche: the invasive niche. Located at the tumor edge, this niche sustains the expression of MMP and induce GBM TICs to undergo epithelial-to-mesenchimal transition by inducing the expression of some of its mediators, such as TWIST1, N-cadherin, STAT3 and NF-kB[51,149,150]. The acquisition of a migratory and invasive phenotype at the tumor leading edge undermine the efficacy of surgical resection, facilitating the relapses.

Globally, GBM niches constitute three diversified but interconnected micro-environments, whose interdependence with GBM TICs generate a broad spectrum of heterogenous and plastic TIC sub-populations, able to nullify the efficacy of therapies targeted against a single peculiar trait of GBM TIC population. The attractor state model implies that effective therapeutic strategies should curb TIC adaptive properties. Ideally, new combinatorial approach should encompass a first treatment, aimed to bottlenecks tumor adaptation by driving and blocking TIC into one particular and fixed state (e.g. differentiated state), against which the second treatment is specifically targeted at[138].

2.10.4 Role of the epigenetic landscape in the stemness maintenance

Normal mammalian development and embryonic stem cell (ESCs) differentiation are physiologically governed by epigenetic mechanism such as histone modifications, DNA methylation, chromatin remodeling and changes in non-coding RNAs. The epigenetic machinery plays a pivotal role in the maintenance of the stemness. Similarly, transcriptional

changes that guide the differentiation process obey not only to the signaling network of a core of transcription factors, but also to finely tuned alterations of the epigenomic landscape[151]. It has been suggested that the accumulation of epigenetic abnormalities may predispose tumor cells to genomic instability, thus increasing tumor mutational burden. Moreover, specific epigenetic changes can dis-regulated stem cell-related pathways, thus sustaining the insurgence of the TIC sub-population. The Wnt/β-catenin pathway, which is physiologically involved in normal tissue development, as well as in TIC self-renewal[152], can be aberrantly activated by DNA methylation[153]; histone modifications can enhance the activity of ASCL1, a transcription factor that activates Wnt signaling by repressing the negative regulator DKK1, and that is essential for the maintenance and *in vivo* tumorigenicity of GBM TICs[139]. The Hedgehog signaling pathway, which regulates stem and progenitor cell proliferation and maintenance, can be dysregulated by histone acetylation[154], and DNA methylation[155]. Finally, enhanced histone acetylation[156], and unbalanced H3K4 and H3K27 methylation[157] can drive aberrant activity of Notch pathway, normally crucial for NSC survival.

Beside the key role of epigenetic alterations in the activation of specific signaling pathways, the extensive plasticity of TICs and their ability to adapt and survive in response to micro-enviromental and therapeutic cues is sustained by their permissive and flexible epigenetic landscape, as previously stated describing the attractor state model[138].

Zhou and colleagues showed that GBM TIC epigenetic landscape is different from that of NSCs, underlying the important role played by epigenetic in GBM TIC compartment. Indeed, they enlightened an abnormal expression of ten-eleven-translocation (TET) family members, instrumental in DNA demethylation, and a distinct enhancer distribution, and hypothesized that these two elements can contribute to shape the transcriptional profile of GBM TICs, influencing the activation of pathways involved in cell proliferation, DNA damage response, apoptosis, and cancer development[158].

Pangeni and colleagues identified subtype-specific epigenetic signatures in GBM. They discovered that TICs isolated from Proneural and Mesenchimal GBMs have a different DNA methylation pattern. Bulk tumors, despite being mildly less methylated compared to TICs, show a similar trend, with Mesenchymal, Neural and Classical subtypes more prone to hypermethylation events compared to Proneural subtype. Further, they claimed the

existence of DNA methylation gene signatures that are unique to GBM subtypes and correlates with their transcriptional profile, underlying the importance of epigenetic in the establishment and the maintenance of GBM TIC and bulk tumor molecular profile[159].

Overall, there are accumulating evidences that stem cell identity and properties in cancer cells are driven not only by the acquisition of their mutational burden, but also by their epigenetic landscape. Thus, the reversible nature of epigenetic alterations paves the way to the development of epigenetic drug aimed to eradicate GBM TIC compartment.

2.11 LSD1

The N-terminal tails of the core histones are a major site of histone post-translational modifications (hPTM), including acetylation, methylation, phosphorylation, ubiquitination and many others. Notably, these modification often occur in close proximity one to each other's, suggesting that their several possible combinations are read as a sort of "histone code," allowing the recruitment of regulatory machinery, including both coactivators and corepressors of transcription, with the final aim to finely regulate gene transcription[160]. One of the most studied hPTM is the methylation or lysine residues, whose biological significance depends on the specific methylated residue: methylation of lysine 4, 36 and 79 within histone H3 (H3K4, H3K36, H3K79) contributes to gene expression activation, while methylation of H3K9, H3K27 and H4K20 leads to gene repression[161].

Lysine methylation is catalyzed by S-adenosilmethionine dependent methyltransferases (SAM-dependent MTases), and can be removed by two different classes of lysine-specific demethylases (KDMs), belonging to either the amino oxidase (AO) or the Jumonji C demethylases (JmjC) family. AOs employ flavin-adenine dinucleotide (FAD) as a cofactor, and demethylates mono- and di-methyl groups of lysine residues, while JmjC employ iron or **α**-ketoglutarate and act on trimethylated lysine residues[162].

The first discovered lysine demethylase was the FAD-dependent Lysine-Specific Histone Demethylase 1A (LSD1, also known as KDM1A or AOF2), whose functions of histone demethylase and transcriptional repressor have been described by Shi and colleagues in 2004[163]. LSD1 belongs to the family of amino oxidase (AO) enzymes and catalyze the demethylation of H3K4me1/me2 and H3K9me1/me2 through an oxidoreductase reaction, by employing FAD as a cofactor and producing formaldehyde as a byproduct[164].

2.11.1 LSD1 structural overview

LSD1 is structured in three main functional domains: the C-terminal amine oxidase-like catalytic domain (AOL), the N-terminal SWIRM domain, and the Tower domain, that protrudes from the central structure of the enzyme. The AOL domain is in turn subdivided in two lobes: the substrate-binding and the FAD-binding domain[165] (**Fig. 9**).

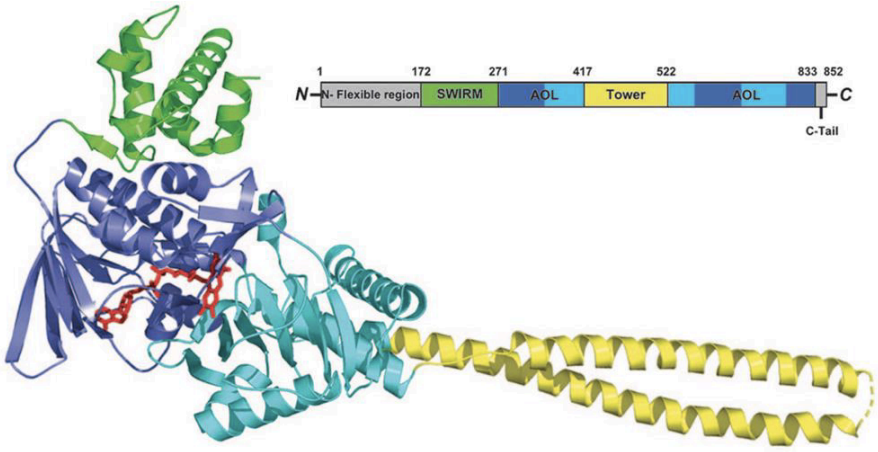

Figure 9. LSD1 structural overview. The SWIRM domain is shown in green, the AOL domain is in blue (the FAD-binding subdomain) and cyan (the substrate-binding subdomain), and the Tower domain is in yellow. The N-terminal flexible region and the C-terminal tail that are not included in the structure determination are colored in gray. FAD is in ball-and-stick representation and is colored in red. Adapted from Chen et al., 2006[165].

The interaction between AOL and SWIRM domains leads to the formation of a globular structure that ensures LSD1 stability and function. In fact, mutations of conserved residues along this interface are associated with defects in LSD1 stability and catalytic activity[166]. Instead, Tower domains mediates protein-protein interaction with the SANT domain of protein complexes such as REST corepressor 1 (CoREST) and The Nucleosome Remodeling and Deacetylase complex (NuRD)[162,167].

2.11.2 LSD1 histone substrate specificity

LSD1 carries out its demethylase functions as part of multi-protein complexes, whose different composition drives LSD1 substrate specificity and, as consequence, LSD1 transcriptional regulator activity[168,169]. Two main repressive complexes such as coREST[170] or NuRD[167] allow LSD1 to demethylate H3K4m1/me2, thus acting as a transcriptional repressor (**Fig. 10**). CoREST complex is a supervisor of cell fate decision during neuronal differentiation, and functions as a transcription repressor that localizes in the promoters of neuron-specific genes. Upon differentiation into a neuron cell, it is largely degraded to activate a neuronal expression program, while upon differentiation into a non-neuronal

cell type, this repressor machinery persists in maintaining neuron-specific genes in a repressive state[171]. CoREST complex protects LSD1 from proteosomal degradation and facilitates its demethylase activity on nucleosomal substrates. Indeed, the coREST complex contains, among the others, also the histone deacetylase (HDAC), whose function is to create a hypo-acetylated chromatin environment that is fundamental to allow LSD1 catalytic activity[168]. BHC80 (also known as PHF21A) is another important member of the LSD1 complex and it is essential to maintain LSD1-target gene repressed. BHC80 is pivotal to permit LSD1 binding to unmethylated H3K4 (H3K4me0), suggesting that BHC80 may be necessary to maintain LSD1 at the target promoters after H3 demethylation, thereby preventing the re-methylation of H3K4[172]. LSD1-coREST recruitment to chromatin, in particular to promoter and enhancer regions, is mediated by its interaction with the SNAG domain of several transcription factors, including Snail1, GFI1 and GFI1b[173,174]. When part of the NuRD complex, instead, LSD1-chromatin interaction is driven by Pax2 or Prox1[175,176]. NuRD complex is involved in several biological processes from human development to the progression of several cancer types[177]. LSD1 acts as a co-repressor of the NuRD complex in a subset of its biological functions, among which enhancer decommissioning during embryonic differentiation[178], lipid homeostasis[176] and aberrant gene-repression in Ewing sarcoma[179].

An additional important partner of LSD1 is the orphan nuclear receptor TLX, which contributes to the proliferation and the stem cell-properties of NSCs and regulates neurogenesis; TLX interact with LSD1 both directly, by binding its AOL and SWIRM domains, and indirectly, by recruiting the CoREST/LSD1 complex[180].

Despite its well-reported activity as transcription repressor, LSD1 can also behave like a co-activator, through the demethylation of H3K9me1/me2. Although LSD1 is not able to demethylate H3K9 *in vitro*[163], its substrate specificity towards this lysine residue is achieved by its interaction with androgen and estrogen receptors (AR and ERα)[169] (**Fig. 10**). The mechanisms underlying this switch remained elusive until Metzger and coworkers enlightened that, upon AR signaling activation, the protein kinase C beta I (PKCb1) phosphorylates H3 at threonine 6, originating steric constrains that prevents LSD1 from demethylating H3K4[181]. Nair and colleagues instead proposed that the histone reader PELP1 acts a co-regulator of ERα, recruiting LSD1 to ERα target genes characterized by the repressive mark H3K9me2 and here switching LSD1 substrate specificity in order to allow ERα de-repression[182].

Moreover, a neuronal-specific splicing variant of LSD1, known as LSD1+8a or LSD1n, regulates neuronal differentiation, memory and spatial learning by eliciting its demethylase activity on H3K9me2 and H4K20me3[183,184].

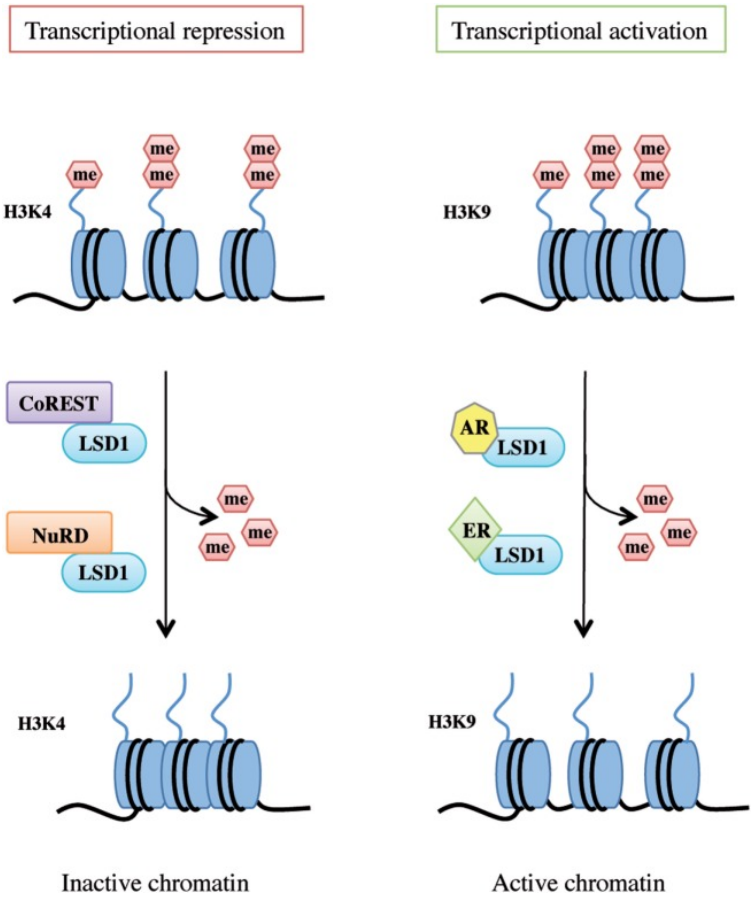

Figure 10. LSD1 substrate specificity. LSD1 dual functions as transcriptional repressor and activator. LSD1 regulates chromatin accessibility through its demethylating activity on H3K4 and H3K9. On the left, LSD1 binds to the CoREST or NuRD thus demethylating mono- and dimethyl-group on histone H3K4 and allowing genes transcriptional repression. On the right, following androgen receptor or estrogen receptor binding, LSD1 promotes transcriptional activation by demethylating mono- and dimethyl-group on histone H3K9. Adapted from Magliulo et al., 2018 [185]

2.11.3 LSD1 non-histone targets

LSD1 demethylates also some non-histone substrates, determining changes in their function or protein stability.

In this way, LSD1 modulates apoptosis, DNA damage response and the activity of cell cycle regulators, such as p53, E2F and Rb.

In particular, LSD1 blocks the p53-dependent pro-apoptotic program by removing mono or di-methyl groups from its K371 residue, thus impairing the interaction with the co-activator p53 Binding Protein (53BP1) and preventing DNA binding[186].

In p53-deficient cancer, instead, LSD1 promotes DNA damage induced cell death by demethylating E2F1 lysine 185 (K185). The unmethylated form is protected from proteasomal degradation and is primed to be acetylated and phosphorylated by PCAF and CHK2, respectively. These modifications stabilize E2F, leading to its accumulation and triggering the pro-apoptotic signaling activation[187].
Further, LSD1-dependent demethylation causes the degradation of negative regulators of Rb phosphorylation. Thus, increasing the levels of phosphorylated Rb, LSD1 contributes to cell cycle progression[188].

Another main non-histone target of LSD1 is HIF-1α, that plays a crucial role in the development of aggressive cell phenotype (through stimulation of angiogenesis, epithelial-mesenchymal transition, and invasion) and in glycolytic and mitochondrial metabolism interplay. LSD1 prevents HIF-1α ubiquitination and degradation by demethylating HIF-1α K32 and K39. Thus, LSD1 acquires a key role in the reprogramming of cancer metabolism inducing the shift from oxidative to glycolytic metabolism, maintenance of redox homeostasis, and cell survival[189].

Finally, Sheng and colleagues highlighted a novel role of LSD1 as negative modulator of tumor immunogenicity. Indeed, LSD1 demethylates the Protein Argonaute 2 (AGO2) lysine 726, thus stabilizing this core component of the RNA-inducing silencing complex (RISC). LSD1 inhibition in melanoma impairs RISC activity, and that leads to dsRNA stress activation. The consequent production of type 1 interferon stimulates an anti-tumor T cell response and facilitates T cell tumor infiltration[190]. Moreover, LSD1 targeting increases the expression of the programmed cell death-ligand 1 (PD-(L)1) in melanoma cells, making them more sensitive to anti-PD-1 blockade-base therapy[190]. Recently, Qin and co-workers confirmed that LSD1 inhibition sensitizes poorly immunogenic breast tumor to immunotherapy[191], supporting the hypothesis that LSD1 regulates anti-tumor immunogenic response.

2.11.4 LSD1 biological functions

LSD1 is a vital gene in mammalian biology, with an essential involvement in developmental programs; indeed, LSD1 knock-out results in mouse embryonic failure[192].

LSD1 is a key regulator of the balance between stemness and differentiation of ESCs. In this cellular context, LSD1 binds the promoters of a group of developmental genes characterized by the presence of bivalent domains, a peculiar chromatin environment that contains both H3K4me2/me3 and H3K27me3. Through the demethylation of H3K4, LSD1 suppress the expression of the developmental genes, thus contributing to the pluripotency maintenance. Coherently, LSD1 silencing induces the expression of cell-lineage commitment genes. Moreover, LSD1 expression is progressively downregulated during ESC differentiation[193]. LSD1 is also a master regulator of hematopoiesis. Its interaction with growth-factor independent (GFI) proteins is crucial to allow the first emergence of hematopoietic stem cells[194], as well as to dynamically coordinates hematopoietic differentiation by promoting the expression of lineage-specific genes[193,195]. *In vitro* and *in vivo* knockdown approaches confirm that normal granulopoiesis, erythropoiesis and thrombopoiesis are all dependent upon LSD1[174]. Similarly, LSD1 was found to finely tune the transition from pluripotent to NSCs, and from progenitor cells to mature neurons. LSD1 is indeed part of a multi-protein complex named BRAF-histone deacetylase complex, which abrogate the expression of neuronal-specific genes and whose timely-regulated disassembly allows mature neuron terminal differentiation[171].

Further confirmation of the involvement of LSD1 in developmental processed has been documented in anterior pituitary gland and oocytes[192].

Additional roles played by LSD1 comprise DNA damage response promotion[196], circadian cycle regulation phase resetting[197] and metabolism regulation. LSD1 was indeed found to drive the metabolic shift from mitochondrial to glycolytic metabolism that hepatocarcinoma cells undergo to adapt to the surrounding environment[198] and to regulate the expression of energy expenditure genes in adipocytes by suppressing mitochondrial respiration[198].

2.11.5 LSD1 in cancer

LSD1 serves as an important oncogenic driver in the context of malignant transformation. LSD1 was first found to be overexpressed in poorly differentiated neuroblastoma[199]. Overexpression of LSD1 has been documented in many solid tumors, including breast, prostate, esophageal, bladder and lung cancer, and acute myeloid leukemia (AML)[200] and is correlated with aggressive clinicopathological features and poor patient outcomes[201–203]. It is plausible that LSD1, through interaction with different factors, might exert distinct molecular mechanisms in various tumor types. Indeed, LSD1 targeting, either by genetic depletion or pharmacological inhibition, inhibits a plethora of cancer-related cellular processes such as proliferation[204,205], differentiation[178,206] , migration and invasion[205,207], beside decreasing tumor growth and metastatisation in animal models[195,208].

There are several forms of malignancy that have been shown to have aberrant LSD1 activity. In breast cancer, LSD1 expression is higher in invasive ductal carcinoma compared to in situ ductal carcinoma, and its upregulation correlates with the progression of the tumor grade[209]. Moreover, it is highly expressed in triple negative breast cancer subtype, characterized by rapid growth, loss of differentiation, and increased propensity to metastatization[210]. LSD1 was found to closely cooperate with HDAC to positively control breast cancer cell growth by inducing an aberrant gene silencing[202]. Further, LSD1 cooperates with the transcription factor Slug to enhance EMT activation, thus conferring migratory ability, and to repress the expression of ERα, thus contributing to make the hormone therapy ineffective[211]

An elevated LSD1 activity is also reported in squamous cell carcinoma (SCC), which is often characterized by the overexpression of the stemness-related transcription factor Sox2[212]. LSD1 binds the enhancer of Sox2 and promotes its expression and that of cell cycle regulatory genes[213]. In turn, Sox2 expression confers sensitivity to LSD1-targeted therapies[214].

LSD1 is also dysregulated in colorectal carcinoma, where it confers a poor prognosis and exerts pro-metastatic activities by enhancing EMT activation[215]. In fact, LSD1 suppress E-cadherin expression through the demethylation of H3K4me residues at the promoter of its coding genes *CDH-1*[216]. In addition, LSD1 sustains EMT also contributing to the activation of Wnt/β-catenin signaling pathway[217].

Several studies highlighted the pro-tumorigenic role of LSD1 in hematological malignancies, and in particular in acute myeloid leukemia (AML), in which LSD1 is often overexpressed independently from molecular subtypes[185]. AML is an heterogenous malignancy characterized by the accumulation of incompletely differentiated progenitor cells (blasts) that impede the normal hematopoiesis. Consistently to what observed in many solid tumors, LSD1 sustains the maintenance of pool of cells endowed with stem cell-like traits, such as clonogenic potential, by suppressing differentiation and apoptotic programs[218]. Moreover, LSD1 inhibition in AML can re-activate the expression of myeloid differentiation-associated genes, sensitizing AML cell to all-*trans* retinoic acid-based therapies, which are otherwise effective only in acute promyelocytic leukemia (APL), a subtype of AML characterized by the PML-RARA fusion[195].

Overall, the molecular mechanisms underpinning LSD1-related phenotypic effects are various and largely context-dependent. Intriguingly, recent reports shed light on novel molecular mechanism through which LSD1 exerts it pro-tumorigenic activities in a catalytic-independent manner. Maiques-Diaz and colleagues reported that LSD1 promotes AML cell differentiation through its protein-scaffolding functions. Specifically, inhibition of LSD1 by OG-86, a highly selective LSD1 inhibitor, results in the disruption of the GFI repressor transcription complex. In turn, this leads to the displacement of GFI1/CoREST from the enhancers that control the expression of a set of transcription factors involved in myeloid differentiation, thereby triggering blast differentiation[206,219] (**Fig. 10**). An analogous mechanism has been described by Ishikawa in a model of AML by using a different LSD1 inhibitor: the compound T- 3775440[220]. Similarly, Ravasio and collaborators demonstrated that LSD1 inhibitors, that are ineffective as single agents in APL treatment, greatly sensitize APL cells to physiological doses of all-*trans* retinoic acid, inducing their differentiation and prolonging the survival of leukemic mice. They found that LSD1 inhibition disrupt its interaction with GFI1 and causes LSD1-complex displacement from GFI1 target genes, leading to the reactivation of the differentiation program[221].

Such demethylase-independent mechanisms are not exclusively conserved in hematological malignancies. Indeed, the interaction between LSD1 and GFI1 repress the expression of genes involved in neuronal commitment and differentiation in

meduloblastoma[222]. Moreover, LSD1 scaffolding functions promote the survival of castration-resistant prostate cancer. Indeed, the allosteric LSD1 inhibitor SP2509 obstacles LSD1 interaction with its binding protein ZNF217, impeding they cooperative activation of a lethal prostate cancer gene network[223]. Finally, Takagi and coworkers demonstrated that the compound T- 3775440 exerts anti-tumorigenic properties in a model of small cell lung cancer (SCLC) by disrupting LSD1 interaction with either GFI1 or the transcriptional repressor INSM1, thereby inhibiting expression of neuroendocrine-associated genes[224].

Whether similar mechanisms are conserved in other malignancies needs further investigations.

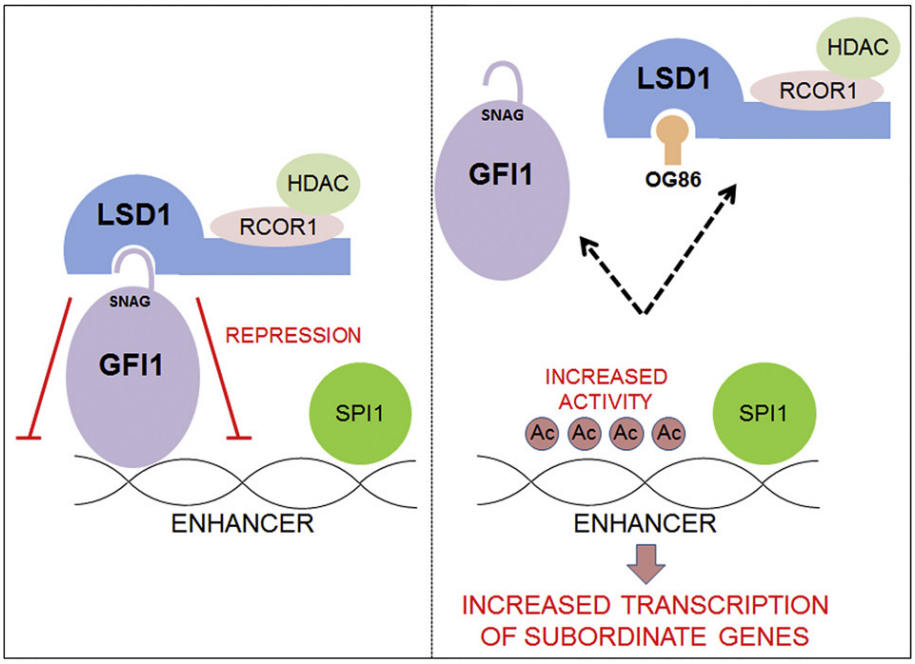

Figure 11. LSD1 demethylase-independent functions. LSD1 inhibition disrupts GFI1/CoREST complexes, whose release from their target enhancers leads to the activation of subordinate myeloid transcription factor genes. Adapted from Maiques Diaz et al., 2018 [206]

2.11.6 LSD1 in GBM

LSD1 is highly expressed in GBM[204,225,226], and its expression correlates with histological malignancy[225]. LSD1 demethylates H3K4me2 at the promoter of p21 and PUMA, and this sustains proliferation of both primary GBM TICs and differentiated, commercially available, glioma cell lines (U87MG, T98G, U138, LN229). Nevertheless, more recently Sareddy and coworkers demonstrated that LSD1 expression is higher in GBM TICs compared to patient-matched differentiated cells and that the effect of LSD1

pharmacological inhibitors, such as NCL-1 and NCD-38, on cell viability, neurosphere formation and apoptosis are more pronounced in GBM TICs than in matched-differentiated cells, toward which they exert only modest effects[227]. Moreover, it has been reported that LSD1 control the expression of c-MYC, which in turn increases the expression of OLIG2, POUF3F and Sox2, all genes involved in the transcriptional reprogramming of GBM cells into stem-like state. Unexpectedly, LSD1 regulates c-MYC expression in a dose-dependent manner. Indeed, when LSD1 is efficiently silenced, MYC expression is reduced and cell death is increased, while in the case of only partial LSD1 silencing, MYC expression is upregulated, leading to tumor growth[228]

As in other cancer types, LSD1 exerts a plethora of different functions in GBM. Above controlling GBM stemness and proliferation, LSD1 blocks also GBM cell apoptosis by demethylating its non-histone substrate p53[225]. Its genetic or pharmacological targeting retards xenograft tumor growth through both a reduction of proliferation and an increased induction of apoptosis[225]. LSD1 pharmacological inhibition drives also GBM TIC death by triggering an hyperactivated unfolded protein response (UPR)[227]. Further, Saccà and co-workers showed that LSD1 inhibition induces DNA-damage response and senescence by inducing HIF1α degradation in a post-transcriptional manner in three GBM cell lines (U87MG, U251 and T98G cells)[226].

Some studies started to address the effect of LSD1 targeting in various combined therapeutic approaches. LSD1 silencing or inhibition sensitizes GBM cell lines and GBM TICs to the treatment with HDAC inhibitors, such as vorinostat or PCI-24781, inducing both caspase-dependent and independent apoptosis. Interestingly, this effect is not photocopied in non-transformed cells (normal astrocytes)[204]. This combined therapeutic approach reduces the tumor size and extend the overall survival of U87MG-transplanted mice[229]. Recently, the attempt to increase cancer-selectivity of therapeutic approaches, leads to the development of a novel dual-action prodrug, which activation depend on high concentrations of H_2O_2. Since cancer cells produce high quantity of reactive oxygen species, including H_2O_2, this ensure specific activation of the prodrug in tumor cells, whereby reducing side effects due to normal tissue damages [230]. This prodrug activation contemporary releases the LSD1 inhibitor *trans*-2-phenylcyclopropylamine (2-PCPA/tranylcypromine) and a glutathione quencher, the *para*-quinone methide.

Glutathione depletion has been linked to caspase 3/7 activation, leading to a synergic triggering of apoptosis in GBM cells[230].

Therefore, owing to its aforementioned pro-oncogenic properties, LSD1 has been pointed out as a promising therapeutic target in GBM, alone or in combination with other drugs.

2.12 LSD1 inhibitors: state of the art

Targeting LSD1 is becoming an emerging option for the treatment of cancers and numerous LSD1 inhibitors have been developed so far. The non-selective MAO inhibitor tranylcypromine (TCP) was the first compound found to be able to irreversibly but weakly inhibits LSD1 by forming covalent TCP-FAD adducts[231]. TCP showed anti-tumorigenic properties in different cellular models[232] and entered in phase 1 clinical trial for AML (ClinicalTrials.gov Identifier: NCT02261779 and NCT02273102).
TCP low potency and selectivity has inspired further efforts for designing a series of TCP-based derivatives with enhanced LSD1 selectivity. The TCP phenyl-ring was modified by the addition of N-alkylations and side groups in order to increase the selectivity towards LSD1, whose catalytic site is larger than those of other MAOs. To date, ORY-1001, GSK-2879552, IMG-7289, INCB059872, and ORY-2001 currently undergo clinical assessment for cancer therapy.

ORY-1001, developed by Oryzon Genomics, potently inactivates LSD1 and is highly selective over other FAD-dependent aminoxidases, while demonstrating excellent oral bioavailability, activity, and target exposure *in vivo*. It entered phase 1 clinical trial for both AML (EUDRACT 2013-002447-29) and SCLC (ClinicalTrials.gov Identifier: NCT02913443).
The compound GSK2879552 was initially chosen due to its high selectivity to FAD utilizing proteins, including LSD1. Despite it has been used also in hepatocellular carcinoma and T-cell lymphoblastic leukemia (T-ALL) an antitumor screening of GSK2879552 against a panel of cell lines showed that its antitumor activity is mainly restricted to SCLC and AML[232]. Although these premises, two clinical phase 1 trials investigating the safety, pharmacokinetics, pharmacodynamics, and clinical activity of GSK2879552 in SCLC (ClinicalTrials.gov Identifier: NCT02034123) and AML (ClinicalTrials.gov Identifier: NCT02177812) have been terminated because the risk/benefit analysis was not favorable.

Other two LSD1 inhibitors recently entered in clinical trial: INCB059872 and IMG-7289. INCB059872, developed by Imago BioSciences, is a FAD-directed LSD1 inhibitor that acts forming FAD adducts. Its preclinical activity has been tested in several cancer models, as AML, SCLC and prostate cancer[232]. It is currently under clinical assessment in Ewing sarcoma patients (Trial Identifier: NCT03514407 and EudraCT 2018-000062-11). Its safety and tolerability are now under investigation also in different types of tumors such as AML/MDS, SCLC, myelofibrosis, Ewing sarcoma, and poorly differentiated neuroendocrine tumors (ClinicalTrials.gov Identifier: NCT02712905). IMG-7289, developed by Imago BioSciences, is currently undergoing phase IIa clinical trial evaluation as a combined treatment with ATRA for treating high risk AML (ClinicalTrials.gov Identifier: NCT02842827).

Many other irreversible LSD1 inhibitor have been developed and tested in pre-clinical studies, but did not enter in clinical trials. Among them, the most effective are OG86, T-3775440 and NCD38. OG86 was shown to trigger AML cell differentiation by altering LSD1 and GFI1 interaction[206], while T-3775440 impaired the proliferation of SCLC and AML cells[220,224]. Beside hematological malignancies, the efficacy of NCD38 was demonstrated also in GBM, in which its administration induces differentiation and trigger apoptosis of immature cells[227].

Numerous efforts have been also dedicated to the development of LSD1 reversible inhibitors, in the attempt to reduce long lasting off-targets effects, especially those impacting on erythropoiesis. Differently from irreversible LSD1 inhibitors, reversible compounds are not TCP-derivatives, from which they differ in their mechanism of action. Indeed, reversible LSD1 inhibitors compete with the LSD1 substrate for the binding to the enzyme. Achieving potent reversible inhibition of LSD1 has proved challenging and a varied group of compounds have been tested[233]. Nevertheless, some exemplars of reversible inhibitors -such as CC-90011, GSK690 and SP2509- have achieved excellent potencies in biochemical assays.

CC-90011, developed by Celgene, was the first reversible LSD1 inhibitor in clinical trials. It currently undergoes phase 1 clinical trial for safety and efficacy evaluation in patients with relapsed/refractory solid tumors and non-Hodgkin's lymphomas (Clinical trial identification: NCT02875223 and EUDRACT 2015-005243-13). Moreover, a phase 1/2

study is evaluating the safety, tolerability, and preliminary efficacy of combined treatment of CC-90011 with cisplatin or etoposide in patients with SCLC (ClinicalTrials.gov Identifier: NCT03850067).

Interesting pre-clinical results have been obtained with GSK690 in multiple AML subtypes, where it elicits its anti-tumorigenic effects both through the inhibition of LSD1 catalytic activity and through the alteration of its scaffolding functions[234]. Additionally, the combination with HDAC inhibitors was proved effective in engaging the intrinsic apoptotic pathway in rhabdomyosarcoma cells[235].

Also the allosteric inhibitor SP2509, alone or in combination with HDAC inhibitors, led to promising results in AML, Ewing Sarcoma and prostate cancer, but the enthusiasm for this compound has been mitigated by a study showing that it was effective also against LSD1-KO cells, highlighting a lack of selectivity[236].

Latterly, novel reversible LSD1 inhibitors have been identified through high-throughput screenings and are currently under early stage investigation. Z. Li and colleagues reported the development of compound 15u, able to induce differentiation of AML cell lines[237], while L. Li and coworkers claimed the design of a series of new compounds, among which Lo5 was confirmed to be highly selective and displayed a marked inhibition of colorectal cancer cell migration[238]. Another novel reversible inhibitor, the compound 10d, has been reported to inhibit migration of colon and lung cancer cell lines[239]. So far, few is known about the potential applications of these newly designed LSD1 inhibitors, and further analyses are necessary to understand if they deserve a deeper investigation as a hit-to-lead in oncology.

2.12.1 The LSD1 inhibitor DDP38003

In this thesis, we evaluated the anti-tumorigenic potential of a novel irreversible LSD1 inhibitor named DDP_38003 (here LSD1i). This compound was born from the collaboration between the Drug Discovery at the European Institute of Oncology, the University of Pavia, La Sapienza University in Rome and the University of Milan. This tight collaboration also led to the development of a series of irreversible LSD1 inhibitors with proved selectivity towards LSD1 compared to other structurally and functionally similar enzymes such as MAOs and LSD2[240].

DDP_38003 was designed using TCP as chemical scaffold. Among the new developed compounds, it performed well in term of potency (LSD1 IC50: 0.06uM) and selectivity (MAO-A IC50: 0.29μM, MAO-B IC50: 84.59μM, LSD2 IC50: 36.6μM). Its administration reduces the clonogenic potential of mouse APL blasts and AML cells, induces their differentiation, and modulates the expression of recognized LSD1 target genes, such as GFI1B and CD11b[240]. Its efficacy has been evaluated in vivo in a murine promyelocytic leukemia model. Mice were treated by oral gavage, testifying the oral availability of this compound. No significant body weight differences among the groups of mice were observed during the treatment, suggesting a good tolerability profile. DDP_38003-treated mice survived longer than vehicle-treated mice, and the effect was dose-dependent (11.25mg/Kg: + 35%; 22.50mg/Kg: +62%)[240]. The anti-tumorigenic effects of DDP_38803 on APL models have been subsequently widely studied by the group of Prof. Saverio Minucci (IEO): its combination with all-trans retinoic acid (ATRA) was of benefit for leukemic models and further encouraged its testing in other cancer types[221].

3. AIMS OF THE STUDY

- Many of the pre-existent studies point to LSD1 as a possible druggable target in GBM. Although, despite the number of the available LSD1 inhibitors, major concerns have been raised about the low selectivity of some of them. In my PhD project, I tested the anti-tumorigenic potential of the novel, irreversible and highly selective LSD1 inhibitor DDP_38003 (here LSD1i) for therapeutic intervention in human GBMs.
- The majority of the LSD1 studies published so far in GBMs has been conducted in established cell lines and few is known about LSD1 specific role in the TIC compartment, which better recapitulates the heterogeneity of the parental tumor, and whose therapeutic targeting may bey the key to defeat GBM. Thus, I focused on the pro-tumorigenic role played by LSD1 in the GBM TIC compartment. In this effort, I took advantage of human patient-derived GBM TICs, already available in the laboratory, and orthotopic GBM patient derived xenograft (PDXs) as model systems.
- Since the mechanism of action of different LSD1 inhibitors seems to depend both on the features of the compounds and on the cellular context in which they are used, we planned to unravel the molecular players underlying LSD1 pro-tumorigenic role in GBM TICs and to dissect the molecular mechanisms underpinning the anti-tumorigenic potential of LSD1i in GBM TICs.

4. MATERIALS AND METHODS

4.1 Experimental model and subject details

4.1.1 Primary cultures:

GBM TICs isolated from human-GBM surgical specimen[241] collected from consenting patients of both genders in the Department of Neurosurgery at Neurological Institute "C. Besta" (Milan, Italy) under "C. Besta research ethics committee approval", were already available in the laboratory. The clinical features of the corresponding patients and the molecular information identified for each patient-derived TIC culture were already available and are provided in Table 5-7. TICs Briefly, tumors were enzymatically digested with papain 2 mg/mL (Worthington Biochemical) at 37°C and mechanically dissociated until achievement of single cell suspension. ACK (Ammonium-Chloride-Potassium) Lysis Buffer was employed to remove red blood cells, upon an incubation of 3-5' at room temperature. Viable single cells were finally resuspended and maintained in serum-free DMEM/F12 medium (Dulbecco's modified Eagle medium/ Ham's F12 Nutrient Mixture; Gibco) supplemented with B27 supplement (Life Technologies), 20 ng/ml human epidermal growth factor, 10 ng/ml human basic fibroblast growth factor (PeproTech), 2mM Glutamin and 1% Penicillin/Streptomycin as cellular floating aggregates known as neurospheres. Human GBM TIC cultures were grown at 37°C in a 5% CO_2 humidified incubator. They were passaged by mechanically dissociation when sphere reached approximately 300-500 microns in diameter, and cell counts were performed at the time of passage.

4.1.2 Animals:

CD1-nude were obtained from Charles River laboratory (Charles River, Wilmington, MA) and maintained in a pathogen-free environment. Mice were given ad libitum access to food and water and randomly assigned to experimental groups.

The whole procedure was carried out using experimental protocols approved by the institutional review board of the European Institute of Oncology, Milan, Italy.

All animal experiments were performed in accordance with the Italian laws (D.L.vo 116/92 and following additions), which enforce EU 86/609 Directive (Council Directive 86/609/EEC of 24 November 1986 on the approximation of laws, regulations and

administrative provisions of the Member States regarding the protection of animals used for experimental and other scientific purposes). Mice have been housed accordingly to the guidelines set out in Commission Recommendation 2007/526/EC - June 18, 2007 on guidelines for the accommodation and care of animals used for experimental and other scientific purposes. The protocol was approved by the Italian Ministry of Health (Authorization 556/2016-PR).

Only 4–6 weeks old female mice were used for xenograft studies. To obtain orthotopic GBM PDX, GBM TICs were mechanically dissociated and 10^5 cells were resuspended in 2 µl of phosphate-buffered saline (PBS) and stereotaxically injected into the mice nucleus caudatus (coordinates from bregma: 1 mm posterior, 3 mm left lateral, 3.5 mm in depth)[241].

4.2 Method details

4.2.1 Compounds

LSD1i (DDP_38003) was produced by the Experimental Therapeutic Unit at the IFOM-IEO Campus[240] and administered as specified for each experiment. L-Histidinol (HisOH, Merck Life Science #H6647) was administered as a single dose (2mM). Thapsigargin (Merck life Science, #T903) was administered as a single dose (2.5uM).

As a complementary approach to L-Histidinol treatment, GBM TICs have been cultured in Glutamine deprivation conditions. (Glutamine standard concentration: 2mM. Glutamine deprivation: 0.5mM.)

4.2.2 Generation of LSD1-silenced or ATF4-overexpressing or ΔN-LSD1 and ΔN-LSD1^{K661A} overexpressing GBM TICs.

LSD1 silencing was achieved by lentiviral transfection with MISSION® pLKO.1-puro Empty Vector Plasmid DNA (Sigma Aldrich) harboring either the sequence targeting human LSD1 (TRCN0000046071, here sh71), or a non-targeting shRNA (SHC002, here shNT) used as a control. For lentivirus production, these two constructs were transfected in 293T cells together with pCMV-DR8.2 packaging plasmid and pMD2G-VSVG envelope expressing plasmid, by using the calcium phosphate method. GBM TICs were incubated with filtered lentiviral supernatant from 293T supplemented with polybrene (8µg/mL) for 72 hours. Cells were then selected in puromycin for 72 hours.

To perform rescue experiment, a N-terminal truncated (172-833) form of LSD1 WT (ΔN-LSD1^{WT}) and LSD1 catalytic mutant (ΔN-LSD1^{K661A}) (gift from Saverio Minucci, European Institute of Oncology, Milan) have been overexpressed in LSD1 KO GBM TICs. Phoenix amphotropic packaging cells had been transfected with either Pinco-GFP-ΔN-LSD1^{WT} or Pinco-GFP-ΔN-LSD1^{K661A}. LSD1 KO GBM TICs were incubated with the filtered retroviral supernatant supplemented with polybrene (8μg/mL) for 48 hours. Cells were then sorted on the base of GFP expression.

GBM TICs expressing ATF4 cDNA were generated by lentiviral infection using lentiviral particles (TLO1001-Lenti-hCMV-ORF-IRES-bsd, transOMIC) harboring human ATF4 cDNA. Empty lentiviral particles were used as controls. Cells were then selected in blasticidin for 72 hours.

4.2.3 Generation of LSD1-KO GBM TICs

LSD1-KO GBM TICs were generated by the genome editing facility of IFOM. GBM#22 TICs have been transduced with all-in-one PX458 vector using Nucleofection (kit V, program T-020). After 48 hours, cells were FACS-sorted for GFP expression and clonally cultured by limiting dilution. NGS sequencing (Ion Proton) and western blot were used to check LSD1 KO efficacy.

4.2.4 Generation of Luc-expressing GBM TICs

Luc-expressing GBM TICs were generated by lentiviral infection. Viral particles were produced through transfection of pLentiLox3.7 vector encoding Luc2 cDNA (gift from Luisa Lanfrancone, European Institute of Oncology, Milan), pRSV-Rev and pMDLg/pRRE packaging plasmids and pMD2G-VSVG in 293T cells. After 48 hours of infection with the filtered viral supernatant, GBM TICs were selected in puromycin for 72 hours and seeded in limiting dilution conditions to obtain single sphere. Luc2^{high} expressing spheres were then selected after incubation with 150ug/ml luciferin in PBS and luminescence analyses using PerkinElmer's IVIS Lumina Series III instrument.

4.2.5 IF staining

Neurospheres were mechanically dissociated until single cell suspension was achieved and spin down by cytospin for 5' at 200rpm. Cells were fixed with 4% paraformaldehyde (PFA) in phosphate-buffered saline (PBS) for 10', permeabilized with 0.1% Triton-X for 10' and blocked with a 5% Bovine Seum Albumin (BSA) in PBS for 30'. Anti-LSD1 (1:100, Cell Signaling, #2139A) primary antibody was used at room temperature (RT) for 60'. Alexa Fluor 647-coniugated goat anti-rabbit secondary antibody was used at RT for 60'. Nuclei were counterstained with DAPI (1:5000). A Leica laser scanning confocal microscope was used to capture fluorescence images.

4.2.6 CD133, Cd15 and α6-Integrin protein expression on GBM TICs by Fluorescence-Activated Cell Sorting Analysis

For antigen extracellular staining, GBM TICs were mechanically dissociated and analyzed by using the Flow cytometry live cell protocol from Cell Signaling Technology and the following primary antibodies: PE-conjugated anti-CD133 antibody (1:10, Miltenyi, Biotec GmbH, #AC133- 10' at 4C), PE-conjugated anti-α6-integrin antibody (1:50, BD-Pharmigen, #555735 - 60' at 4C), PE-conjugated anti-CD15 antibody (1:50, BD Bioscience, #332778 - 60' at 4C). The isotype control sample was used to establish a gate in the PE channel. Gating for single cells was established using forward scatter in the isotype control sample. Stained cells were analyzed by flow cytometry (FACS Vantage SE flow cytometer (BD Biosciences, Franklin Lakes, NJ). At least 20,000 events were acquired.

4.2.7 Western blot

GBM TICs were collected by centrifugation and washed twice with PBS, then lysed in RIPA Buffer (50 mM Tris-HCl buffer (pH=8), 10 mM CaCl2, 5mM EGTA [pH 8], 250 mM NaCl, Glycerol 10%, triton-x 100 1%) supplemented with a cocktail of proteinase inhibitors (50 mM NAF, 10 mM NAPP, 10mM NaOrtoV, PMSF (0.1mg/ml), Leupeptin 10 μM, Aprotinin 10 μM). Lysates were left for 30' on ice, and then centrifugated at 13000 rpm for 30' in a refrigerated centrifuge. Cleared supernatants were recovered and the concentration of protein lysates was measured by Bradford assay according to manufacturer protocol. 10-30 μg of proteins were mixed with Laemmly buffer, supplemented with 100 mM DTT, and denaturated for 5 minutes at 95°C. Proteins were resolved by SDS-page, transferred to

Nitrocellulose or PVDF membranes at 100V for 90 minutes or 30V overnight at 4C, and blocked with 5% bovine serum albumin (BSA) in Tris Buffered Saline (TBS) solution with Tween 20 (TBS-Twenn buffer: 50mM Tris, 150 mM NaCl, 0.1% Tween 20) for 1 hour at room temperature (RT). Primary antibody were incubated in 5% BSA TBS-Tween overnight at 4°C or for 1 hour at RT. After three 10 minutes washes with TBS-Tween buffer, antibody binding was assessed by horseradish peroxidase (HRP) conjugated secondary antibody (1:5000, Sigma Aldrich). Images were acquired on a ChemiDoc XRS instrument (Biorad). Primary antibodies included: anti-LSD1 (1:1000, Cell Signaling #2139A), anti-ΔN-LSD1 (1:1000, Abcam #ab17721), anti-ATF4 (1:500, Cell signaling #11815S), anti-eIF2**α** (1:1000, Cell Signaling #5324S), anti Phospho-eIF2**α** (1:1000, Cell Signaling #3398S), anti-ASNS (1:1000, Santa Cruz, SC-365809), anti-CBP (1:1000, Santa Cruz #SC-7300), anti-GAPDH (1:1000, Santa Cruz, SC-322223), anti-Lamin B1 (1:1000, Abcam, AB16048), anti-β-actin (Clone AC-74, 1:2000, Sigma Aldrich, A5316) and anti-Vinculin (1:5000 Sigma Aldrich, #V9131).

4.2.8 EC50 assessment and growth assay

To determine LSD1i EC50, single GBM#22, GBM#7 and GBM#18 TICs obtained through mechanical dissociation of neurospheres were seeded in 3 wells of a 24 well plates (10.000 cells/well) and treated with a single administration of vehicle or increasing doses of LSD1i (0.5 - 1-0 - 2.5 - 5.0 and 10.0uM). Viable cells were manually counted after 7 days. EC50 was calculated with "Quest Graph™ EC50 Calculator (v.1)." *AAT Bioquest, Inc*, 10 Aug. 2020 (https://www.aatbio.com/tools/ec50-calculator-v1)

To assess cell growth upon LSD1 inhibition, GBM TICs were plated as described above in 3 wells of a 24 well plates (10.000 cells/well) and treated with a single administration of vehicle or LSD1i. GBM#22 and GBM#7 TICs were treated with LSD1i 2.5um. GBM#18 TICs were treated with LSD1i 5uM. Viability was assessed by manual count on indicated days.

Similarly, to assess cell growth upon LSD1 genetic targeting, LSD1-silenced GBM TICs (sh71-GBM#22, -GBM#7 and -GBM#18 TICs) or LSD1-KO GBM TICs (KO#1 and KO#2 GBM#22) and their respective controls were plated as described above in 3 wells of a 24 well plates (10.000 cells/well) and viable cells were counted at the indicated days.

4.2.9 Self-renewal assay

Single cells obtained from mechanical dissociation of GBM#22, GBM#7 and GBM#18 TIC neurosphere cultures were seeded in Dulbecco's modified Eagle medium/F12 medium containing 50% of methylcellulose (MethoCult SF, STEMCELL Technology) in a 35 mm culture plates (1000-3000 cells/dish). Two weeks after plating, the number of neurospherse was manually counted. When needed, a second serial plating has been done according to the same protocol. LSD1i 2.5uM was administered as a single treatment at the first plating.

The effect of LSD1 genetic targeting on GBM TIC self-renewal was similarly assessed in LSD1-silenced GBM TICs (sh71-GBM#22, -GBM#18 and -GBM#10 TICs) or LSD1-KO GBM TICs (KO#1 and KO#2 GBM#22) and their respective controls.

4.2.10 *In vitro* extreme limiting dilution assay

After neurosphere mechanical dissociation, LSD1-silenced GBM TICs (sh71-GBM#22, -GBM#18 and -GBM#10 TICs) and their respective controls were seeded at decreasing concentration (100- 50- 10- 1- 0.5 cells/well) in a 96 well plate. Sphere formation was evaluated after two weeks. Results have been analyzed by means of the extreme limiting dilution analysis (ELDA) algorithm[242].

4.2.11 Apoptosis

GBM TICs were seeded as single cells in a final volume of 100ul, in a 96 well plate (10.000 cells/well) and treated with a single administration of vehicle or LSD1i (GBM#22 and GBM#7 TICs were treated with LSD1i 2.5uM. GBM#18 were treated with LSD1i 5uM) for 7 days. Caspase 3/7 activity of treated cells was measured with Caspas-Glo assay kit (Promega). Briefly, the plate containing cells was removed from the incubator and allowed to equilibrate to room temperature. 100µl of Caspase-Glo reagent was added to each well and the plate was gently mixed with a plate shaker for 30 seconds. The plate was then incubated at room temperature for 30 minutes. The luminescence of each sample was measured in a plate-reading luminometer (GloMax). The experiments were performed in triplicate.

The effect of LSD1 genetic targeting was similarly assessed in LSD1-silenced GBM TICs (sh71-GBM#22 and -GBM#7 TICs) and their respective controls.

4.2.12 LSD1i tolerability

GBM#22 TICs were orthotopically implanted in the nucleus caudatus of female CD-1 nude mice. Animals were weighted and then treated with vehicle or 17mg/kg of LSD1i at day 14 and 21 after TICs injection. 5 hours after the second treatment mice blood was withdrawal through cardiac puncture and 250 µl of blood analyzed using a Beckman Coulter Hematologial Analyzer to assess the total number of platelets and red and white blood cells.

4.2.13 Cellular Thermal Shift Assay (CETSA) on brain extracts from LSD1i-treated mice

CD-1 nude mice were treated with vehicle or 17mg/kg of LSD1i at day 14 and 17 after GBM#22 injection; 5 hours after the second treatment mice were sacrificed, organs collected and briefly rinsed in ice-cold PBS before snap-freezing in liquid nitrogen and storage at -80°C. Brains were grinded afterwards in a Potter-Helvehjem homogenizer with a Teflon pestle, in 4 volumes of ice-cold Hypotonic Buffer (HB: 10mM Hepes pH7.5, 10mM KCl, 1.5mM $MgCl_2$ and 1mM DTT/protease inhibitor cocktail (PIC) freshly added); brain homogenates were next forced through a 26-gauge syringe-needle four to five times and then incubated 30min at 4°C after addition of 0,5vol of Nuclear Extraction Buffer-3x (NEB-3x: 10mM Hepes pH7.5, 1.5mM $MgCl_2$, 600mM NaCl, 0.4mM EDTA, 0.9% TritonX-100, 1mM DTT/PIC freshly added), followed by centrifugation at 20000xg for 10min at 4°C. Protein content of supernatants was determined by Bradford assay and lysates from different mice were equalized by addition of NEB-1x prior to 1:6-dilution to reduce NaCl and TritonX-100 respectively to 100mM and 0.05% (Dilution Buffer: 10mM Hepes pH7.5, 1.5mM $MgCl_2$, 80mM NaCl, 0.15mM EDTA, 1mM DTT/PIC freshly added). Diluted lysates were aliquoted in strip-PCR tubes and heated for 3min to different temperatures in a Veriti Thermal Cycler (Applied Biosystems) with a 3°C-step gradient to generate melting curves, followed by rapid cooling to 25°C for 3min. Aggregated proteins were removed by centrifugation at 20000xg for 30min at 4°C; equal amounts of the supernatants were separated on 8% SDS-PAGE gels, blotted onto nitrocellulose

membranes and protein of interest was detected with primary anti-LSD1 antibody (1:3000, Cell Signaling, #2139 in 5% BSA-TBST buffer) and secondary anti-rabbit IRDye-800CW antibody (LI-COR, 1:20000). Fluorescent signals were acquired on Odyssey CLx and quantified using ImageStudioLite (LI-COR). Data were normalized by setting band intensities of lowest and highest temperature of the gradient to 100% and 0% respectively. Melting curves were fitted using the Blotzmann sigmoidal equation to determine the apparent aggregation temperature. The reported data were obtained from 3 animals in each experimental group (vehicle or treatment) and are presented as mean with error bars representing the standard error of the mean (S.E.M.).

4.2.14 Mice survival analysis

To evaluate the time of appearance of the tumor symptomatology after *in vivo* treatment with LSD1i, $10^{\wedge 5}$ GBM#22 or Luciferase positive-GBM#18 TICs were mechanically dissociated and stereotaxically injected into the mice nucleus caudatus. Treatments started two weeks after GBM TIC injection. LSD1i (17mg/kg) or vehicle was administered twice/week for 4 weeks by oral gavage. Tumor-bearing mice were sacrificed at the appearance of neurological signs (weight loss, lack of grooming, kyphotic posture).

To evaluate the effect of LSD1 genetic targeting on the time of appearance of the tumor symptomatology, $10^{\wedge 5}$ LSD1-silenced (sh71-GBM#22 and -GBM#18) or LSD1-KO GBM TICs (KO#1- and KO#2 GBM#22 TICs) and their respective controls were mechanically dissociated and stereotaxically injected. Tumor-bearing mice were sacrificed at the appearance of neurological signs.

Survival differences were compared by Log-rank test with control and non-targeted GBM TICs.

4.2.15 Bioluminescence Monitoring

Tumor growth was monitored through a non-invasive in vivo analysis of bioluminescence starting from the week following the orthotopic injection and carried out weekly until the appearance of neurological symptoms. The bioluminescence measure was performed by intraperitoneal inoculation of 150 mg/kg of luciferin (60µl of D-luciferin potassium salt

diluted in PBS up to a concentration of 50 mg/ml to allow non-invasive monitoring of luciferase) about 10 minutes before in vivo image capture. The mice were anesthetized in special chambers with 1-4% isofluorane. The images were acquired using PerkinElmer's IVIS Lumina Series III instrument wavelengths (600 - 800 nm) depending on the organ involved (lungs, lymph nodes, liver, brain) [243]. Treatment group and time effects, with the interaction, taken as fixed factors, and mice effect as random, were evaluated in a mixed-effect model (PROC MIXED, SAS). Repeated-measures models investigated the effect of arms in changes of intensity from baseline at different time points adjusting for baseline values. Normal distribution of residuals was checked using residual plots from saturated models. All statistical tests were two-sided, and $P<0.05$ was considered statistically significant. The statistical analyses were performed with the Statistical Analysis System Version 9.2 (SAS Institute, Cary, NC).

4.2.16 Limiting Dilution Transplantation Assay (LDA)

Progressively smaller numbers ($10^{\wedge 5}$, $10^{\wedge 4}$, $10^{\wedge 3}$ and $10^{\wedge 2}$) of LSD1-silenced GBM TIC#22 or GBM#18 and their relative controls were orthotopically implanted and TIC frequency was estimated by means of the extreme limiting dilution analysis function [242]
The incidences of tumors per number of injected cells and injected TICs were compared by means of Log-linear analysis (G^2 test; http://biostathandbook.com/gtestgof.html).

4.2.17 Immunohistochemistry:

Immunohistochemical staining was performed on formaline-fixed and paraffin-embedded tissue specimens (mouse and human). The paraffin blocks were sliced into 2μM thick sections, deparaffinized with histolemon (Carlo Erba), and rehydrated with decreasing concentrations of ethanol in water. Before incubation with the primary antibody (2h at RT), tissue sections were subjected to heat-induced epitope retrieval using Citrate Buffer pH 6 for anti-GFAP, anti-Nestin, anti-Sox2 antibodies and EDTA 1mM ph8 for anti-LSD1 antibody. Bound antibody was revealed using EnVision Plus/HRP detection system (DAKO) and diaminobenzidine as chromogenic substrate, then counterstained with Hematoxylin solution (Leica). Representative images were acquired with the Aperio ScanScope XT instrument. The immunohistochemical analysis of LSD1 expression was

carried out on a panel of human GBMs. For quantification of LSD1 staining, 10 different fields were counted for each section from 51 independent samples, and was evaluated by counting the percentage of LSD1-positive tumor cells (P) and the intensity of nuclear staining (I). The signal intensity was scored as follow: 0, no staining; 1 weak staining; 2 moderate staining; 3 strong staining. By performing an IxP score, we identified three categories: 0-100 low expression, 100-200 moderate expression, 200-300 high expression. IHC staining antibody: The following primary antibodies were used: LSD1 polyclonal antibody (1:600, Cell Signaling #2139), GFAP polyclonal antibody (1:200, Dako #Z0334), Nestin monoclonal antibody (1:200, Millipore # MAB5326), SOX2 polyclonal antibody (1:50, Stem Cell Technologies, #01438).

4.2.18 RNA extraction and RT- qPCR

RNA was isolated from GBM TICs using Quick-RNA Miniprep Kit (Zymo Research) following manufacturer's specifications. RNA was isolated from frozen brain tissue using Quick-RNA Miniprep Kit (Zymo Research) after tissue homogenization in TRIzol Reagent (ThermoFisher). cDNA was synthesized with High Capacity cDNA reverse transcription kit (Thermo Fisher). RT-qPCR was performed by Viia7 Real-Time PCR system (ThermoFisher) using Fast SYBR Green (Applied Biosystems). Threshold cycle (Ct) values for each gene were normalized to the housekeeping (HK) gene expression level. Relative expression levels were determined by the 2-ΔΔ where ΔCt was calculated as follows: ΔCt= Ct (gene of interest) – Ct (HK).

To assess LSD1 expression in LSD1-silenced (sh71) and control (shNT) GBM PDXs, two microdissected sections/PDX have been analyzed. Data were normalized on mean LSD1 expression levels in shNT group.

PRIMER ID	FORWARD	REVERSE
TBP	TGCACAGGAGCCAAGAGTGAA	CACATCACAGCTCCCCACCA
GAPDH	AGCCACATCGCTCAGACAC	GCCCAATACGACCAAATCC
LSD1	GATTCCAGGTGCCCCACAGCCG	ACATGGGCCTCTTCCCTTAGAATGC
ΔN-LSD1	TTTGATCGGGTGTTCTGGGA	AGGCATCGGCCAACAATCA
TUBB	AGTGATGAGCATGGCATCG	ACGTACTTGTGAGAAGAGGCC
NES	GGTGGCCACGTACAGGACCC	TGGGGTCCTAGGGAATTGC
GFAP	GGTACCGCTCCAAGTTTGC	AGGTCAAGGACTGCAACTGG
ASNS	ACTGTCGGGATGTACCCCTG	AAAGGCAGCCAATCCTTCTGT
DDIT3	GGAAACAGAGTGGTCATTC	CTGCTTGAGCCGTTCATTCT

CHAC1	GTGTGGTGACGCTCCTTGAAGA	TGCTCCCCTTGCACTTGGTAT
FAM89A	TCCGCAAAGAGATGGTTGGTC	GCATGCCCCCTTGTACTCC
GAL	CGACAAGAATGGCCTCACCA	GACCGCTCGATGTCTTCTGA
GDF15	CCTGCAGTCCGGATACTCAC	CCCGAGAGATACGCAGGTG
NARS	ATGATCCAAGTCTCCCAGAGC	GTGGACCCAGCCAAACACCT
PSAT1	GGTGACAGGAGCTTGGTCAG	CCATGCACCGTCTCATTTGC
XPOT	TGGTGGATCGTGATGTGGTG	ATGCACTGTTCCCTCATGGT
SLC7A11	AGAGGGATTGGCTTCGTCCAT	GGCAGATTGCCAAGATCTC
ATF3	CTCGGGGTGTCCATCACAAAAG	AGCTTCTCCGACTCTTTCTGC
ATF5	GCTGGGATGGCTCGTAGAC	TCGCTCAGTCATCCAGTCAG
EIF1AY	TCTCACGAGGCTGTCATCACC	ACACAATGCTTCCAATCGTCC
KDELR3	TGTTTGCTCTCGTCTTCACCA	AGAAACTCCAGGCGGAATGTG
CRYAB	GGAAAACATGAAGAGCGCCAG	GGTGAGAGGGTCTACATCAGC
ASCT1	GCTGTGGACTGGATTGTGGA	TGCTCGCCTTTCTTTGTTGC
ASCT2	TCATGTGGTACGCCCCTGT	GCGGGCAAAGAGTAAACCCA
SNAT2	CTTGCCGCCCTCTTTGGATA	ACAGCCAGACGGACAATGAG
LAT1	CCGTGAACTGCTACAGCGT	CTTCCCGATCTGGACGAAGC
4F2HC	CTGGTGCCGTGGTCATAATC	GCTCAGGTAATCGAGACGCC

Table 1. List of primer sequences used in RT-qPCR assays

TaqMan assays were employed to assess the expression of TRIB3 (Thermo Fisher, Hs01082394_m1) and CBP (Thermo Fisher, Hs00932878_m1)

4.2.19 RNA-sequencing

Total RNA was extracted as described. RNA integrity was checked on a Byoanalyzer 2000 (Agilent). 500-1000ug of high quality RNA (RIN>9) have been used to prepare RNA-libraries using TruSeq RNA Library Prep Kit v2 kit (Illumina) according to manufacturer's instructions. Library quality was checked on Byoanalyzer 2000 (Agilent). Libraries were multiplexed, clustered, and sequenced on an Illumina NovaSeq 6000.

RNA-seq analysis was performed by Elena Ceccacci (Saverio Minucci's group).
Raw reads were mapped to the human reference genome using STAR aligner[244]. Reads quantification was calculated using the featureCount function of the Subread package[245]. edgeR was used to assess differential expression[246]. Differentially expressed genes (DEGs) were defined as those showing FDR ≤0.05 and linear fold-change ≥1.5. Pathway analysis and transcription factor prediction analysis were performed with QIAGEN's Ingenuity Pathway Analysis (IPA, QIAGEN Redwood City, www.qiagen.com/inenuity). The bigwig files for UCSC browser visualization of genome profiles were normalized with the deepToos suite using RPKM.

4.2.20 Measure of ATF4 translation rate

The ATF4 reporter viral particles, pseudotyped with the vesicular stomatitis virus G (VSVG) protein using the pMD.G vector and third-generation pMDLg/pRRE and pRSVRev vectors, were packaged in 293T cells using calcium-phosphate transfection and used to transduced GBM TICs. The bidirectional ATF4 lentiviral reporter vector (gift from Piergiuseppe Pelicci, European Institute of Oncology, Milan), allow the constitutive expression of BFP and ATF4–GFP. As such, all GBM TICs were marked by either BFP, as a read-out of transduction, and GFP as a measure of the ATF4 mRNA translation rate. Following infection, BFP fluorescence was measured using FACS Vantage SE FACSCantoII flow cytometer (BD Biosciences). ATF4 promoter activity was calculated as the transgene ratio between GFP and BFP (TGR = GFP mean fluorescence intensity/TagBFP mean fluorescence intensity).

4.2.21 ChIP-sequencing and ChIP-qPCR

Cells were cross-linked in culture medium containing 1% formaldehyde with gentle rocking at room temperature for 10 minutes. Cross-linking was arrested by addition of 0.125M glycine with gentle rocking at room temperature for 5 minutes. Cross-linked cells were washed twice with ice-cold PBS, resuspended in SDS-Buffer (NaCl 100mM, Tris-Cl pH 8.0 50mM, NaN3 0.02%, SDS 0.5%) and then conserved at -80C for at least one overnight incubation. Before Chromatin sonication, ½ volume of Triton-buffer (NaCl 100mM, Tris-Cl pH 8.5 100mM, EDTA 5mM, NaN3 0.02%, Triton-X-100 5.0%) was added to the samples in order to obtain the IP buffer condition (NaCl 100mM, Tris-Cl pH8.0 33mM, Tris-Cl pH 8.5 33mM, EDTA 5mM, NaN3 0.02%, SDS 0.33%, Triton-X-100 1.7%). Chromatin was sheared to an average fragment size of 200bp using a Branson Sonifier and then pre-cleared by incubation with protein A-Sepharose beads (Amersham) for 1 hours on a rotating wheel at 4C. Precleared chromatin was centrifuged to discard the beads and the supernatant was used for immunoprecipitation. The antibody of interest or Normal Rabbit IgG control (Invitrogen) were added to chromatin samples, followed by overnight incubation on a rotating wheel at 4C. The day after, antibody-chromatin complexes were captured with Protein G Dynabeads (Life Technologies) at 4C for 4 hours with rotation. Subsequently, beads were washed 3X with Mixed Micelle Buffer (NaCl 150mM, Tris-Cl 200mM, EDTA 5mM, sucrose 5.2%, NaN3 0.02%, Triton-X-100 1%), 3X with Buffer 500 (deoxycholic acid 0.1%, EDTA 1mM, HEPES 50mM, NaCl 500mM, NaN3

0.02%, SDS 0.2%, Triton-X-100 1%), 3X with LiCl detergent (deoxycholic acid 0.5%, EDTA 1mM, LiCl 250mM, NP-40 0.5%, Tris-Cl 10mM, NaN3 0.02%) and 1X with TE Buffer. Cross links were reversed by resuspending beads in de-crosslinking solution (NaHCO3 100mM, SDS 1%) and incubating samples overnight at 65°C in agitation. RNAse-A and Proteinase K were added to remove RNA and protein contaminants. Input samples, constituted by pre-cleared chromatin collected before immunoprecipitation, were decrosslinked in the same way. The day after, DNA was purified using a QIAquick PCR purification kit (Qiagen). RT-qPCR was performed using Fast SYBR Green (Applied Biosystems).

The antibodies used for ChIP-sequencing are: Anti-LSD1 (10ug, Abcam, Ab17721, 10ug), anti-ATF4 (10ug, Merck, ABE387), anti H3K4me1 (1ug, Abcam, Ab8895), anti H3K4me2 (1ug, Abcam, Ab32356), anti H3K4me3 (1ug, Abcam, Ab8580).

DNA libraries were prepared by the sequencing facility at IEO campus according to the protocol described by Blecher-Gonen and colleagues[247]. Results have been validated by ChIP-qPCR performed by Viia7 Real-Time PCR system (ThermoFisher) using Fast SYBR Green (Applied Biosystems).

PRIMER_ID	FORWARD	REVERSE
P_ATF4	AGGATTTGTGGGCGAGGTTG	TTCACTGGGCCACACAAGTA
P_ASNS	CGTAAGCAGGTCAGGGTGAT	CGCGCTGGTTGGTCCT
P_DDIT3	ATGGTCTCCCCTGGCCTAA	GTAGTGTGCTGGGACTTGAC
P_TRIB3	CGGACCGGGGGATTAGC	CACTTCCGCTGCGAGTCT
P_NARS	TCTCACCCACCTAGCACCAT	GCAGGCGCCCTCAGATCTAC
P_GDF15	ATAGAAGTTTGTGATGGGCAGAGC	CTCGTTGCATGTGACTTTAGCAG
P_PSAT1	CCAGGCAGGTGGTCAACTTT	CTCCCGCCTGAACCTCACTC

Table 2. List of primer sequences used in LSD1- and ATF4-ChIP-qPCR. The "P" that comes before the gene name indicates that primers have been designed in the promoter region.

The ChIP-seq analysis were performed by Elena Ceccaci (Saverio Minucci's group). Short reads obtained from Illumina Genome Analyzer II were quality-filtered according to the Illumina pipeline. Reads were aligned to the hg18 reference genome using Bowtie v1.0.1[248] and MACS version 1.4.1[249] was used as peak caller to identify regions of ChIP-seq enrichment over background. Only reads with a unique match to the genome and with two or fewer mismatches (-m 1 –v 2) were retained. MACS was used with a p-values threshold of 10^{-5} for all the data sets. Each sample was compared to input DNA derived from GBM#22 TICs.

For the LSD1 ChIPseq analysis common regions were defined as regions with peaks in both condition and at least 1bp of overlap between LSD1i-treated and vehicle-treated cells. Gain and loss regions were defined as regions with identified peaks only in LSD1i-treated (gain) or vehicle-treated (loss) cells. Reads count were calculated inside these regions with bedtools suite and only regions with a Log2 FC (RPKM) > 2 were kept. LSD1-treated, vehicle-treated enriched regions as well as common, gain and lost regions were annotated with R package ChIPseeker. The bigwig files for UCSC browser visualization of genome profiles were normalized with the deepToos suite using RPKM.

4.2.22 Analysis of LSD1 and ATF4 ChIP data in K562 cells

We studied the interplay between ATF4 and LSD1 binding sites by means of published data from the ENCODE consortium[250]. We downloaded from the ENCODE database (https://www.encodeproject.org/) conservative IDR thresholded peaks for ATF4 and LSD1 (KDM1A) ChIP-seq in K562 cells. These datasets where composed by 36375 peaks and 28409 peaks respectively. Subsequently, starting from the Ensembl database[251], promoter regions (-2500, + 2500 around the TSS) were defined for all protein coding genes annotated on the human genome. All the genomic annotation referred to human GRCh37 /hg19 genome. Bedtools[252] was subsequently used to determine the overlaps between ATF4/LSD1 peaks and the set of human protein coding gene promoters previously defined. This resulted in 5234 potential protein coding target genes for ATF4 and 4846 potential protein coding target genes for LSD1. Of them, 2169 protein coding genes where in common (p-value < 10^-188, Fisher exact test).

4.2.23 ATF4 enrichment in LSD1 modulated genes

We studied the enrichment of computationally predicted ATF4 binding sites on the promoter of LSD1 modulated genes by means of a simulation strategy. First, the whole-genome mapping in human of predicted ATF4 binding sites was downloaded from the Jaspar database (http://jaspar.genereg.net/,[253]). Subsequently, starting from the Ensembl database[251], a promoter regions (-2500, + 2500 around the TSS) was defined for all protein coding genes annotated on the human genome, considering for each gene only the longest transcript. Bedtools[252] was used to identify the set of ATF4 binding sites predicted by Jaspar located on the promoter regions for all the considered protein coding genes.

All the genomic annotation referred to human GRCh37/hg19 genome. Based on these definitions, we generated 1000 random gene sets consisting of 44 genes each (equal to the number of genes we found modulated by LSD1 and on which an ATF4 binding site is present) recording the total number of ATF4 binding sites associated to each of them. Finally, a Z-score was evaluated between the number of ATF4 binding sites detected on the group of 44 genes we found modulated by LSD1, equal to 197, and the distribution of ATF4 sites found in the random gene sets, resulting in Z = 1.858 (empirical p-value <0.05)

4.2.24 ATAC-seq

We conducted ATAC-seq using a home-made Tn5 kindly gifted by Giuseppe Testa's group. We collected 50,000 GBM#22 TICs by centrifugation and briefly resuspended them in ice-cold ATAC Resuspension Buffer (ATAC-RSB buffer: Tris-HCl pH 7.4 10mM, NaCl 10mM, MgCl2 3mM) supplemented with NP-40 0.1%, Tween-20 0.1% and Digitonin 0.01%. Samples were incubated on ice for 3 minutes. Lysis was washed out with ATAC-RSB supplemented with Tween-20 0.1%. To allow transposase reaction, samples were pelleted and resuspended in ice-cold transposition mixture (TD buffer 2X, MEDS-loaded Tn5 100nM, PBS 33%, digitonin 0.01%, Tween-20 0.1%) and then incubated for 30 minutes at 37C on agitation (1000 rpm). Tn5 was pre-loaded with pre-annealed Mosaic End double-stranded (MEDS) oligonucleotides as in Picelli protocol[254]. To clean up transposase reaction, samples were purified with Zymo DNA Clean and Concentrator-5 kit (Zymo Research), according to manufacture instructions. Tagmented-DNA was amplified and barcoded by PCR to construct DNA library. 8 cycles of PCR amplification were performed by Viia7 Real-Time PCR system (ThermoFisher) using NEBNext Master Mix (NEB).

Cycling Conditions	
72 C	5 min
98 C	30 sec
5 cycles of	
98 C	10 sec
63 C	30 sec
72 C	1 min
Hold at 4 C	

Table 3. ATAC-seq PCR conditions

SAMPLE	BARCODE I7+I5
VEHICLE	UDI0002_TTATAACC_GATATCGA
LSD1I	UDI0004_AAGTCCAA_TATGAGTA

Table 4. ATAC-seq barcode sequences

PCR products were purified with Zymo DNA Clean and Concentrator-5 kit (Zymo Research). DNA fragments underwent a doubled-side size selection to remove primer dimers and fragments larger than 1000bp. To remove DNA fragments > 1000bp, 0.5X volumes of Agencourt AMPure beads XP (Beckman Coulter) were added to the samples, then incubated for 10 minutes at room temperature. The supernatant, containing DNA fragments < 1000bp, was transferred in a new tube and incubated for 10 minutes at room temperature with 1.3X original volume AMPure beads. Supernatant, containing primer dimers, has been discarded and the DNA-beads complex was washed 3X with Ethanol 80% and eluted in water. Library was quantified by QuBit DNA High sensitivity (Thermo Fisher), checked with Bioanalyzer 1000 and sequenced on an Illumina NovaSeq 6000.

ATAC-seq analysis was performed by Elena Ceccacci (Saverio Minucci's group). Reads obtained were aligned to the hg18 reference genome with Bowtie2 with very-sensitive and -X 2000 options. Accessible regions were identified by MACS, with bampe and keep-dup options.

4.2.25 LC-MS/MS analysis of histone PTMs

Histones were enriched from 0.5-1*10^6 GBM primary cells treated with LSD1i or vehicle as described[255]. About 4 µg of histones per run per sample were mixed with an approximately equal amount of a heavy-labelled histone super-SILAC mix, which was used as an internal standard for quantification[256]. After separating the samples on a 17% SDS-PAGE gel, bands corresponding to histones H3 were excised, chemically alkylated with D6-acetic anhydride, in-gel digested with trypsin and desalted on handmade nanocolumns (StageTips), as previously described. Peptide mixtures were separated by reversed-phase chromatography on an EASY-Spray column (Thermo Fisher Scientic), 25-cm long (inner diameter 75 µm, PepMap C18, 2 µm particles), which was connected online to a Q Exactive HF instrument (Thermo Fisher Scientific) through an EASY-Spray™ Ion Sources (Thermo Fisher Scientific). Peptide separation, MS acquisition and histone

peptide data analysis were performed as described[257]. Extracted ion chromatograms (XIC) were constructed for each doubly charged precursor based on its m/z value. For each histone modified peptide, the relative abundance (RA) was estimated by dividing the area under the curve (AUC) of each modified peptide for the sum of the areas corresponding to all the observed forms of that peptide. The heavy form of each modified peptide was quantified from its XIC and the relative abundance quantified. L/H ratios of relative abundances were compared in different conditions by Student's t- test analysis.

4.3 Data-sets analysis

Normalized RNA-seq/microarray expression data were downloaded from The Cancer Genome Atlas (TCGA) public database (http://cancergenome.nih.gov/) and Sun dataset (GEO, GSE4290).

4.4 Quantification and statistical analysis

The specific statistical tests used are indicated in the figure legends and in methods details and were calculated using GraphPad Prism unless otherwise specified. Unpaired Student's t-test was used to compare two groups unless otherwise specified. Details for analysis are included in figure legends and methods details. Three biological replicates have been performed for each experiment, and one representative experiment have been shown, unless otherwise specified.

5. RESULTS

The results presented in this thesis have been obtained by taking advantage of GBM TICs isolated from human fresh surgical specimen as model system that better resemble human GBM compared to differentiated commercially available cell lines.

The GBM TICs sample used had been previously isolated and characterized in Giuliana Pelicci's laboratory[127].

GBM TIC isolation procedure has been discussed in Material and Methods section.
In absence of reliable and specific stem cell markers for GBM, our cohort of GBM TICs has been defined by functional criteria, namely *in vitro* self-renewal, *in vivo* tumorigenicity and self-renewal ability, phenotypical recapitulation of the primary tumor and aberrant expression of both stem cell and differentiation markers (**Fig. 12**). Moreover, the stem cell frequency of each GBM TIC sample has been calculated by *in vivo* limiting dilution[127,133].

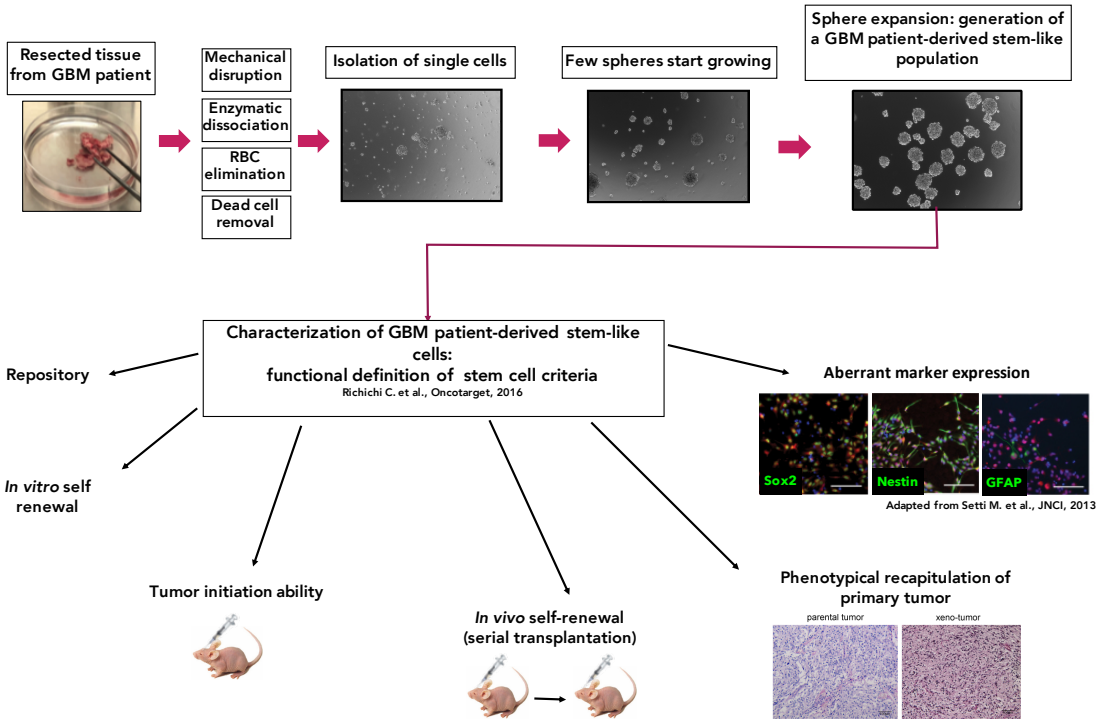

Figure 12. Workflow of GBM TIC isolation and functional characterization. GBM TICs are isolated from fresh human GBM surgical specimen through mechanical and enzymatic dissociation and cultivated in a selective serum-free medium. They are subsequently defined based on their tumorigenicity upon orthotopic transplantation and their ability to self-renew (both *in vitro* and *in vivo*). GBM TICs are also defined by aberrant expression of both stem cell and differentiation markers and their ability to phenotypical recapitulate the primary tumor.

TICs have been isolated from tumors that had been homogenously diagnosed as primary or recurrent GBM (WHO grade IV) without any age- or gender-based selection (**Table 5**). In particular, the results that will be reported in this thesis have been obtained using 4 different patient-derived GBM TIC samples, highlighted in red in **Table 5-7.** GBM TICs and the corresponding GBM tumor were both subjected to molecular analysis in order to assign a molecular subtype. Notably, the definition of the molecular subtype relies on the concordant outcome from the analysis of matched GBM TICs and tumor specimen (**Table 5**). GBM#22 TICs have been isolated from a primary tumor with a Proneural subtype. GBM#18 and GBM#7 TICs have been isolated from recurrent tumors with Mesenchimal subtype. GBM#10 TICs have been isolated from a recurrent tumor with a Proneural subtype.

Consistently with the high prevalence of IDH wild type tumors among primary GBMs, no alterations in IDH1 and IDH2 genes have been reported in our GBM TIC cohort; the IDH status has been assessed by immunohistochemistry and confirmed by both targeted next generation sequencing and PCR techniques (**Table 5**).

SAMPLE ID	TUMOR TYPE	SURGERY	SEX	SUBTYPE	IDH
HGBM#8	GBM	I	M	PN	WT
HGBM#22	GBM	I	M	PN	WT
HGBM#9	GBM	II	F	nd	WT
HGBM#18	GBM	II	M	MES	WT
HGBM#10	GBM	II	M	PN	WT
HGBM#161	GBM	I	M	nd	WT
HGBM#23	GBM	I	M	nd	WT
HGBM#11	GBM	II	M	MES	WT
HGBM#7	GBM	II	M	MES	WT
HGBM#20	GBM	I	M	PN	WT
HGBM#25	GBM	II	M	nd	WT
HGBM#153	GBM	II	M	nd	WT

Table 5. GBM TICs characterization. Molecular subtype assignment and IDH1/IDH2 status assessment in our cohort of GBM TICs and paired GBM tumor specimen. All the tumors have been hysto-pathologically defined as GBM (WHO grade IV). Surgery I and II indicate a tumor resected at its first onset or at its

recurrence, respectively. For each tumor, the gender of the patient is indicated. M: male; F: female. The samples used in this thesis are highlighted in red.

Our cohort has been further molecularly characterized to assess the mutational status of a subset of genes whose alterations are commonly found in GBM. To this aim, we exploited an approach based on targeted next generation sequencing followed by PCR validation. The genetic mutations found in our cohort are reported in **Table 6**. Other genes have been analyzed without finding any alterations in our samples, and are not included in the table (PIK3A, PIK3R1, CDK4, CDKN2A, CDKN2B, TERT promoter). Further, we defined the methylation status of MGMT promoter by PCR (**Table 6**).

Each sample used in this thesis (GBM#22, GBM#18, GBM#10 and GBM#7 TICs) showed a peculiar mutational landscape. Alterations of TP53 have been reported in all these samples. EGFR, PDGFR, PTEN, RB1 and NOTCH1 mutations are instead heterogeneously distributed. GBM#22 TICs are also uniquely characterized by the presence of FGFR3-TACC3 fusion protein. Finally, the promoter of MGMT is methylated in GBM#18 and GBM#10, but not in GBM#22 and GBM#7 TICs (**Table 6**)

SAMPLE ID	TP53	EGFR	PDGFRA.	PTEN	RB1	NOTCH1	FGFR3	TACC3	MGMT
HGBM#8									n.d.
HGBM#22	C/C	**T/T**			A/G		FGFR3-TACC3 FUSION PROTEIN		unmet
HGBM#9					A/G				n.d.
HGBM#18	T/T								met
HGBM#10	**T/T;** GC/GC		A/G		A/G				met
HGBM#161	T/T			A/A	G/G; A/G	C/T			n.d.
HGBM#23	**T/T**								n.d.
HGBM#11						GT/TC			n.d.
HGBM#7	CG/CG	**T/T**	G/T		A/G	CGTT/C			unmet
HGBM#20	G/A				A/G				unmet
HGBM#25					A/G				unmet
HGBM#153	**T/T;** GC/GC				A/G				unmet

Table 6. Mutational profiling of GBM TICs. Targeted next generation sequencing-based assessment of genetic alteration within a subset of GBM-related genes. PCR was applied to validate these results and to assess MGMT promoter methylation. Pathogenic mutation already reported in GBM are highlighted in bold. The samples used in this thesis are highlighted in red.

GBM TICs have been analyzed by western blot to assess the expression of P53, EGFR, EGFR vIII and PTEN. The expression of EGFRvIII has been validated by PCR (**Table 7**). The samples used in this thesis (GBM#22, GBM#18, GBM#10 and GBM#7 TICs) heterogeneously express these markers (**Table 7**)

SAMPLE ID	P53 EXPRESSION	EGFR EXPRESSION	EGFR vIII	PTEN EXPRESSION
HGBM#8		+	+	
HGBM#22	-	+	n.d.	+
HGBM#9	-	+	n.d.	-
HGBM#18	+	+	+	+
HGBM#10	+	+	-	-
HGBM#161	n.d.	n.d.	n.d.	n.d.
HGBM#23	+	+	-	-
HGBM#11	+	+	n.d.	-
HGBM#7	-	+	+	+
HGBM#20	-	+	n.d.	+
HGBM#25	-	+	n.d.	+
HGBM#153	-	+	+	+

Table 7. P53, EGFR, EGFRvIII, and PTEN expression in GBM TICs. Western blot evaluation of the expression of the indicated proteins in GBM TICs. The presence of EGFRvIII has been confirmed by PCR. The samples used in this thesis are highlighted in red.

Thus, the subset of GBM TICs used in this thesis to test the effect of LSD1 pharmacological inhibition are molecularly heterogeneous and resemble the peculiar inter-tumoral heterogeneity of GBM.

5.1 LSD1 is strongly expressed in human GBM and GBM TIC compartment

LSD1 pro-tumorigenic role runs parallel to its overexpression in many cancer types[199,202,258]. Gene expression data from the publicly available datasets of Sun and The Cancer Genome Atlas (TCGA) cohorts, comprising results from 81 and 442 human tumors respectively, revealed that LSD1 is significantly enriched in human GBM in comparison with non-neoplastic brain tissues (**Fig. 13**).

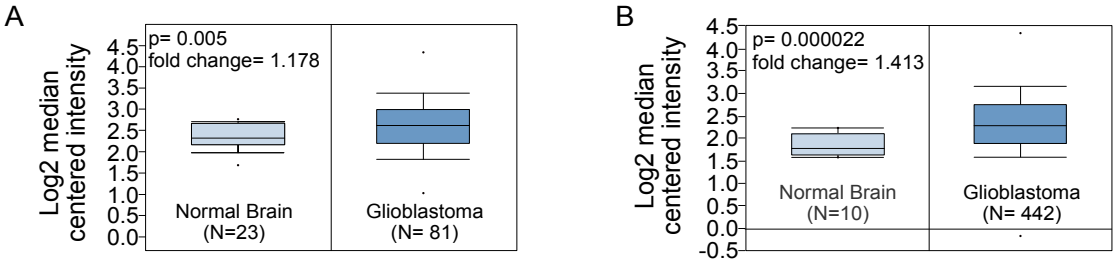

Figure 13. LSD1 mRNA levels in human GBM tissue. (A-B) LSD1 mRNA expression in GBMs versus non-neoplastic brains. Data from SUN (A) and TCGA (B) database are shown.

GBM are sub-classified on the base of their molecular profile, with each class being characterized by specific markers expression and genomic alterations. The molecular classification is now gaining growing importance, since it correlates with patient survival, with IDH-mutated and Proneural tumors linked to longer survival[29,37]. Remarkably, LSD1 is well expressed in all GBMs, but its mRNA levels reach a maximum in the Proneural subtype. According to Verhaak classification, this subtype is defined by the expression of recognized stem-cell markers, such as Sox2 and Olig2[48], suggesting that LSD1 may correlate with a stem-cell like phenotype in GBM (**Fig. 14A**). Interestingly, LSD1 expression is also more pronounced in IDH1 mutated tumors (**Fig. 14B**) but is not correlated with overall survival (**Fig. 14C**).

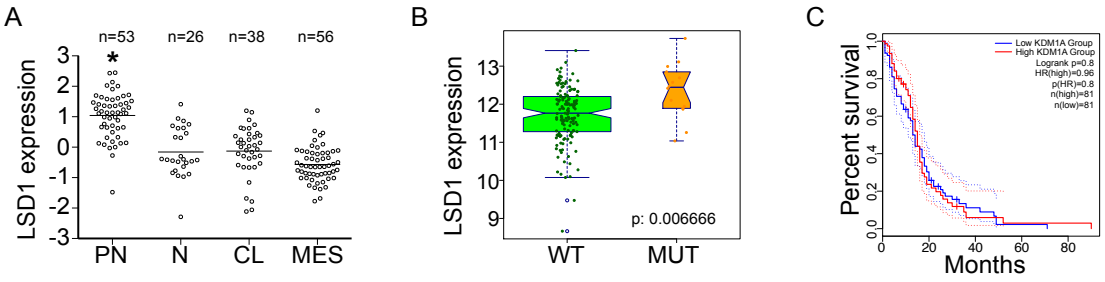

Figure 14. LSD1 mRNA levels in GBM subtypes. LSD1 mRNA expression in the GBM subtypes (PN: Proneural, N: Neural, CL: Classical, MES: Mesenchymal) derived from Verhaak classification. Data from TCGA dataset. (B) LSD1 mRNA expression in GBM according to IDH mutational status. Data from TCGA dataset.

IDH WT n= 141; IDH mut n=14. (C) Correlation between LSD1 expression and GBM patient survival. Data from GEPIA2 dataset.

To confirm this *in silico* data, we analyzed the expression pattern of LSD1 in an independent cohort of human GBM tissues by immunohistochemistry. As expected, LSD1 staining is nuclear. Importantly, LSD1 is well appreciable in all the samples analyzed, although the percentage of positive nuclei and the intensity of the staining is variable among patients, coherently with the high grade of inter-tumoral GBM heterogeneity (**Fig. 15** and **Table 8**).

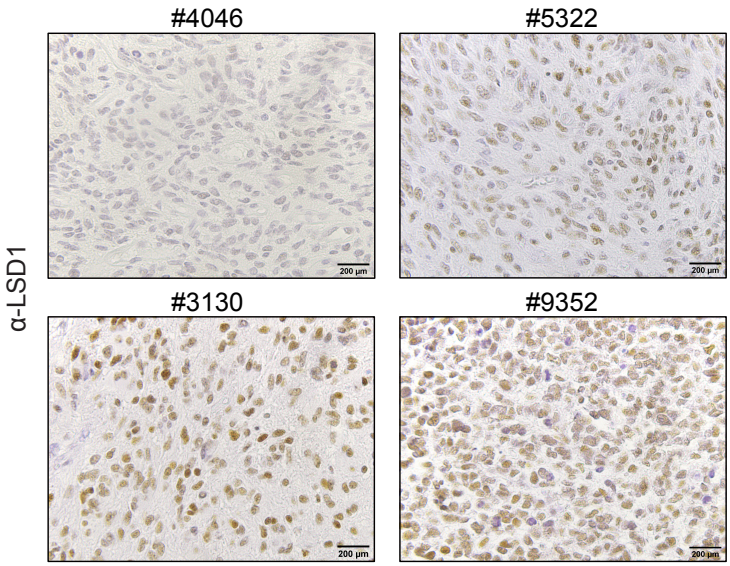

Figure 15. LSD1 protein levels in human GBM. Representative images of LSD1 expression patterns in human GBMs. Scale bars, 200um. See Table 8.

ID CASO	HYSTOPHOLOGY	WHO GRADE	% POSITIVE NUCLEI	NUCLEI INTENSITY	SCORE
4046/12	GBM	IV	40	1	40
5781/10	GBM	IV	50	2	100
4598/11	GBM	IV	50	2	100
4509/13	GBM	IV	60	2	120
9253/11	GBM	IV	60	2	120
7565/09	GBM	IV	70	2	140
8902/09	GBM	IV	70	2	140
1976/11	GBM	IV	70	2	140
6240/13	GBM	IV	70	2	140
7669/07	GBM	IV	70	2	140
1073/11	GBM	IV	70	2	140
14939/09	GBM	IV	70	2	140
7921/11	GBM	IV	70	2	140
6686/12	GBM	IV	70	2	140
532/16	GBM	IV	70	2	140
6708/11	GBM	IV	80	2	160
3816/13	GBM	IV	80	2	160
1198/09	GBM	IV	80	2	160
4515/09	GBM	IV	80	2	160
4474/10	GBM	IV	80	2	160
6812/13	GBM	IV	80	2	160
7020/06	GBM	IV	80	2	160
5322/07	GBM	IV	80	2	160
13176/07	GBM	IV	80	2	160
12408/08	GBM	IV	80	2	160
14063/10	GBM	IV	80	2	160
6723/15	GBM	IV	80	2	160
754/	GBM	IV	80	2	160
430/13	GBM	IV	85	2	170
7366/11	GBM	IV	90	2	180
10453/10	GBM	IV	90	2	180
7083/12	GBM	IV	90	2	180
792/06	GBM	IV	90	2	180
4165/08	GBM	IV	90	2	180
12802/13	GBM	IV	100	2	200
4603/13	GBM	IV	70	3	210
13256/15	GBM	IV	80	3	240
1848/07	GBM	IV	80	3	240
639/11	GBM	IV	90	3	270
12149/08	GBM	IV	90	3	270
12333/06	GBM	IV	90	3	270
11505/07	GBM	IV	90	3	270
4305/08	GBM	IV	90	3	270
7565/08	GBM	IV	90	3	270
637/10	GBM	IV	90	3	270
3972/15	GBM	IV	90	3	270
3130/09	GBM	IV	95	3	285
9352/06	GBM	IV	95	3	285
2834/07	GBM	IV	95	3	285
1848/07	GBM	IV	100	3	300
11245/16	GBM	IV	100	3	300

Table 8. LSD1 expression in a cohort of human GBM Semi-quantitative evaluation of LSD1 expression in human GBM samples: LSD1 expression was examined by immunohistochemistry in 51 GBM specimen. For each sample analyzed, the final score of LSD1 staining has been calculated as the product of the percentage

of positive nuclei and the intensity of nuclear LSD1 staining. (Intensity 1:low, 2: medium, 3:high) (LSD1 score <100: Low, 100-200: Moderate, > 200: High).

We then sought to determine LSD1 expression in the GBM TIC compartment. Performing western blot analysis, we showed that LSD1 is highly expressed in our cohort of patient-derived molecularly heterogeneous GBM TICs (**Fig. 16).** Moreover, LSD1 is enriched in GBM TICs compared to neural normal human progenitor cells, here used as non-tumoral counterpart (**Fig. 16**).

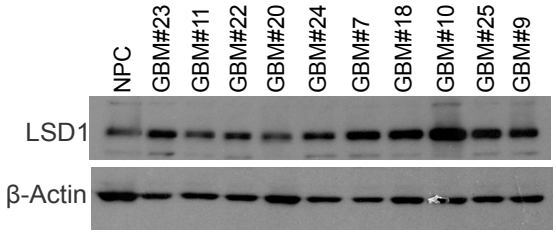

Figure 16. LSD1 protein expression in GBM TICs. LSD1 protein levels by western blot in human GBM TICs isolated from different patients. NPC (human Neural Progenitor Cells) were used as non-tumoral counterpart. β-actin was used as loading control.

5.2 LSD1 is uniformly expressed in GBM TIC heterogeneous population

In vitro GBM TIC culture are obtained by processing fresh human GBM specimen and are grown in a selective serum-free medium. Due to the lack of specific and selective GBM cancer stem cell markers allowing the isolation of a pure stem cell population, the results are floating clusters of cells, known as neurospheres, composed by immature cells, cells at different stages of differentiation, and differentiated cells. To gain insight into LSD1 expression in GBM TIC compartment, we exploited confocal imaging on single cells obtained by neurospheres mechanical dissociation. Despite its variable expression among different patients (**Fig. 16**), LSD1 was uniformly expressed in GBM TIC cultures. Indeed, confocal images show that all cell nuclei from the same GBM patient TIC expressed LSD1 (**Fig. 17**).

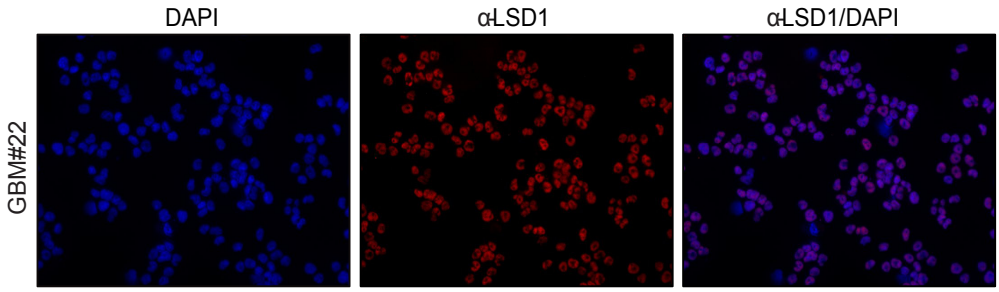

Figure 17. LSD1 staining in GBM TICs. Representative confocal images of GBM#22 TICs stained for LSD1 (red) and DNA (blue)

In line with this, LSD1 was equally expressed by either the putative GBM stem-like cells, defined as CD133[103], or CD15[259] or Itga6[260] positive cells, and by the negative counterparts, all of them composing the GBM TICs *in vitro*. (**Fig. 18**).

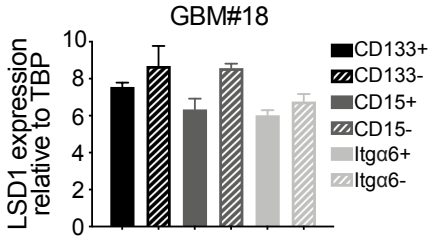

Figure 18. LSD1 correlation with stem cell marker expression. GBM#18 TICs have been FACS sorted on the base of the expression of the indicated markers. LSD1 mRNA levels by qRT-PCR in the putative GBM stem-like cells (CD133-, or CD15- or Itga6- positive cells) and in the negative counterparts. TBP was used to normalize gene expression. Results are the average of 3 technical replicates. Error bars represent mean +/− SD. p-values were calculated by a two-tailed Student's t-test.

LSD1 is therefore uniformly expressed in the GBM TIC compartment, and its specific enrichment in both GBM tissues and primary GBM TICs might help in discriminating between tumor and normal brain cells, leading the groundwork to test LSD1 role as a therapeutic target in GBM.

5.3 LSD1i is able to cross the brain blood barrier and is well tolerated by GBM PDX-bearing mice

We then started to test the efficacy of DDP_38003 (hereafter LSD1i), a novel LSD1 inhibitor already characterized in terms of selectivity, efficacy and tolerability in a murine promyelocytic leukemia model[221,240], as a potential anti GBM therapy.

Of note, poor BBB penetration is one of the major issue responsible of drug failure in GBM therapy. For this reason, we first assessed the ability of LSD1i to penetrate mouse BBB. GBM TICs were orthotopically implanted in the *nucleus caudatus* of CD-1 nude mice. 14 days after implantation, when tumor had already started to form, tumors-bearing mice were treated twice with LSD1i (17mg/kg) and sacrificed 5 hours after the second administration. Through Cellular Thermal Shift Assay (CETSA assay) conducted on brain homogenates by Experimental Therapeutics Program in IFOM, we revealed a clear increase of thermodynamic stability of LSD1 (**Fig. 19A**) but not of vinculin, here used as negative control (**Fig. 19B**) in the treated group compared to the controls, demonstrating the ability of LSD1i to engage LSD1 inside the brain.

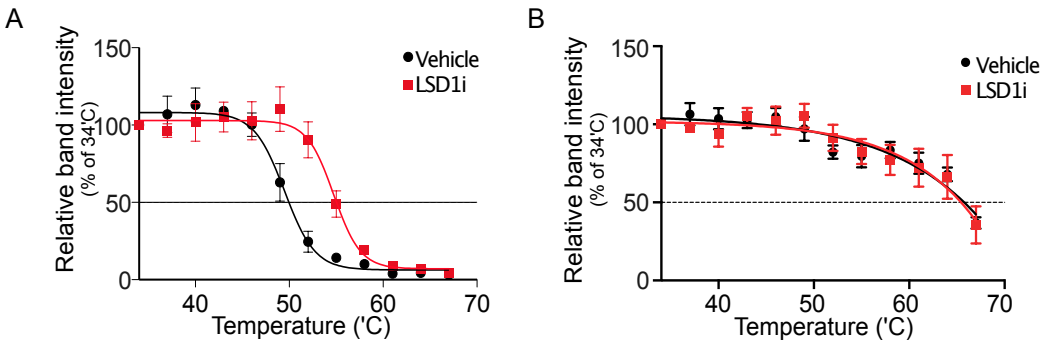

Figure 19. LSD1i ability to cross the brain blood barrier. (A-B) LSD1i ability to bind LSD1 (A) and vinculin (B) within the brain by CETSA assay. GBM#22 TICs have been orthotopically injected in CD1-nude mice. Mice were treated by oral gavage with vehicle or 17mg/kg of LSD1i at day 14 and 17 after injection; 5 hours after the second treatment mice were sacrificed. The reported data were obtained from 3 animals in each experimental group (vehicle or treatment) and are presented as mean with error bars representing the standard error of the mean (S.E.M.).

Importantly, LSD1i treatment was well tolerated *in vivo.* Indeed, when it was administered 2 days per week for two weeks, no modification of grooming behavior (data not shown), no weight loss (**Fig. 20A**) and no alteration of hematological parameters (**Fig. 20B**) were observed.

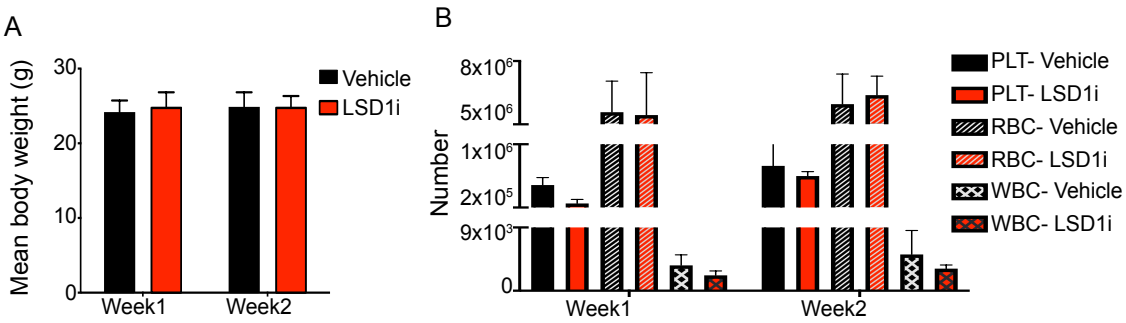

Figure 20. LSD1 tolerability *in vivo*. (A and B) Mean body weight (A) and hematological parameters (B) (PLT: Platelets, RBC: Red Blood Cells, WBC: White Blood Cells) of LSD1i- or vehicle-treated mice. Animals were weighted and then treated by oral gavage with vehicle or 17mg/kg of LSD1i starting from 14 days after GBM#22 TIC injection. LSD1i tolerability was assessed 1 and 2 weeks after LSD1i treatment start.

5.4 LSD1 inhibition prolongs survival of orthotopic GBM PDXs

As such, we administered LSD1i to GBM PDXs to validated LSD1 as a potential target in GBM. GBM#22 were orthotopically implanted inside the *nucleus caudatus* of CD-1 nude mice. 14 days after implantation, tumors-bearing mice were treated with LSD1i (17 mg/kg) or vehicle, 2 days per week for 4 weeks. Kaplan-Meier survival curves demonstrated that LSD1i significantly extended mice survival (**Fig. 21A**). To gain insights into the effects of LSD1 pharmacological inhibition, we killed subgroups of mice at early time points. Hematoxylin and eosin (H&E) staining revealed that one week after LSD1i administration, the tumor was appreciable in 50% of control mice and 25% of treated mice. The percentage of control mice developing a tumor grew rapidly to 87,5% at week 2, and 100% at week 3. Strikingly, the percentage of LSD1i-treated mice developing the tumor remained stable (20%) by week2, week 3 and week 4, indicating that tumor initiation and growth was inhibited during LSD1i treatment **(Fig. 21B).**

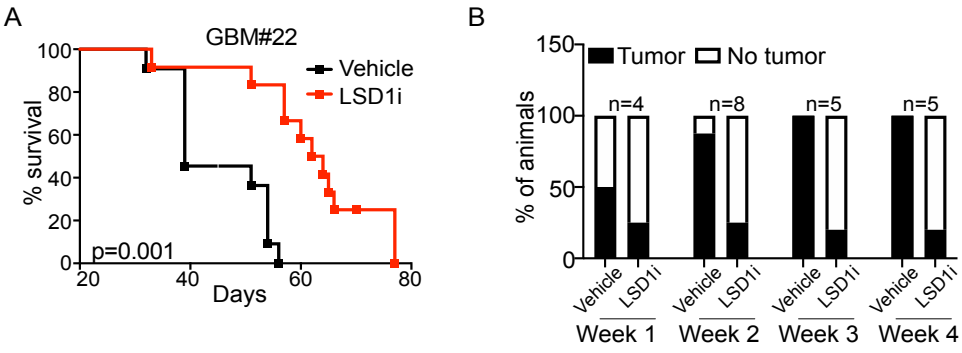

Figure 21. GBM TIC tumorigenic potential upon LSD1 inhibition. (A) Survival curve (p=0.001) of LSD1i- or vehicle-treated GBM#22 PDXs. 11 Vehicle-treated mice and 11 LSD1i treated mice have been included in the survival analysis. Results of two independent experiments have been pooled. (B) Tumor incidence at 1, 2,

3 and 4 weeks after beginning of LSD1i treatment. 22 Vehicle-treated mice and 22 LSD1i treated mice have been included in these analyses Results of two independent experiments have been pooled. LSD1i treatment started 2 weeks after GBM#22 TICs orthotopic injection. LSD1i was administered at 17mg/Kg/o.s. twice a week for 4 consecutive weeks

Mice were sacrificed at the appearance of neurological signs. At the time of death, when the treatment was already finished, LSD1i-treated tumors were histologically similar to their controls. Indeed, cytoarchitecture of vehicle and treated tumor was indistinguishable. Despite LSD1 well known role in stemness maintenance, no differential pattern of expression of stem (Nestin, Sox2) and differentiation (GFAP) markers have been detected (**Fig. 22**).

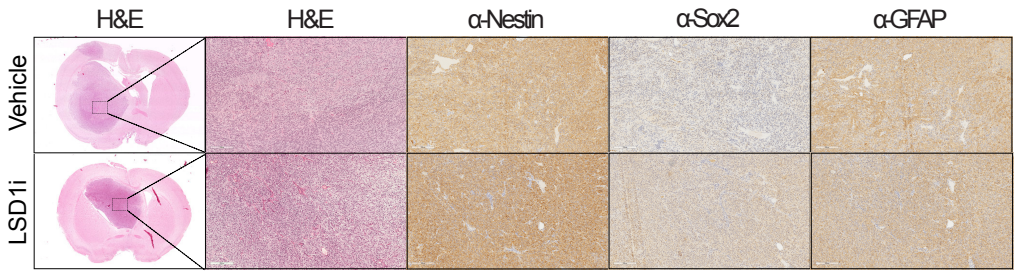

Figure 22. Histological characterization of GBM PDXs upon LSD1i treatment. H&E staining and IHC for the indicated markers in LSD1i- or vehicle-treated GBM#22 PDXs. Data from a representative mouse for each group are shown.

We substantiated the previous results by exploiting luciferase-positive TICs derived from a different GBM patient. CD1-nude mice were transplanted with Luc^{+} GBM#18 TICs and treated as previously described. Survival curves confirmed LSD1i therapeutic potential in term of prolonged survival (**Fig. 23A**). Tumor growth, monitored by bioluminescence images, was significantly delayed in LSD1i-treated mice (**Fig. 23B-C**).

Overall, these results highlight the therapeutic efficacy of LSD1i for GBM treatment: by effectively binding LSD1 inside the brain, the compound affects GBM growth in molecularly different GBM PDXs.

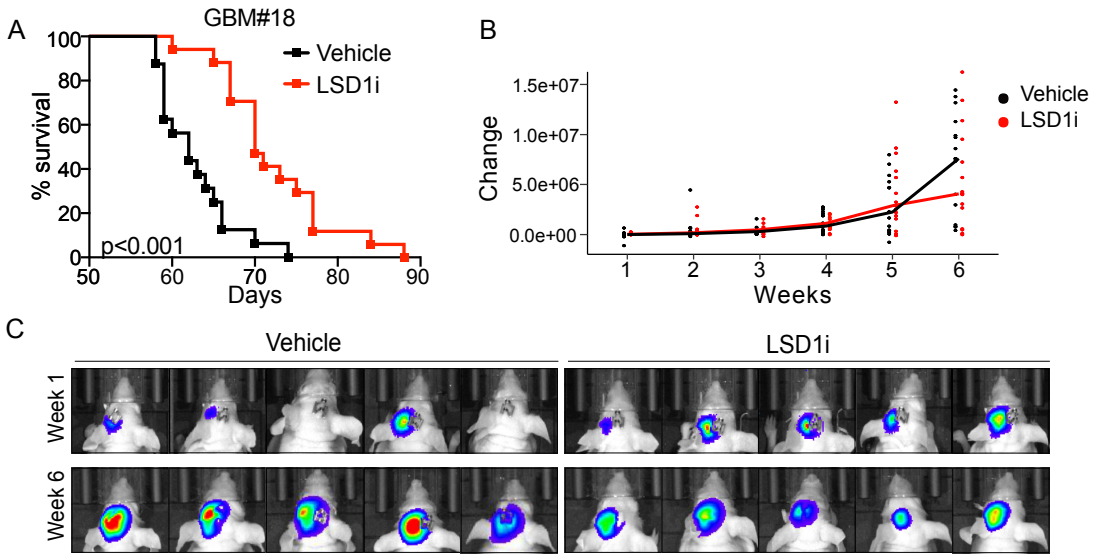

Figure 23. LSD1 inhibition prolong survival of GBM#18 PDXs. (A-C) Survival curve ($p<0.001$) (B), luminescent intensity quantification (B) and representative bioluminescence images (C) of LSD1i- or vehicle-treated mice transplanted with the luciferase-positive GBM#18 TICs. Luciferase signals were measured from week 1 to week 6 after LSD1i treatment start. LSD1i treatment started 2 weeks after Luc^{+}GBM#18 TICs orthotopic injection. LSD1i was administered at 17mg/Kg/o.s. twice a week for 4 consecutive weeks. 16 Vehicle-treated mice and 18 LSD1i treated mice have been included in these analyses. Results of two independent experiments have been pooled.

5.5 LSD1 pharmacological inhibition reduces GBM TIC growth and self-renewal

5.5.1 GBM TICs are sensitive to LSD1i

As human GBMs are maintained by a TIC subpopulation endowed with stem cell-related features[125], and LSD1 has a role in either adult[194], embryonic[261] and pluripotent[262] stem cells, we decided to exploit *in vitro* assays sought to figure out the effect of LSD1i on GBM TICs properties.

First, we sought to assess if LSD1i effectively affects LSD1 demethylase activity in GBM TICs. To this aim, in collaboration with Tiziana Bonaldi's group, we employed mass spectrometry to compare the levels of H3K4me2 and H3K4me1, the canonical LSD1 targets, in LSD1i- or vehicle-treated cells. Of note, after 24 hours of treatment, LSD1i-treated cells exhibited a mild but statistically significant increase in the levels of H3K4me2 (**Fig. 24A**) demonstrating that LSD1i effectively reduce LSD1 demethylase activity in multiple patient derived GBM TICs. H3K4me1 levels were instead unaffected (**Fig. 24B**), suggesting that, in the GBM TIC context, LSD1i effects on the global H3K4 mono-methylation are weak, and can be better addressed with a locus-specific approach (**see Fig. 72**).

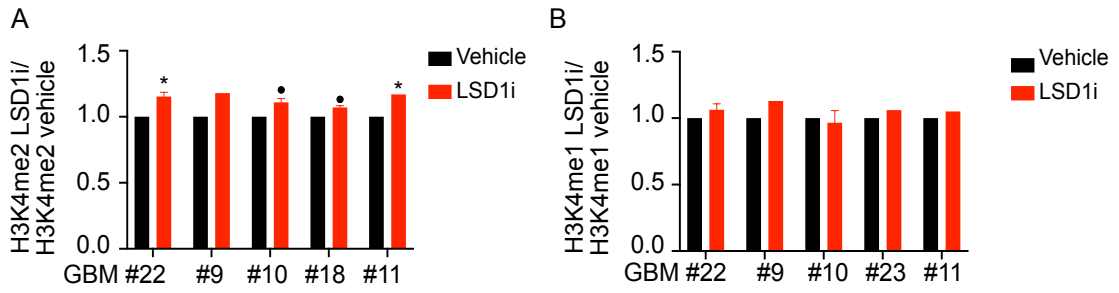

Figure 24. GBM TICs are sensitive to LSD1i. (A) H3K4me2 and (B) H3K4me1 levels by MS in LSD1i- or vehicle-treated GBM TICs from different patients. LSD1i was administered 2.5uM for 24 hours. H3K4me2 levels were normalized over matching vehicle-treated controls. All quantitative data are the average of 2/3 technical replicates. Error bars represent mean +/− SE. Matching LSD1i- and vehicle-treated cells were compared by paired Student's t-test. • indicates p<0.1. * indicates p<0.05.

Then, we calculated LSD1i EC50 in our model system. By treating GBM TICs once with increasing concentrations of LSD1i, we observed a clear dose-dependent reduction of cell viability. The EC50 values revealed that the tested GBM TICs were all sensitive to LSD1i (EC5O GBM#22 TICs: 2.483μM, EC50 GBM#7 TICs: 2.588 μM, EC50 GBM#18 TICs: 7.9 μM) (**Fig. 25**).

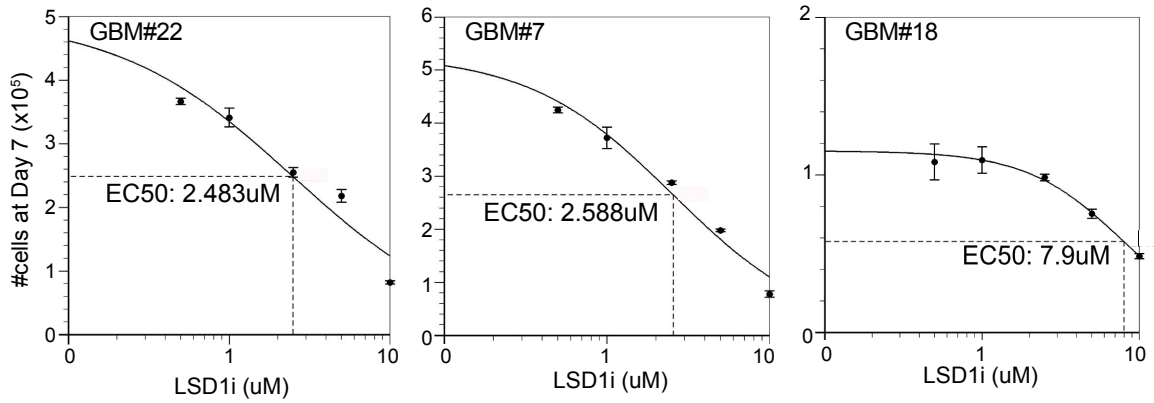

Figure 25. LSD1i EC50 calculation. The dose-dependent effects of LSD1i on GBM TICs from three representative patients (GBM#22, GBM#7 and GBM#18) treated once with vehicle or increasing concentrations of LSD1i (0.5μM, 1μM, 2.5μM, 5μM and 10μM). Viable cells have been manually counted after 7 days. Results are the average of 3 technical replicates. Error bars represent mean +/− SD.

5.5.1 LSD1i impairs GBM TIC growth

As a confirmation, we measured the *in vitro* efficacy of LSD1i on cell growth rate: GBM TICs were treated with a single administration of LSD1i or vehicle and cell growth has been evaluated by manual counting for a period up to 7 days. Consistently with GBM inter-tumoral heterogeneity, the timing and the extent of the effect of LSD1i depended on the GBM TIC sample. GBM#22 TICs showed a reduction of 35% at day 5 and of 42% at day 7. GBM#7 and GBM#18 TICs responded later, with no effect at day 5, but with a reduction of, respectively, 45% and 30% at day 7. However, all the samples analyzed were sensible to LSD1i in a dose range in which this compound is therapeutic and specific[240] (**Fig. 26**).

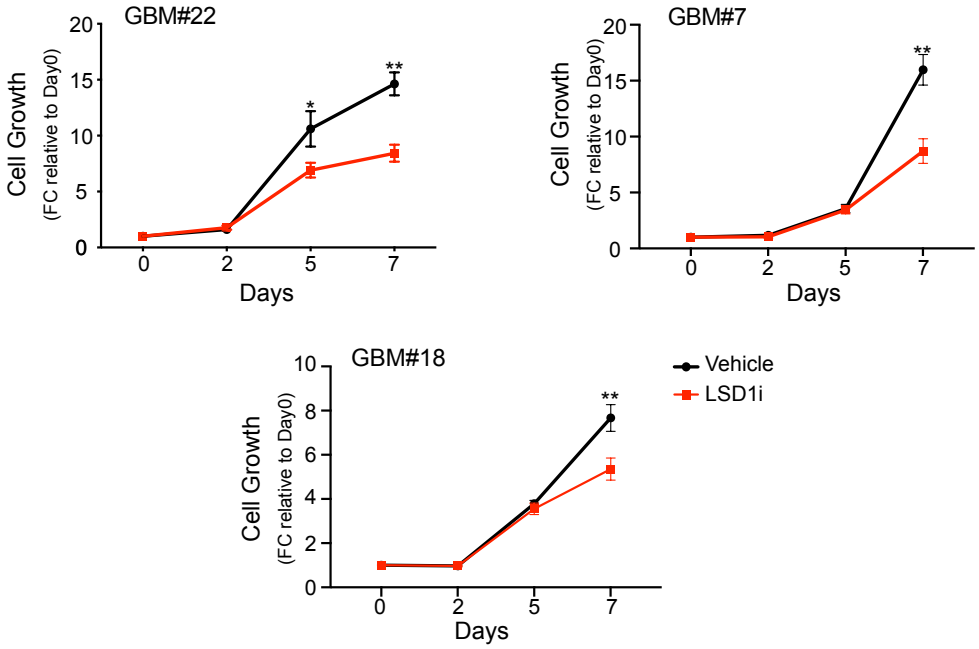

Figure 26. GBM TIC growth upon LSD1 inhibition. Growth of the indicated LSD1i- or vehicle-treated GBM TICs. GBM#22 and GBM#7 TICs have been treated with LSD1i 2.5uM. GBM#18 TICs have been treated with LSD1i 5uM. Viable cells have been manually counted at the indicated days. Results are the average of 3 technical replicates. Error bars represent mean +/− SD. p-values were calculated by a two-tailed Student's t-test. * indicates p<0.05. ** indicates p<0.01. *** indicates p<0.001.

To assess if the reduction of cell growth was due to increased cell death, we measured apoptosis of GBM TICs upon LSD1i treatment. 7 days after drug administration, the activity of caspase 3/7, a well-known read-out of apoptosis, was 30% higher in all the LSD1i treated cells compared to controls, thus revealing that LSD1i treatment affects cell survival (**Fig. 27**).

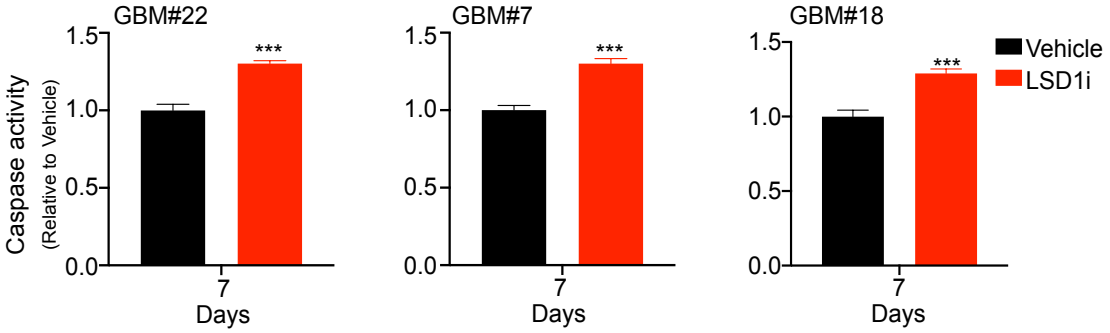

Figure 27. GBM TIC apoptosis upon LSD1 inhibition. Caspase 3/7 of the indicated LSD1i- or vehicle-treated GBM TICs. GBM#22 and GBM#7 TICs have been treated with LSD1i 2.5uM. GBM#18 TICs have been treated with LSD1i 5uM. Results are the average of 3 technical replicates. Error bars represent mean +/− SD. p-values were calculated by a two-tailed Student's t-test. * indicates p<0.05. ** indicates p<0.01. *** indicates p<0.001.

5.5.1 LSD1i impairs GBM TIC self-renewal

GBM TICs are *in vitro* functionally defined by the ability to self-renew, for which sphere formation ability on clonogenic assays represents a surrogate. As such, we evaluated the effect of the inhibitor on sphere formation. Interestingly, we found a significant reduction in sphere number in LSD1i-treated GBM TICs compared to controls (**Fig. 28**). Albeit the drop of sphere formation efficiency was not quantifiable in all the patient-derived GBM TICs at the first plating, it significantly augmented at the second plating, indicating that LSD1 pharmacological inhibition curtailed the subset of cells able to self-renew (GBM#22 TIC: -28% first plating, -78% second plating. GBM#7 TICs: -32% second plating. GBM#18 TICs -41% first plating, -42% second plating) (**Fig. 28**).

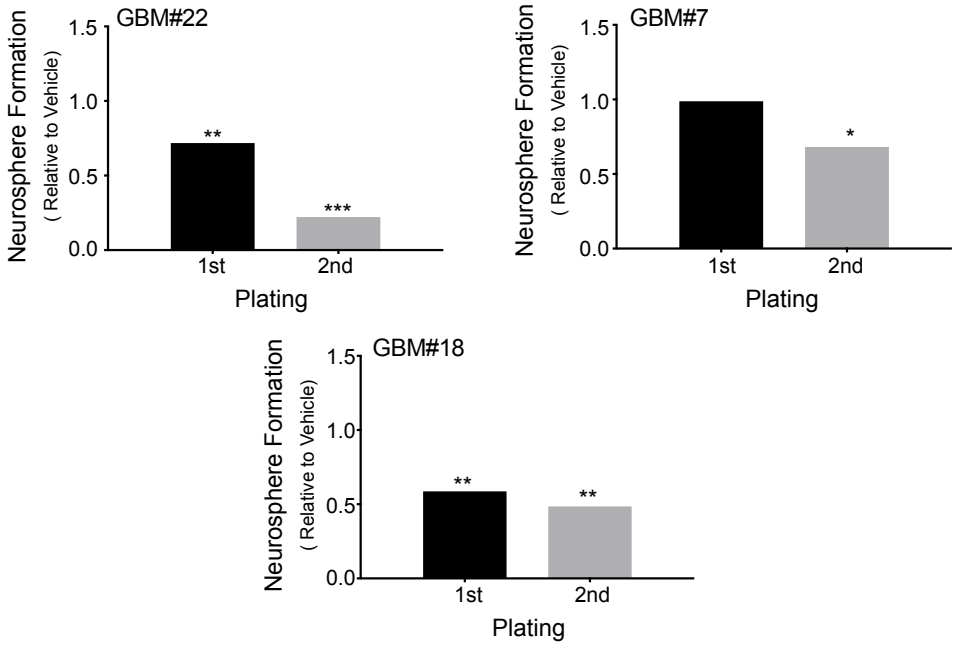

Figure 28. GBM TIC self-renewal upon LSD1 inhibition. Neurosphere formation efficency of GBM#22, GBM#7 and GBM#18 TICs treated with LSD1i 2.5uM or vehicle. Sphere formation ability was evaluated after 2 serial platings. Results are the average of 3 technical replicates. Error bars represent mean +/− SD. p-values were calculated by a two-tailed Student's t-test. * indicates p<0.05. ** indicates p<0.01. *** indicates p<0.001.

Notably, despite LSD1 involvement in the regulation of the balance between stem cell like state and differentiation[193], LSD1 pharmacological inhibition did not induce nor modified GBM TIC differentiation: no differences in the expression of putative stem cell-related (Nestin) and differentiation markers (GFAP, β-Tubulin) were measured (**Fig. 29**).

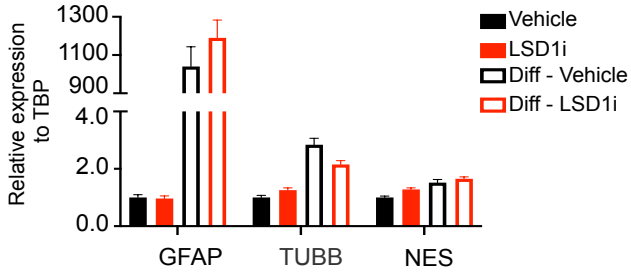

Figure 29. Stem and differentiated markers expression upon LSD1i treatment. mRNA levels of the indicated genes by qRT-PCR in GBM#22 TICs grown as neurosphere or upon differentiation (Diff), treated or not with LSD1i 2.5uM. TBP was used to normalize gene expression. Results are the average of 3 technical replicates. Error bars represent mean +/− SD. p-values were calculated by a two-tailed Student's t-test. * indicates p<0.05. ** indicates p<0.01. *** indicates p<0.001.

Overall, these results indicate that LSD1i successfully inhibits LSD1 enzymatic activity in GBM TICs and is effective in reducing either cell viability and stemness *in vitro*, independently of GBM TIC molecular profile.

5.6 LSD1 genetic targeting mirrors LSD1 pharmacological inhibition in GBM TICs

To validate the specificity of the phenotype obtained by LSD1 pharmacological inhibition, we decided to genetically abrogate LSD1 expression in GBM TICs. Two different LSD1-KO clones derived from the same GBM#22 patient (hereby LSD1-KO#1 and LSD1-KO#2) have been generated by the Genome Editing Unit (Cogentech) through CRISPR/Cas9 technology (**Fig. 30A**). As a complementary approach, we exploited lentiviral vectors to silenced LSD1 in different patient-derived GBM TIC samples using a LSD1-specific shRNA (sh71). A non-targeting shRNA (shNT) was used as a control (**Fig. 30B**).

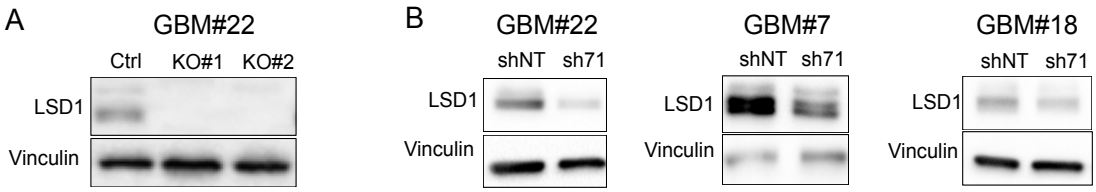

Figure 30. Western blot evaluation of LSD1 KO or silencing efficiency. (A) LSD1 protein expression levels of LSD1-KO GBM TICs (KO#1 and KO#2) compared to control GBM#22 TICs are shown (B) LSD1 protein expression levels of LSD1 silenced (sh71) and control (shNT) GBM TICs. Data relative to GBM#22, GBM#7 and GBM#18 TICs are shown. Vinculin was used as loading control.

5.6.1 LSD1 KO hampers GBM TIC growth and self-renewal

First, we evaluated the effects of LSD1-KO on GBM TIC biological properties by exploiting *in vitro* assays.

Cell growth has been evaluated for a period of up to 8 days of culture, during which both LSD1 KO clones halved GBM TIC growth rate. (**Fig. 31**).

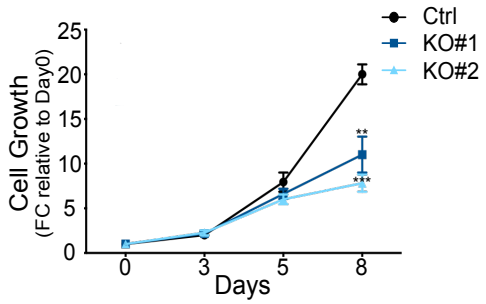

Figure 31. GBM TIC cell growth upon LSD1 genetic abrogation. Growth of LSD1-KO GBM TICs (KO#1 and KO#2) compared to their control. Viable cells have been manually counted at the indicated days. Results are the average of 3 technical replicates. Error bars represent mean +/− SD. p-values were calculated by a two-tailed Student's t-test. * indicates $p<0.05$. ** indicates $p<0.01$. *** indicates $p<0.001$.

In clonogenic assays, LSD1 KO dramatically diminished GBM TIC *in vitro* self-renewal potential. Similarly to what observed upon LSD1i treatment, the effect, already clearly noticeable at first plating (LSD1-KO#1 -64%, LSD1-KO#2 -69%), became even more striking after the second plating (LSD1-KO#1 -91%, LSD1-KO#2 -90%), implying a specific effect of LSD1 abrogation against the stem cell-like cell compartment (**Fig. 32**).

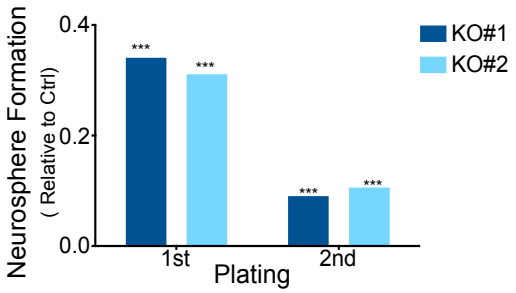

Figure 32. GBM TIC self-renewal upon LSD1 genetic abrogation. Neurosphere formation efficency of the indicated LSD1-KO (KO#1 and KO#2) and control GBM#22 TICs. Sphere formation ability was evaluated after 2 serial platings. Results are the average of 3 technical replicates. Error bars represent mean +/− SD. p-values were calculated by a two-tailed Student's t-test. * indicates $p<0.05$. ** indicates $p<0.01$. *** indicates $p<0.001$.

5.6.2 LSD1-KO impairs GBM TIC tumorigenic potential

Importantly, LSD1 deletion compromised GBM TIC tumorigenic potential. The life-span of mice orthotopically injected with LSD1-KO#1 cells significantly increased relative to controls. Indeed, by day 50 after tumor induction all control mice have been sacrificed at the appearance of neurological signs, while mice transplanted with LSD1-KO#1 cells survived longer (**Fig. 33**). LSD1-KO#2 cells exhibited an even more striking phenotype, having completely lost their tumorigenicity (**Fig. 33**). To shed light on the anti-tumorigenic effect of LSD1 abrogation, we performed an *in vivo* extreme limiting dilution assay, implanting a progressively smaller number of LSD1-KO#1 GBM TICs or control GBM TICs in the *nucleus caudatus* of immunocompromised mice. LSD1 deletion significantly reduced the stem cell content (estimated stem cell frequency: Crtl [1\1073]; LSD1-KO#1 [1\33743]). This result is coherent with the self-renewal drop observed *in vitro* and suggests that LSD1 loss can affect GBM TIC tumorigenic properties by impairing their stem cell like traits.

However, at the time of death, LSD1-KO#1 GBM PDXs were similar to their controls in term of cytoarchitecture and expression of stem cell and differentiation markers (**Fig. 34**), mirroring the effects of LSD1 pharmacological inhibition on GBM TICs (**Fig. 29**) and GBM derived PDXs (**Fig. 22**)

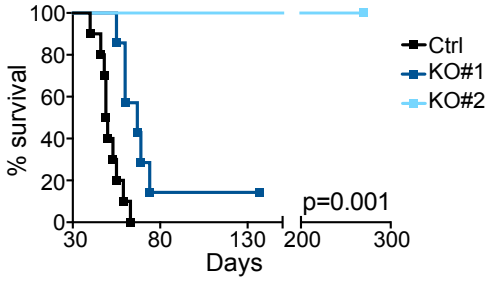

Figure 33. GBM TIC tumorigenic potential upon LSD1 genetic abrogation. Survival curves (p=0.001) of mice transplanted with the indicated LSD1-KO (KO#1 and KO#2) and control GBM#22. 10 mice injected with control cells, 7 mice injected with LSD1-KO#1 TICs and 8 mice injected with LSD1-KO#2 TICs have been included in this analysis. Results of two independent experiment have been pooled.

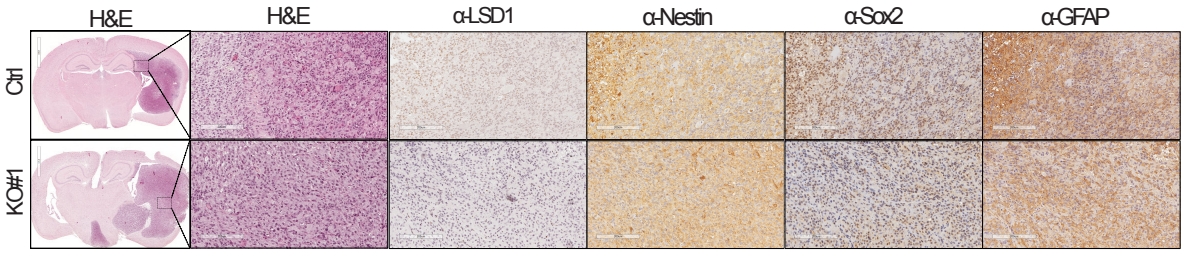

Figure 34. Histological characterization of GBM PDX upon LSD1 genetic abrogation. Hematoxylin and eosin (H&E) staining and IHC for the indicated markers in LSD1-KO#1 or control GBM#22 PDXs. Data from a representative mouse for each group are shown.

5.6.3 LSD1 silencing hampers GBM TIC growth and self-renewal

These phenotypes were recapitulated by exploiting LSD1-silenced GBM TICs. LSD1-silenced cells (sh71) showed a reduced *in vitro* growth compared to their controls (shNT). As observed upon LSD1i treatment, the timing and the extent of this effect was patient-dependent (GBM#22 TICs -50% at day 5, -65% at day 7; GBM#7 TICs: -75% at day 5, -68% at day 7; GBM#18 TICs: -42% at day 2, -46% at day 5) (**Fig. 35**).

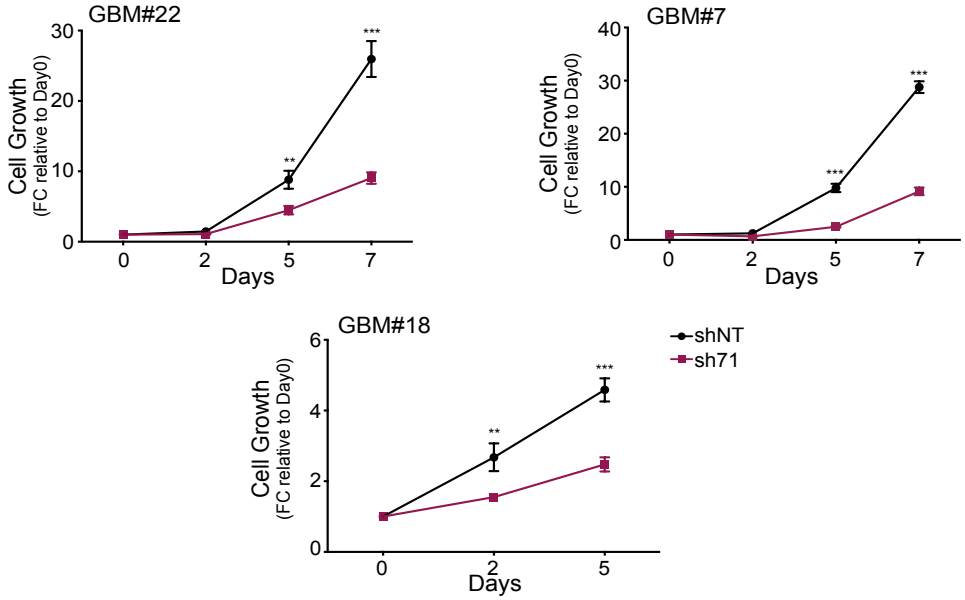

Figure 35. GBM TIC cell growth upon LSD1 silencing. Growth of the LSD1-silenced (sh71) GBM TICs from different patients (GBM#22, GBM#7 and GBM#18) compared to their non targeting control (shNT). Viable cells have been manually counted after 7 days. Results are the average of 3 technical replicates. Error bars represent mean +/− SD. p-values were calculated by a two-tailed Student's t-test. * indicates $p<0.05$. ** indicates $p<0.01$. *** indicates $p<0.001$.

The reduction of LSD1 silenced cell growth was at least in part due to their increased cell death, measured as an increase in caspase 3/7 activity of nearly 44% in both GBM#22 and GBM#7 TICs. (**Fig. 36**).

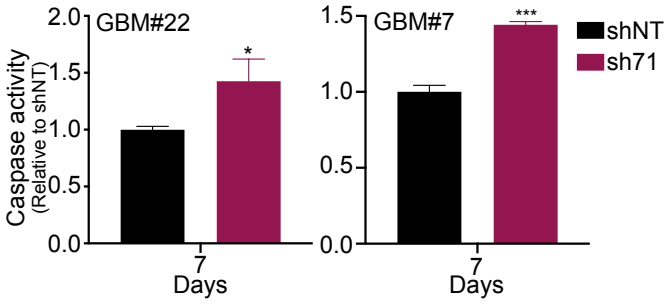

Figure 36. GBM TIC apoptosis apon LSD1 silencing. Caspase 3/7 of the indicated LSD1i silenced (sh71) or control (shNT) GBM TICs. Results are the average of 3 technical replicates. Error bars represent mean +/− SD.

p-values were calculated by a two-tailed Student's t-test. * indicates p<0.05. ** indicates p<0.01. *** indicates p<0.001.

Further, LSD1 silencing significantly reduced GBM TIC self-renewal ability (GBM#22 TICs -88%, GBM#18 -91%, GBM#10 -95%) (**Fig. 37A**) and stem cell content (**Fig. 37B**), measured by either sphere formation and limiting dilution *in vitro* assays, respectively.

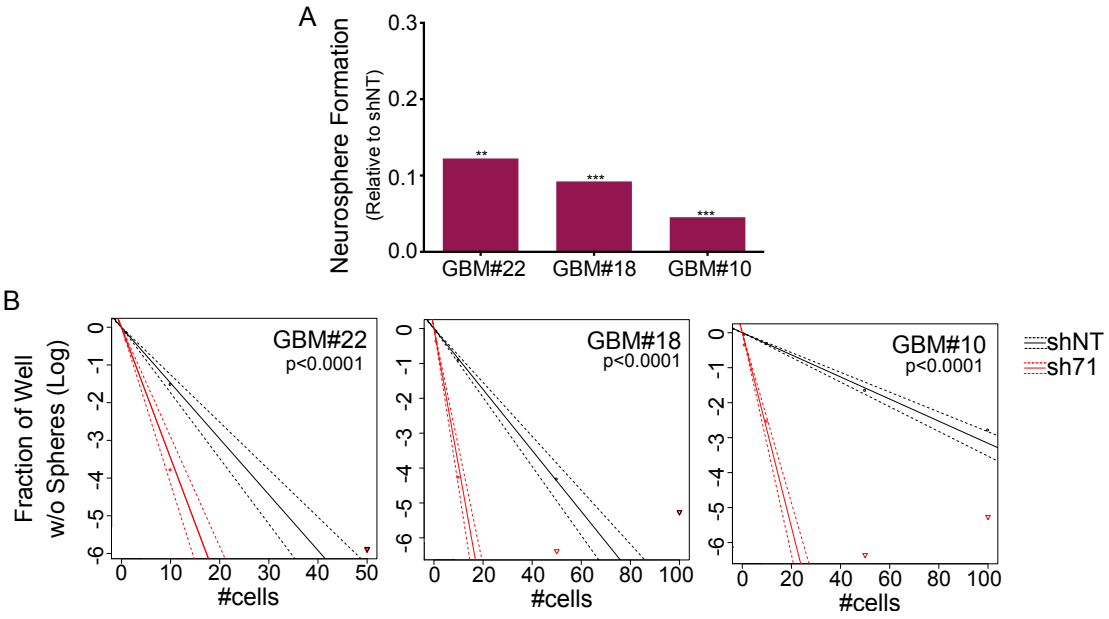

Figure 37. GBM TIC self-renewal upon LSD1 silencing. (A) Neurosphere formation efficency and (B) *in vitro* limiting dilution assays of the indicated samples upon LSD1 silencing. Results are the average of three technical replicates.

5.6.4 LSD1 silencing impairs GBM TIC tumorigenic potential

In vivo, the injection of LSD1 silenced GBM TICs significantly prolonged the life-span of tumor-bearing mice relative to controls (**Fig. 38A**) and lowered the stem cell frequency as measured by limiting dilution cell injection (**Fig. 38B**). To study the impact of LSD1 knock-down on GBM initiation, we killed the mice at an early time point before the onset of neurological signs (i.e. four weeks after GBM LSD1-KO#1 TICs injection): 66% of control mice developed large tumors while LSD1-silenced tumors were still undetectable by H&E staining at that timing (shNT: 2/3 mice; sh71: 0/3 mice). Thus, LSD1-silenced tumors started to appear later after intracranial injection, suggesting that LSD1 loss retarded tumor growth, as already observed upon LSD1 pharmacological inhibition.

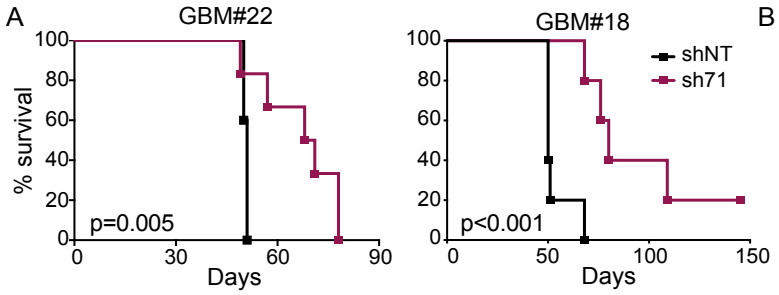

Estimated stem cell frequency		
sample	shNT	sh71
GBM#22	1/77	1/2157
GBM#18	1/507	1/13066

Figure 38. GBM TIC tumorigenic potential upon LSD1 silencing (A) Survival curves of mice injected with LSD1-silenced and control TICs. Results from two representative samples (GBM#22: p=0.005, left; GBM#18: p<0.001, right) are shown. 5 mice injected with shNT-GBM#22 TICs and 6 mice injected with sh71-GBM#22 TICs have been included in the survival analysis. 5 mice injected with shNT-GBM#18 TICs and 4 mice injected with sh71-GBM#18 TICs have been included in the survival analysis. (B) The *in vivo* estimated stem cell frequency for the indicated LSD1-silenced and control cells. 3 mice for each cell dose ($10^{\wedge 5}$, $10^{\wedge 4}$, $10^{\wedge 3}$ and $10^{\wedge 2}$ GBM TICs) have been included in this analysis.

At the time of death, LSD1-silenced tumors displayed histological and cytoarchitectural features similar to that of controls (data not shown), while expressing LSD1 mRNA (**Fig. 39A**) and protein levels (**Fig. 39B**) at level comparable to controls. This might suggest that LSD1-silenced cells have been counter-selected to allow tumor growth.

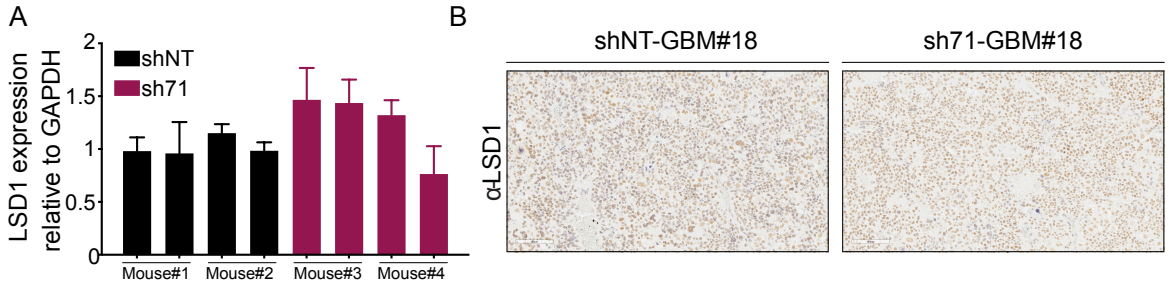

Figure 39. LSD1 expression in GBM PDX at the experimental end-point. (A) LSD1 expression levels by qRT-PCR in LSD1-silenced (sh71) and control (shNT) GBM#22 PDXs at the experiment end-point. Data relative to two microdissected sections/PDX are shown. Data are normalized on mean LSD1 expression levels in shNT group. GAPDH was used to normalize gene expression. Results are the average of 3 technical replicates. Error bars represent mean +/− SD. p-values were calculated by a two-tailed Student's t-test. (B) IHC analysis of LSD1 levels in sh71-GBM#18 and shNT-GBM#18 PDXs collected at the experiment end-point. Data from a representative mouse for each group are shown.

Overall, these results demonstrate that LSD1 expression is critical to tumor growth, and its genetic abrogation strongly reduces viability, stemness and tumor forming potential in multiple patient-derived GBM TICs, thus resembling the phenotype induced by LSD1 pharmacological inhibition.

5.7 LSD1 genetic targeting affects ATF4-mediated ISR in GBM TICs

5.7.1 LSD1 regulates genes involved in response to unfolded proteins and amino acid deprivation

To dissect the molecular mechanisms through which LSD1 sustains GBM TIC tumorigenic properties, we exploited RNA-sequencing to perform a global transcriptomic profiling of LSD1 silenced and control GBM#22 TICs.

A gene set enrichment analysis (GSEA) revealed that LSD1 expression is negatively associated with that of genes involved in response to unfolded/misfolded proteins and in amino acid metabolism (**Fig. 40**).

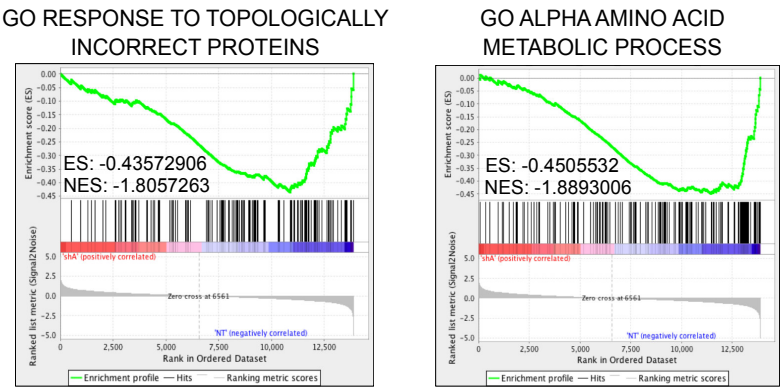

Figure 40. Gene set enrichment analysis of GBM TIC upon LSD1 silencing. GSEA enrichment score curves of LSD1-silenced (sh71) and control (shNT) GBM#22 TICs. (ES: enrichment score. NES: normalized enrichment score).

The differential expression analysis yielded a list of 48 differentially expressed genes (DEGs) (|Log2FC|>1.2, FDR≤0.05) (**Fig. 41**). Surprisingly, almost all of them were down-regulated upon LSD1 silencing, despite LSD1 canonically acts as a transcriptional repressor.

To unravel the biological process in which they are involved, we performed a Gene Ontology (GO) analysis, that confirmed their participation in the response to unfolded/misfolded proteins and in amino-acid metabolism regulation. Indeed, these DEGs are entangled in PERK-mediated unfolded protein response (UPR) and in the

apoptotic pathway in response to endoplasmatic reticulum (ER) stress, as well as in the response to starvation and in t-RNA aminoacylation for protein synthesis (**Fig. 42**).

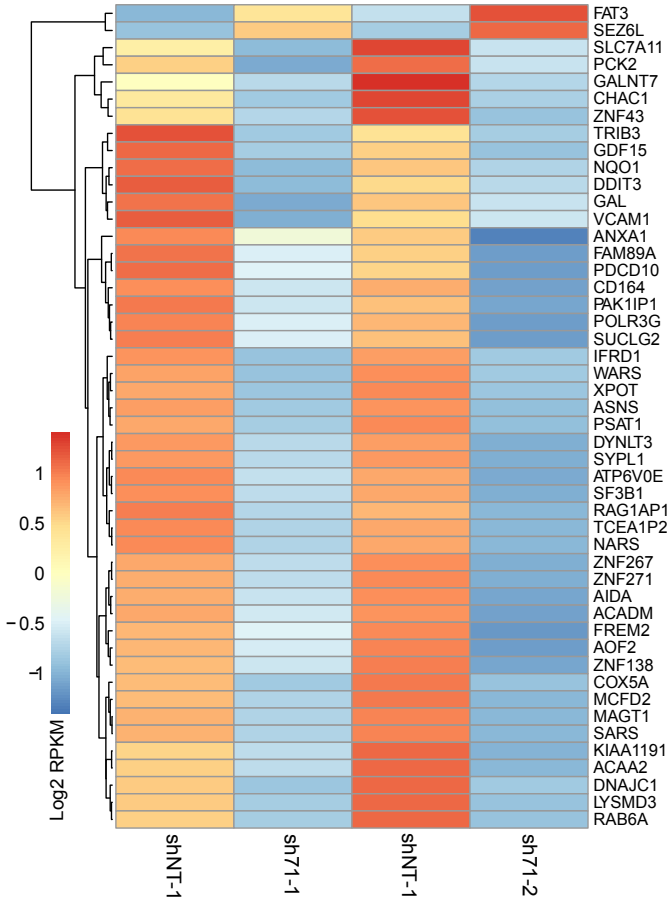

Figure 41. Differential gene expression in GBM TIC upon LSD1 silencing. Heatmap showing differentially expressed genes in LSD1-silenced (sh71) and control (shNT) GBM#22 TICs, as assessed by RNA-seq. Data from two biological replicates are shown.

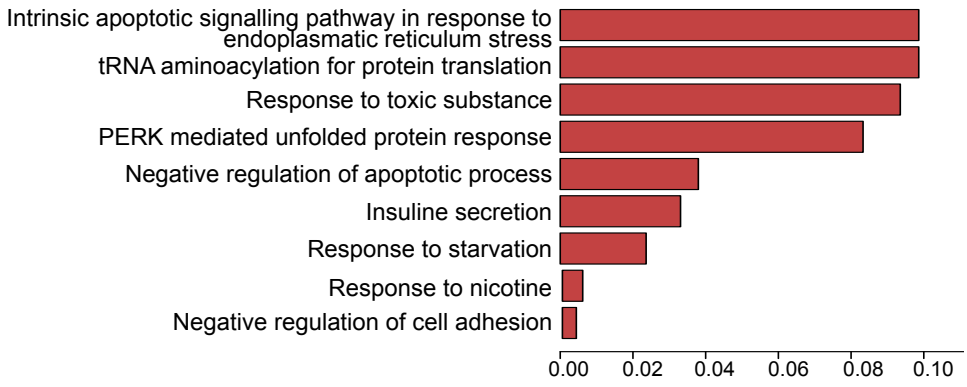

Figure 42. LSD1-dependent biological processes. Gene Ontology analysis illustrating the biological processes potentially regulated by LSD1. The analysis is based on the DEGs showed in Fig. 40.

5.7.2 LSD1 regulates ATF4 transcription

Tumor progression inevitably entails an exacerbation of intrinsic and extrinsic cellular stresses. The tumoral microenvironment is often subjected to lack of nutrients, including amino acids and the enhanced protein synthesis, necessary to sustain cellular proliferation, likely exceeds the protein folding capacity resulting in proteostasis perturbation. The unfolded protein response (UPR) and the cellular response to amino acid deprivation (AAR) converge in the so called Integrated Stress Response (ISR), whose aim is to promote stress adaptation and survival[263]. ISR activation is mediated by the catalytic activity of specific serine/threonine kinases, such as PERK[264] and GCN2[265,266], respectively activated by the accumulation of misfolded/unfolded proteins and by the lack of charge tRNA during amino acid deprivation. PERK and GCN2 phosphorylates the **α**-subunit of the eukaryotic translation initiation factor 2 (eIF2**α**), thereby inhibiting its function and abolishing general translation. Concurrently, eIF2**α** phosphorylation increases the translation of the activating transcription factor 4 (ATF4) mRNA, thus considered the hub of the ISR, which promotes the transcription of its effector genes with the final aim to solve the stress and restore cell homeostasis[267].

The results of IPA upstream regulators analysis revealed that ATF4 was one of the upstream regulators predicted as significantly inhibited upon LSD1 silencing (**Fig. 43**). Accordingly, the ER stress response to Tunicamycin was predicted to be inhibited as well (**Fig. 43**), while the human homolog of Drosophila tribbles (TRIB3)-dependent response was activated in accordance with the increased cell death measured upon LSD1 targeting (**Fig. 43**). Notably, TRIB3 is known to be involved in the control of cell death[268] and in the regulation of the ISR by a negative feed-back mechanism[269].

Upstream Regulator	Predicted Activation State	Ativation z-score	p-value of overlap	Target molecules in dataset
GNE	*Activated*	2,000	1,28E-09	ASNS,CHAC1,DDIT3,TRIB3
miR-124-3p	*Activated*	2,987	5,70E-09	ACAA2,ATP6V0E1,CD164,DNAJC1,MAGT1,POLR3G,SLC50A1,SUCLG2,SYPL1
miR-30c-5p	*Activated*	2,000	1,80E-04	GALNT7,IFRD1,SLC7A11,SYPL1
TRIB3	*Activated*	2,401	5,63E-11	ASNS,DDIT3,GDF15,PCK2,PSAT1,TRIB3
tosedostat	*Inhibited*	-2,800	5,53E-15	ASNS,CHAC1,DDIT3,PSAT1,SARS,SLC7A11,TRIB3,WARS
HIF1A	*Inhibited*	-2,186	4,27E-03	ASNS,CD164,HIST1H2AC,VCAM1,ZNF267
UCP1	*Inhibited*	-2,596	1,83E-07	ASNS,DDIT3,GDF15,PCK2,PSAT1,TRIB3,XPOT
STK11	*Inhibited*	-2,000	5,49E-03	ATP6V0E1,COX5A,PCK2,PSAT1
ATF4	*Inhibited*	-3,234	5,15E-15	ASNS,CHAC1,DDIT3,GDF15,NARS,PCK2,PSAT1,SARS,SLC7A11,TRIB3,WARS,XPOT
EIF2AK4	*Inhibited*	-2,194	1,39E-08	ASNS,CHAC1,DDIT3,PCK2,PSAT1
tunicamycin	*Inhibited*	-2,230	1,82E-09	ASNS,CHAC1,DDIT3,IFRD1,NARS,PCK2,SLC7A11,VCAM1,WARS

Figure 43. Upstream regulators of LSD1 target genes. Ingenuity Pathway Analysis (IPA) revealing upstream regulator prediction based on the list of LSD1-regulated genes showed in (Fig. 40).

These *in silico* data prompted us to hypothesize that LSD1 can mediate the activation of the ISR through the regulation of ATF4. Thus, we decided to assess if LSD1 targeting regulates ATF4 expression.

A significant reduction of ATF4 transcript levels was measured in either LSD1-silenced (**Fig. 44A**) and LSD1-KO GBM TICs (**Fig. 44B**). Strikingly, this downregulation was measured in TICs isolated from different GBM patients (**Fig. 44A**).

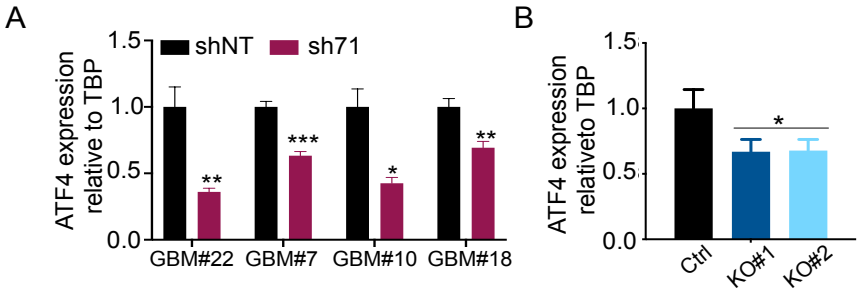

Figure 44. ATF4 mRNA levels upon LSD1 genetic targeting. (A-B) ATF4 expression levels by qRT-PCR upon LSD1 silencing (sh71) in GBM TICs from different patients (GBM#22, GBM#7, GBM#10 and GBM#18) (A) and LSD1-KO (KO#1 and KO#2) and control GBM#22 TICs (B). TBP was used to normalize gene expression. Results are the average of 3 technical replicates. Error bars represent mean +/− SD. p-values were calculated by a two-tailed Student's t-test. * indicates p<0.05. ** indicates p<0.01. *** indicates p<0.001.

As a confirmation, we transduced control and LSD1-silenced GBM TICs with a lentiviral reporter vector in which GFP expression reflects ATF4 promoter activity[270]. As assessed by FACS analysis, the GFP levels were strongly decreased by LSD1 silencing (**Fig. 45**). Notably, stress-induced ATF4 is mainly regulated at the protein level[267], thus implying that LSD1 regulates ATF4 expression through a non-canonical mechanism.

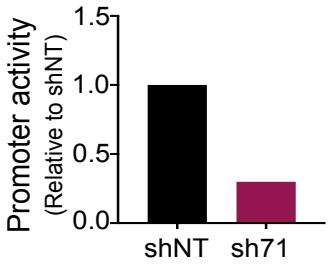

Figure 45. ATF4 promoter activity upon LSD1 silencing. ATF4 promoter activity in LSD1-silenced (sh71) and control (shNT) GBM#22 TICs

5.7.3 LSD1 targeting impairs ISR activation in GBM TICs

To verify if LSD1 was necessary for the induction of ATF4 in GBM TICs, we forced ATF4 activation by treating cells with the stressors Thapsigargin and L-Histidinol, two known inducers of UPR and AAR, respectively[271,272]. In non-stressed conditions, p-eIF2a and ATF4 proteins were nearly undetectable in GBM TICs (**Fig. 46**). Upon Thapsigargin treatment, both control (shNT-GBM#22) and LSD1-silenced (sh71-GBM#22) cells responded by increasing the phosphorylation of eIF2a, which in turn resulted in upregulated ATF4 protein level (**Fig. 46A, left**). ATF4 up-regulation was remarkably reduced upon LSD1 silencing, while the levels of both eIF2 phosphorylation and total eIF2a were not affected (**Fig. 46A, left**). Similar results were obtained upon L-Histidinol treatment (**Fig. 46A, right**). Consistently with the results obtained in LSD1-silenced GBM TICs, LSD1-KO diminished ATF4 protein induction without affecting the levels of both p-eEIF2a and total eIF2a (**Fig. 46B**).

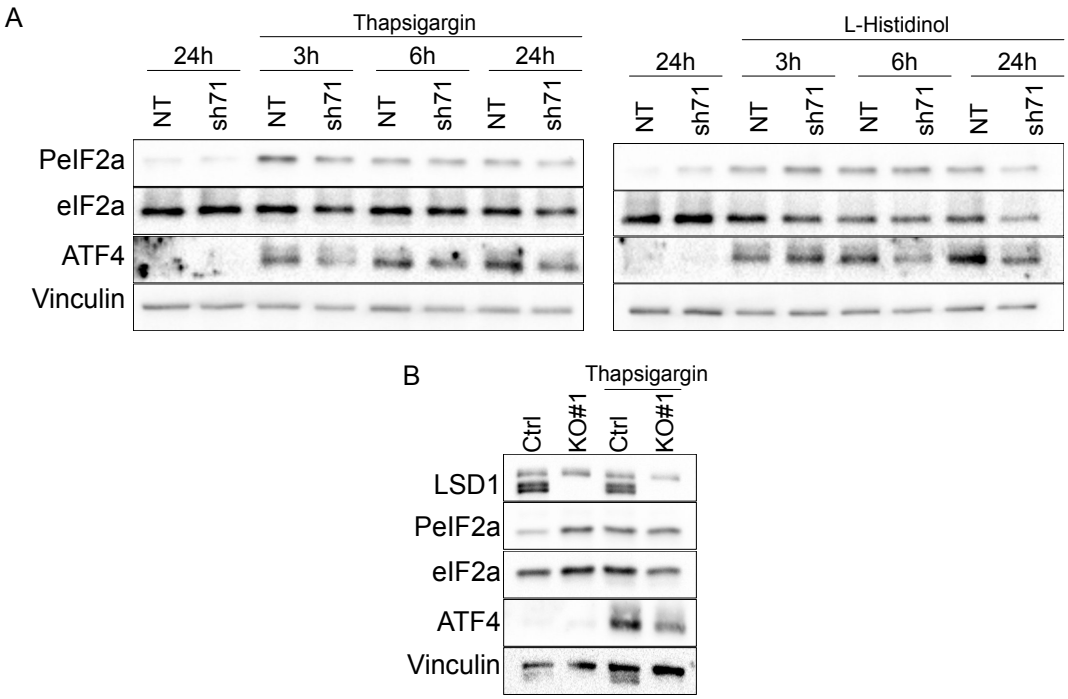

Figure 46. ISR activation upon LSD1 genetic targeting. (A) ISR signalling by western blot in LSD1-silenced (sh71) and control (shNT) GBM#22 TICs upon Thapsigargin 2.5uM (left) or L-histidinol 2mM (right) treatment. (B) ISR signalling by western blot in the indicated LSD1-KO and control GBM TICs upon Thapsigargin 2.5uM treatment. Vinculin was used as loading control.

ATF4 regulates the expression of many genes involved in cell metabolism, amino acid transport and resistance to oxidative stress in different cell types[263]. Of note, some of the DEGs identified in the RNA-seq are known ATF4 downstream genes and belong to these categories (i.e. ASNS, CHAC1, DDIT3/CHOP, GDF15, NARS, PSAT1, SLC7A11, TRIB3,

and XPOT). We confirmed their downregulation, and that of other known ATF4 target genes, by quantitative RT-PCR (qRT-PCR) (**Fig. 47A**). Importantly, we substantiated these findings also in other different LSD1-silenced (**Fig. 47B**) as well as in LSD1-KO GBM TICs (**Fig. 47C**).

Overall, these findings suggest that LSD1 drives the expression of either ATF4 and its target genes in GBM TICs independently from eIF2a phosphorylation.

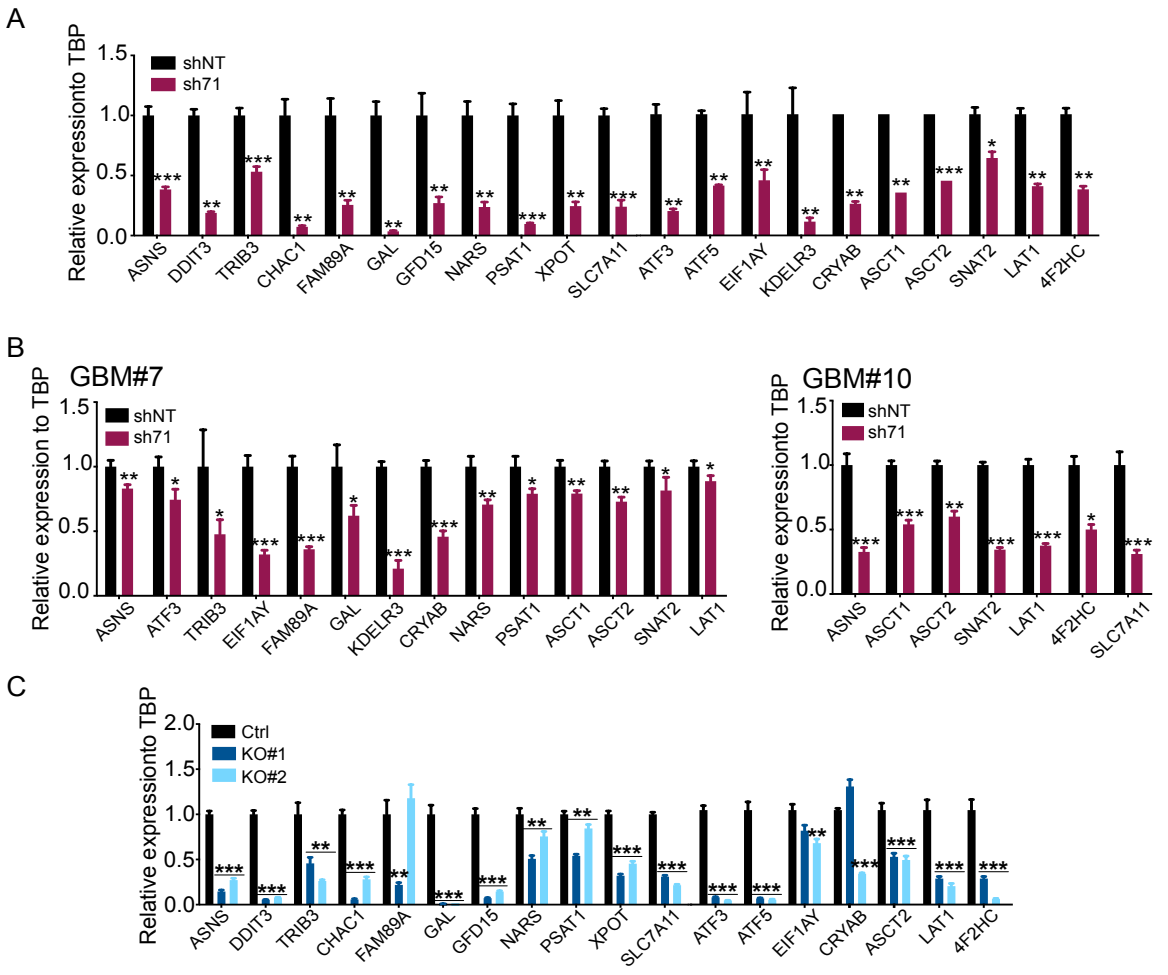

Figure 47. Expression of ISR mediators upon LSD1 genetic targeting. (A-B) ATF4 target gene expression levels by qRT-PCR in LSD1-silenced (sh71) and control (shNT) GBM#22 TICs (A) and their validation in other indicated patient-derived GBM TICs (B). (C) ATF4 target gene expression levels by qRT-PCR in the indicated LSD1-KO and control GBM TICs. TBP was used to normalize gene expression. Results are the average of 3 technical replicates Error bars represent mean +/− SD. p-values were calculated by a two-tailed Student's t-test. * indicates p<0.05. ** indicates p<0.01. *** indicates p<0.001.

5.8 Ectopic LSD1 expression rescue ATF4 expression and GBM TIC growth and self-renewal

To further demonstrate that LSD1 regulates ATF4 expression, we ectopically overexpressed a truncated form of LSD1 (ΔN-LSD1^{WT}) in LSD1-KO GBM TICs. Remarkably, ectopic LSD1 expression significantly increase ATF4 mRNA levels in LSD1-KO#2 cells (**Fig. 48A**). Similarly, LSD-KO#1 GBM TICs transfected with ΔN-LSD1^{WT} showed a robust expression of ATF4 compared to LSD1-KO cells transfected with the empty vector, despite the ectopic expression of ΔN-LSD1^{WT} was not comparable to the expression of endogenous LSD1 in control cells (**Fig. 48B**). The weak entity of ATF4 induction does not undermine the validity of this results, since it should be kept in mind that ATF4 expression level in absence of stressful stimuli is low

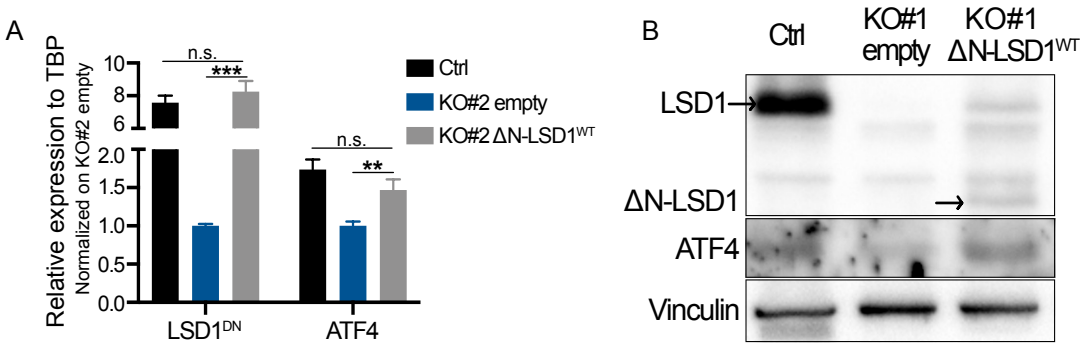

Figure 48. LSD1 and ATF4 expression upon LSD1 ectopic expression. (A) LSD1 and ATF4 expression levels by RT-qPCR in LSD1-KO GBM TICs expressing ΔN-LSD1^{WT} or an empty vector compared to control GBM#22 TICs. TBP was used to normalize gene expression. Results are the average of 3 technical replicates Error bars represent mean +/− SD. p-values were calculated by a two-tailed Student's t-test. * indicates $p<0.05$. ** indicates $p<0.01$. *** indicates $p<0.001$ (B) LSD1 and ATF4 expression levels by wester blot in LSD1-KO GBM TICs expressing ΔN-LSD1^{WT} or an empty vector compared to control GBM#22 TICs. Vinculin was used as loading control.

In addition, we sought to determine if LSD1 ectopic expression was able to rescue the phenotype observed upon LSD1 deletion.

We therefore tested the effects of LSD1 ectopic expression on GBM TICs *in vitro* biological properties. Compared to mock-transduced LSD1-KO#1 TICs, LSD1 ectopic expression effectively increased cell growth (+53% at day 3, + 60% at day 6) of LSD1-KO#1 TICs (**Fig. 49**).

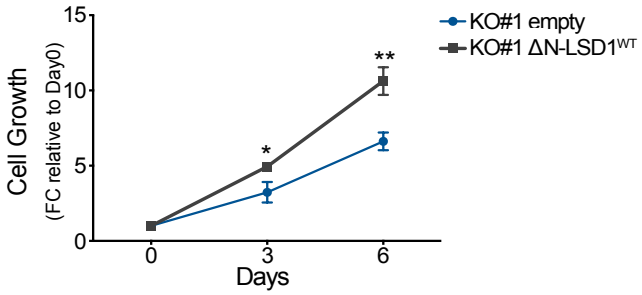

Figure 49. GBM TIC cell growth upon LSD1 ectopic expression. Growth of LSD1-KO#1 GBM TICs upon ΔN-LSD1^{WT} overexpression (KO#1 ΔN-LSD1^{WT}). Mock-transduced LSD1-KO#1 GBM TICs (KO#1 empty) were used as a control. Viable cells have been manually counted at the indicated days. Results are the average of 3 technical replicates. Error bars represent mean +/− SD. p-values were calculated by a two-tailed Student's t-test. * indicates p<0.05. ** indicates p<0.01. *** indicates p<0.001.

Similarly, by analyzing the effect of LSD1 ectopic expression on GBM TIC sphere forming potential, we found that LSD1-KO#1 TICs expressing ΔN-LSD1^{WT} formed 21% more spheres compared to empty vector-transduced controls. (**Fig. 50**).

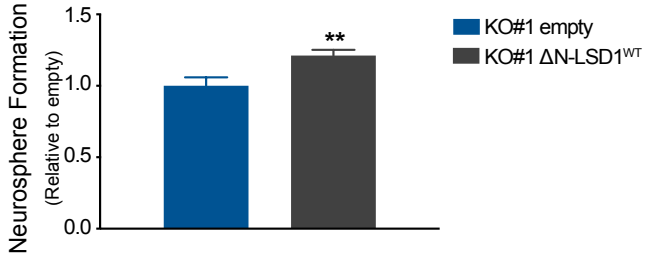

Figure 50. GBM TIC self-renewal upon LSD1 ectopic expression. Sphere formation efficiency of LSD1-KO#1 GBM TICs upon ΔN-LSD1^{WT} overexpression (KO#1 ΔN-LSD1^{WT}). Mock-transduced LSD1-KO#1 GBM TICs (KO#1 empty) were used as a control. Results are the average of 3 technical replicates. Error bars represent mean +/− SD. p-values were calculated by a two-tailed Student's t-test. * indicates p<0.05. ** indicates p<0.01. *** indicates p<0.001.

5.9 Ectopic ATF4 expression rescue GBM TIC growth and self-renewal

We then sought to assess ATF4 role in the LSD1-dependent regulation of GBM TIC biological properties. To this aim, we over-expressed ATF4 in LSD1-silenced GBM TICs (**Fig. 51**).

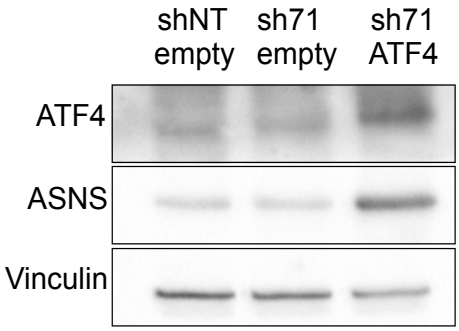

Figure 51. ATF4 and ASNS expression upon ATF4 ectopic expression. ATF4 and ASNS expression levels by western blot in LSD1-silenced GBM#22 TICs with (sh71-ATF4) or without (sh71 empty) ATF4 overexpression. Non-targeted-mock-transduced GBM#22 TICs (shNT empty) were used as a control. Vinculin was used as loading control.

ATF4 ectopic expression completely rescue the cell growth defect of LSD1-silenced cells. Indeed, while LSD1 silencing halved the growth of GBM TIC compared to control cells at both day 5 and day 7, ATF4 expressing cells started to show a growth-advantage at day 5, and grew comparably to shNT-GBM TICs at day 7 (**Fig. 52**).

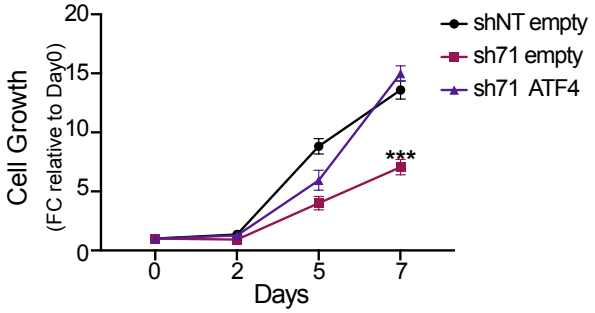

Figure 52. GBM TIC cell growth upon ATF4 ectopic expression. Growth of LSD1-silenced GBM#22 TICs with (sh71-ATF4) or without (sh71 empty) ATF4 overexpression. Non-targeted-mock-transduced GBM#22 TICs (shNT empty) were used as a control. Viable cells have been manually counted at the indicated days. Results are the average of 3 technical replicates. Error bars represent mean +/− SD. p-values were calculated by a two-tailed Student's t-test. * indicates $p<0.05$. ** indicates $p<0.01$. *** indicates $p<0.001$

ATF4 over-expression also mitigated cell death. Indeed, compared to shNT GBM TICs, caspase 3/7 activity was increased of 43% in sh71-GBM TICs transduced with an empty vector, and of only 18% in ATF4-expressing sh71-GBM TICs (**Fig. 53**).

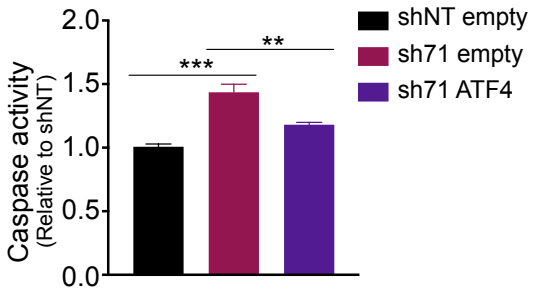

Figure 53. GBM TIC apoptosis upon ATF4 ectopic expression. Caspase 3/7 activity of LSD1-silenced GBM#22 TICs with (sh71-ATF4) or without (sh71 empty) ATF4 overexpression. Non-targeted-mock-transduced GBM#22 TICs (shNT empty) were used as a control. Results are the average of 3 technical replicates. Error bars represent mean +/− SD. p-values were calculated by a two-tailed Student's t-test. * indicates p<0.05. ** indicates p<0.01. *** indicates p<0.001

In addition, ATF4 ectopic expression partially rescued sphere formation ability, with ATF4-expressing sh71-GBM TICs forming 41% more spheres than sh71-GBM TICs transduced with an empty vector (**Fig. 54**).

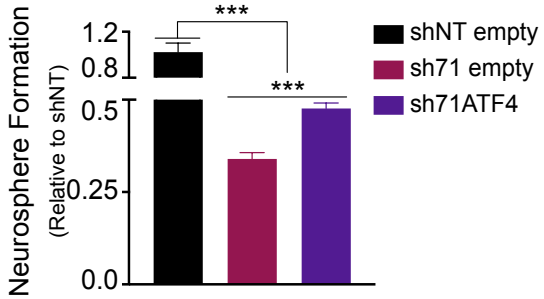

Figure 54. GBM TIC self-renewal upon ATF4 ectopic expression. Sphere formation efficency in LSD1-silenced GBM#22 TICs with (sh71-ATF4) or without (sh71 empty) ATF4 overexpression. Non-targeted-mock-transduced GBM#22 TICs (shNT empty) were used as a control. Results are the average of 3 technical replicates. Error bars represent mean +/− SD. p-values were calculated by a two-tailed Student's t-test. * indicates p<0.05. ** indicates p<0.01. *** indicates p<0.001.

Finally, ATF4 overexpression specifically rescued the expression level of some of its downstream genes (**Fig. 55**).

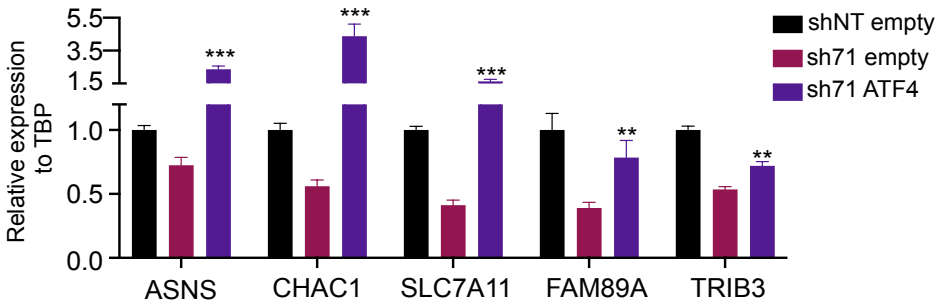

Figure 55. Expression of ISR mediators upon ATF4 ectopic expression. ATF4 target gene expression levels by qRT-PCR in LSD1-silenced GBM#22 TICs with (sh71-ATF4) or without (sh71 empty) ATF4 overexpression. Non-targeted-mock-transduced GBM#22 TICs (shNT empty) were used as a control. TBP was used to normalize gene expression. Results are the average of 3 technical replicates. Error bars represent mean +/− SD. p-values were calculated by a two-tailed Student's t-test. * indicates $p<0.05$. ** indicates $p<0.01$. *** indicates $p<0.001$.

These results demonstrate that ATF4 actually mediates the phenotypic effects observed upon LSD1 silencing.

5.10 LSD1i induced an aberrant ISR activation in GBM TICs

5.10.1 LSD1i weakens and prolongs ISR in GBM TICs

Consistently with the results obtained through LSD1 genetic targeting, LSD1i treatment reduced and slowed down ATF4 induction at protein level in response to either Thapsigargin and L-Histidinol (**Fig. 56**). Indeed, while Thapsigargin strongly burst ATF4 expression in controls GBM#22 TICs, this effect was strongly mitigated in LSD1i-treated cells (**Fig. 56A, left**). Similarly, upon L-Histidinol treatment, ATF4 expression reached a peak at 3h of treatment in controls and dropped at 6 hours and 24. hours, indicating that cells were solving the stress. Conversely, ATF4 induction in LSD1i-treated GBM TICs was weaker but prolonged, being maintained for up to 24 hours (**Fig. 56A, right**). Similar results were obtained with GBM TICs from different patients. In fact, in GBM#18 TICs, Thapsigargin induced a strong activation of ATF4, whose protein expression level reached a peak at 6 hours followed by a slow decline within 72 hours. LSD1 inhibition decreased the intensity of ATF4 burst, but prolonged the activation of the ISR (**Fig. 56B**). Control GBM#7 TICs responded to L-Histidinol stimulation with a more rapid kinetics: ATF4 expression markedly increased at 6 h after treatment and decreased to the initial level at 24 h. LSD1 inhibition decrease ATF4 protein levels at 6 hours, but contributed to maintain them high until 24 hours, similar to what observed in other samples (**Fig. 56C**) Irrespectively of the stimuli used, no modulation of either eIF2 phosphorylation or total eIF2a was observed upon LSD1i treatment (**Fig. 56A-C**).

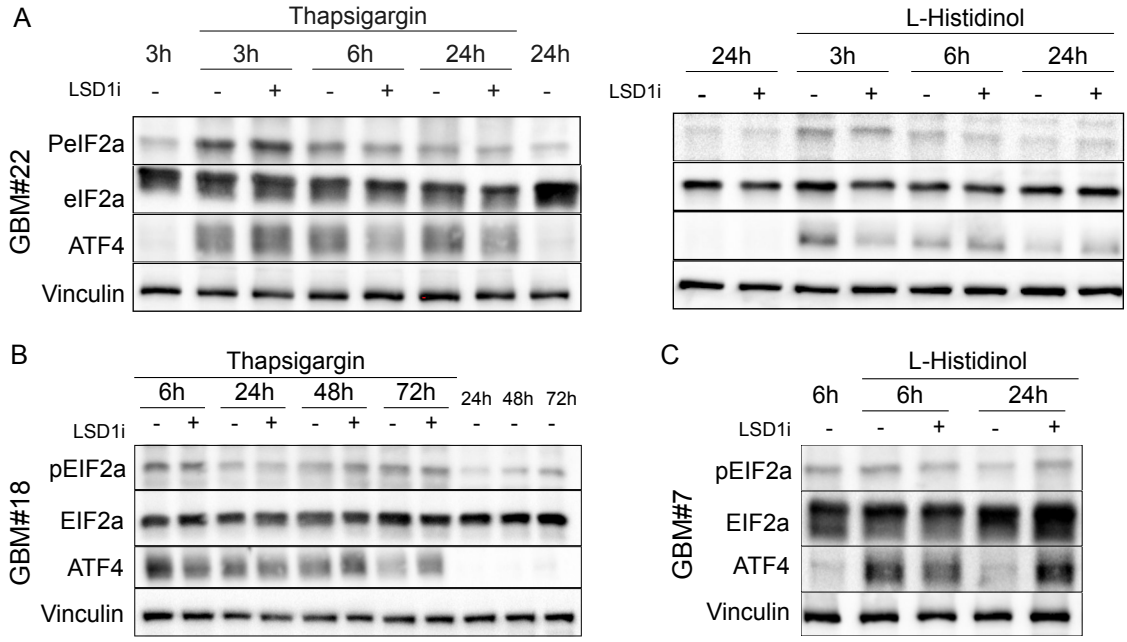

Figure 56. ISR activation upon LSD1 pharmacological inhibition and ISR activation. (A) ISR signalling by western blot in LSD1i- and vehicle-treated GBM#22 TICs upon Thapsigargin 2.5uM (left) or L-histidinol 2mM (right) treatment. (B) ISR signalling by western blot in LSD1i- and vehicle-treated GBM#18 TICs upon Thapsigargin 2.5uM treatment. (C) ISR signalling by western blot in LSD1i- and vehicle-treated GBM#7 TICs upon L-histidinol 2mM treatment. LSD1i was administered 2.5uM. Vinculin was used as loading control

To better understand how LSD1i affects ISR activation over time, we decide to verify how LSD1i regulates the expression of ISR mediator genes in response to L-Histidinol-induced stress. The induction of ATF4 target genes involved in stress response, while being rapid but transient in controls, significantly persisted in LSD1i-treated GBM TICs (**Fig. 57**). Indeed, while in control cells the expression of the majority of the ISR genes reached a peak 3-6 hours after treatment and decrease after 24 hours, LSD1i prolonged the activation of most of the genes analyzed.

ATF3 and ATF5, which contribute to ISR activation[273] were more expressed in the LSD1i treated GBM#22 compared to control cells after 6 and 24 hours of L-Histidinol stimulation. The mRNA levels of down-stream mediators deputed to sustain protein synthesis and cell proliferation during stress showed a similar trend: indeed, asparagine synthetase (ASNS), which restore asparagine levels in response to stress[274], was more than two-fold higher in the inhibitor-treated than in vehicle-treated cells after 24 hours of treatment, as well as PSAT1, involved in serine biosynthesis, critical process for cancer proliferation[275]. At the same time point, LSD1i prolonged the activation of genes that, functioning as amino acid sensors, contribute to GCN2 activation in response to amino acid starvation. In fact, the aminoacyl tRNA synthase genes (NARS and WARS) and the exportin-encoding gene XPOT, involved in charged tRNA exit from the nucleus, where all more robustly

transcribed in LSD1-inhibited cells compared to controls cells. Moreover, also the up-regulation of many solute carrier genes, deputed to restore amino acid uptake in case of amino-acid deprivation, was prolonged by LSD1i (**Fig. 57**).

Intriguingly, above prolonging the expression of genes that are normally activated by stressed cell to survive, LSD1i protracted also the transcription of pro-apoptotic genes. Among these, DDIT3 which is the transcription factor directly involved in the UPR-induced cell death pathway[276], TRIB3, that is implicated in ATF4-mediated cell death signaling[268] and CHAC1, whose overexpression has been associated to enhanced apoptosis[277] (**Fig. 57**).

These results suggest that LSD1i. treated GBM-TICs were not able to solve the stress and switch off the ISR pathway, raising the hypothesis that LSD1i impairs GBM-TIC ability to cope with stressful cues and restore homeostasis (**Fig. 57**).

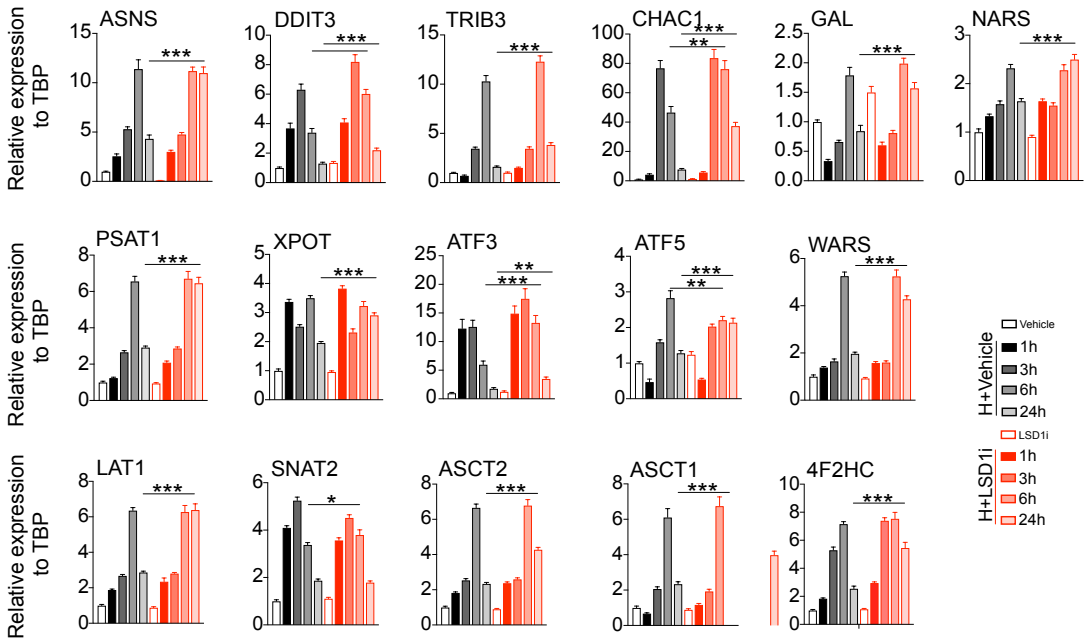

Figure 57. Expression of the ISR mediators upon LSD1 pharmacological inhibition and ISR activation. ATF4 target gene expression levels by qRT-PCR in LSD1i- and vehicle-treated GBM#22 TICs, in non-stressed conditions and upon L-Histidinol 2mM treatment for the indicated time points. LSD1i was administered 2.5uM. TBP was used to normalize gene expression. Results are the average of 3 technical replicates. A two-tailed t Student's t test was applied to compare LSD1i and control-treated samples within each time point. Error bars represent mean +/− SD. p-values were calculated by a two-tailed Student's t-test. * indicates p<0,05. ** indicates p<0,01. *** indicates p<0,001.

5.10.2 LSD1i sensitizes GBM TICs to stress

To verify this hypothesis, we decided to test whether LSD1i treatment hampers GBM TICs ability to cope with stressful cues.

Hence, we determined the cellular growth of LSD1i- or vehicle-treated GBM TICs upon Thapsigargin or L-Histidinol stimulation. LSD1i-treated cells were more sensitive to either Thapsigargin and L-Histidinol compared to control cells. Thapsigargin-treated GBM#22 TICs grew 63% less than vehicle treated cells. The combined addition of LSD1i and Thapsigargin reduced GBM TIC growth of 81% compared to LSD1i as single agents and of 85% compared to vehicle-treated cells (**Fig. 58A, left**). L-Histidinol-treated GBM#22 TICs grew 50% less than vehicle treated cells. The combined addition of LSD1i and L-Histidinol reduced GBM TIC growth of 67% compared to LSD1i as single agents and of 75% compared to vehicle-treated cells. (**Fig. 58A, right**). Of note, despite GBM#7 TICs showed high resistance to L-Histidinol treatment, LSD1i was sufficient to sensitize cells to this stressor. The combined addition of LSD1i and L-Histidinol reduced cell growth of 24% compared to LSD1i as single agents and of 46% compared to vehicle-treated cells (**Fig. 58B**).

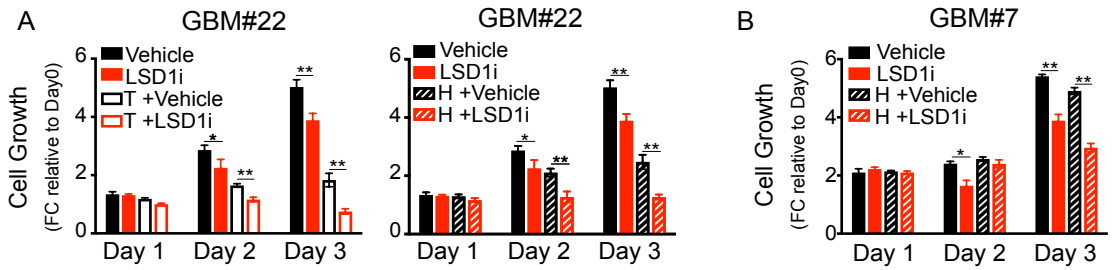

Figure 58. GBM TIC cell growth upon LSD1 pharmacological inhibition and ISR activation. Growth of LSD1i- or vehicle-treated GBM#22 TICs upon Thapsigargin 2.5uM (left) or L-Histidinol 2mM (right) treatment. (B) Growth of LSD1i- or vehicle-treated GBM#7 TICs upon L-Histidinol 2mM treatment. LSD1i was administered 2.5uM. Viable cells have been manually counted at the indicated days. Results are the average of 3 technical replicates. Error bars represent mean +/− SD. p-values were calculated by a two-tailed Student's t-test. * indicates p<0,05. ** indicates p<0,01. *** indicates p<0,001.

5.10.3 LSD1i sensitizes GBM TICs glutamine deprivation

As a further demonstration, we decided to assess if LSD1i could affect GBM TIC response to glutamine deprivation, that mimics amino-acid deprivation and triggers AAR response in a more physiological way compared to L-Histidinol administration. Thus, we cultured GBM TIC both in standard conditions (SG: Gln 2mM) and lowering glutamine concentration (LG: Gln 0.5mM). Control GBM TICs slowly responded to glutamine reduction, by overexpressing ATF4 only after 72 hours of culture, and LSD1i mitigated the intensity of this response (**Fig. 59**).

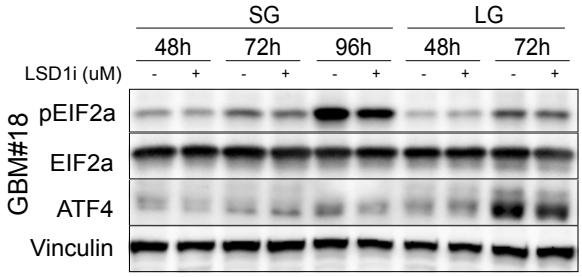

Figure 59. ISR activation upon LSD1 pharmacological inhibition and nutrient deprivation. ISR signalling by western blot in LSD1i- and vehicle-treated GBM#18 TICs cultured in standard- (SG: Gln 2mM) and low-glutamine (LG. Gln 0.5mM) medium. LSD1i was administered 2.5uM. Vinculin was used as loading control.

Likewise, LSD1i sensitized GBM TICs to nutrient stress. Indeed, glutamine deprivation alone (LG Vehicle) was almost ineffective in reducing GBM TIC growth compared to standard culture conditions (SG Vehicle). Although, LSDi1-treated cells cultured in low glutamine conditions (LG LSD1i) grew 40% less than LSD1i-treated cells cultured in standard condition (SG LSD1i) and 66% less than control cells (SG Vehicle) (**Fig. 60**).

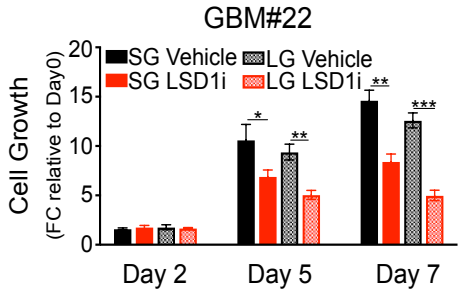

Figure 60. GBM TIC cell growth upon LSD1 pharmacological inhibition and nutrient deprivation. Growth of LSD1i- or vehicle-treated GBM#22 TICs cultured in standard- (SG. Gln 2mM) and low-glutamine (LG. Gln 0.5mM) medium. LSD1i was administered 2.5uM. Viable cells have been manually counted at the indicated days. Results are the average of 3 technical replicates. Error bars represent mean +/− SD. p-values were calculated by a two-tailed Student's t-test. * indicates $p<0.05$. ** indicates $p<0.01$. *** indicates $p<0.001$.

Overall, these results suggest that LSD1 pharmacological inhibition impairs the ability of GBM TICs to promptly and properly activate the ISR. The result is the prolonged activation of the ISR, which in turn affects GBM TIC survival under different stress conditions.

5.11 LSD1 and ATF4 share DNA binding sites in GBM TICs

To better understand how LSD1 regulates the expression of its target genes, we profiled LSD1 genome-wide binding on GBM TIC genome by exploiting chromatin immunoprecipitation followed by next generation sequencing (ChIP-seq). A total of 112,221 LSD1 peaks were identified (p. $<10^{-5}$). 25.76% of LSD1 binding sites were distributed over promoter regions. Specifically, 18.93% lie within the 1-Kbp region surrounding the transcription start site (TSS). Distal-intergenic and intronic regions were occupied by 30.26% and 29.85% of LSD1 peaks, respectively (**Fig. 61**). Notably, the broad LSD1 binding in the genome is in agreement with results from other cellular models[206].

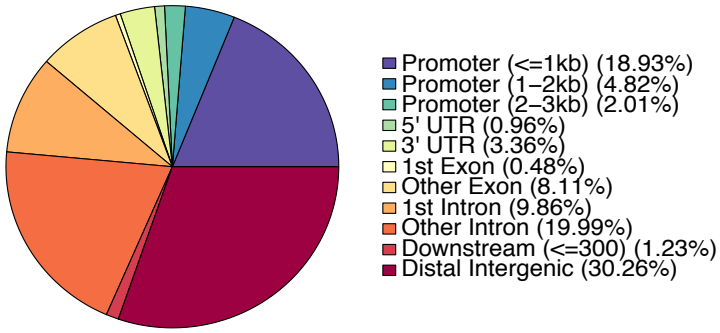

Figure 61. LSD1 binding profile on GBM TICs genome. Genomic annotation of the 112,221 LSD1-binding sites on the genome of GBM#22 TICs.

Importantly, a site-specific analysis of LSD1-ChIP-seq revealed that LSD1 bound the promoters (a region of +/- 2.5Kbp around TSS) of 44 out of 48 LSD1 regulated genes identified by RNA-seq (**Fig. 62**).

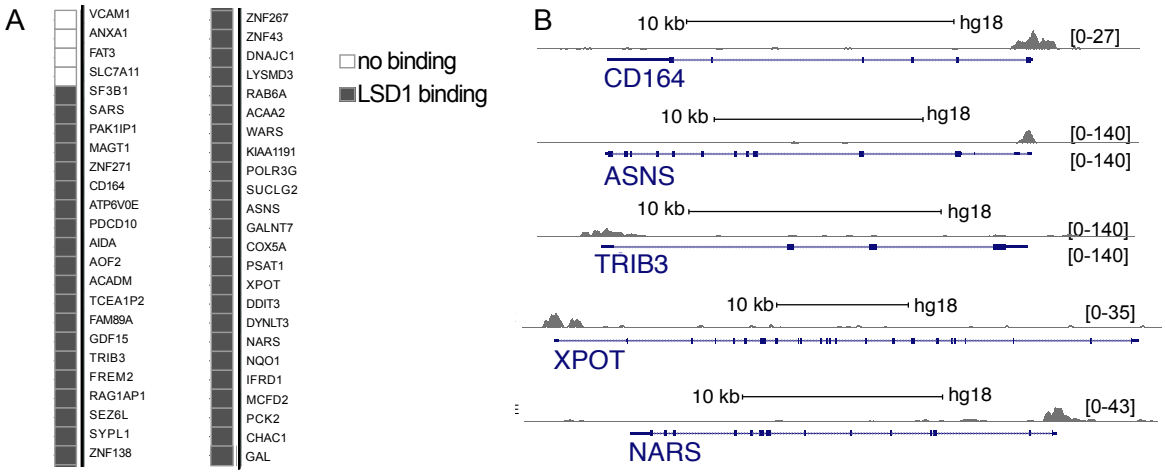

Figure 62. LSD1 binding to the promoter of its target genes. (A) LSD1 binding to the 48 DEGs identified in shLSD1 RNA-seq as assessed by LSD1 ChIP-seq. Flags indicate presence or absence of LSD1 peaks at the promoter (+/- 2.5Kbp around TSS) of the corresponding gene. Black: LSD1-binding peak. White: no LSD1 binding. (B) ChIP-seq signal tracks showing LSD1-binding peak (black bars) within representative DEGs identified in shLSD1 RNA-seq. Tracks are visualized with University of California Santa Cruz Genome Browser.

We confirmed these results performing an independent LSD1 ChIP followed by quantitative PCR (ChIP-qPCR) (**Fig. 63A**). Importantly, we have also demonstrated LSD1 binding to the promoter of ATF4 **(Fig. 63B**). This may explain how LSD1 regulates the activity of the promoter of ATF4 in GBM TICs (**Fig. 45**) and furnish a mechanism underlying the transcriptional regulation of ATF4 observed upon LSD1 genetic targeting (**Fig. 44**).

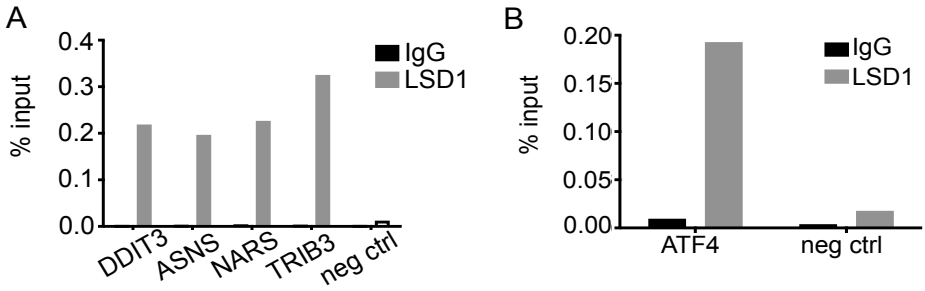

Figure 63. LSD1 binding to the promoter of its target genes (2). (A)LSD1 ChIP-qPCR at the promoter of the indicated genes. (B) LSD1 ChIP-qPCR at the promoter of ATF4. IgG and a gene desert region on human chromosome 12 have been used as controls.

As previously reported, the majority of these DEGs are known ATF4 downstream effectors. Intriguingly, we found that a previously recognized ATF4-binding motif was significantly enriched among LSD1-binding sites located within the promoter regions of LSD1-bound target genes (p-value=0,032).

By immuno-precipitating the chromatin bound by ATF4 in GBM TICs, we demonstrated that ATF4 bound LSD1 target genes in the same region already occupied by LSD1 (**Fig. 64**).

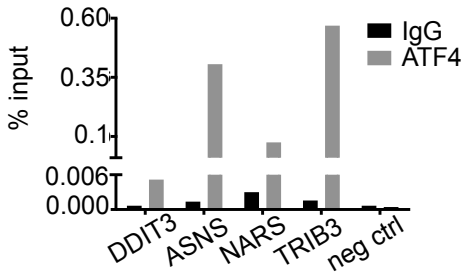

Figure 64. ATF4 binding to the promoter of LSD1 target genes. ATF4 ChIP-qPCR at the promoter of the indicated genes, within LSD1-binding region. IgG and a gene desert region on human chromosome 12 have been used as controls.

The fact that LSD1 and ATF4 share a binding site inside the promoter of LSD1 target genes indicates that they might cooperate to regulate the expression of their common target genes.

5.12 LSD1 and ATF4 share DNA binding sites in K562

We took advantage of *in silico* analysis of publicly available dataset to gains insights about LSD1 and ATF4 genome distribution in different model systems. Specifically, we compared the results of LSD1 (ENCODE accession number ENCSR360HRA) and ATF4 (ENCODE accession number ENCSR145TSJ) ChIP-seq in K562 cells, a cellular model of chronic myeloid leukemia. Considering that ATF4 is a transcription factor, we decided to narrow down the analysis focusing our attention only on LSD1 and ATF4 peaks located within the promoter (+/- 2.5Kbp around TSS) of protein coding genes. This analysis highlighted that 44.8% of LSD1-bound promoter of protein coding genes were bound also by ATF4. *Viceversa*, 41.4% of ATF4-bound protein coding genes were also bound by LSD1, revealing a strongly significant overlap of LSD1 and ATF4 within protein coding genes promoters in K562 (p-value: $10^{\wedge -188}$) (**Fig. 65**).

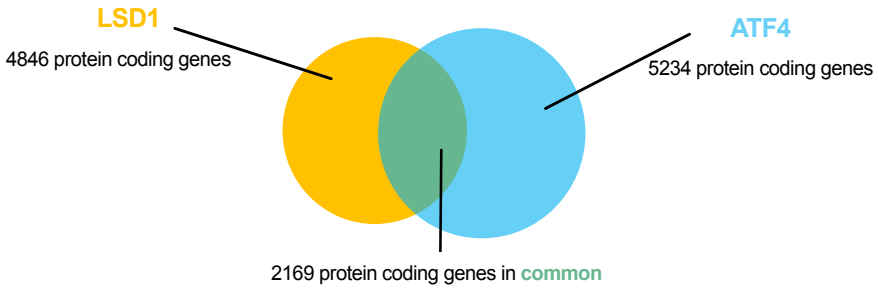

Figure 65. LSD1 and ATF4 overlap in K562. Venn diagram showing the overlap of LSD1 and ATF4 around the promoters of protein coding genes in K562 cells. Yellow: LSD1-bound genes. Blue: ATF4-bound genes. Green: common genes.

5.13 LSD1i does not displace LSD1 from the genome of GBM TICs

We then sought to clarify the mechanism by which LSD1i achieves its effects. Many LSD1 inhibitors are available so far, and some of them are able to displace LSD1 from its targets genes, thus affecting its regulatory functions[206,221,223]. We treated cells with our compound LSD1i 2.5uM for 24 hours, to verify whether it is able to modify LSD1 binding profile. Genomic annotation of LSD1 peaks was substantially unvaried by LSD1i treatment (**Fig. 66**), meaning that LSD1i did not induce massive LSD1 binding or displacement from specific classes of DNA regions, including regulatory regions.

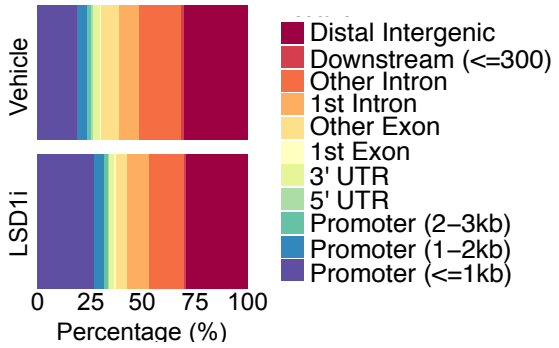

Figure 66. LSD1 binding profile on GBM TIC genome upon LSD1 pharmacological inhibition. Genomic annotation of LSD1-binding sites on the genome of LSD1i- and vehicle-treated GBM#22 TICs. LSD1i was administered 2.5uM for 24 hours.

Genome-wide, we classified LSD1-bound regions as "common" if conserved independently by LSD1i, "Gain" if present only in LSD1i-treated cells, and "Lost" if present only in vehicle-treated cells. Around 75% of LSD1 peaks have been identified as common regions, 8% as gain regions and 16% as lost regions (**Fig. 67A**).

Importantly, promoter regions were predominantly included in the common regions, and much less present among gain and lost peaks (**Fig. 67B**).

MACS scores of peaks within common regions were also significantly higher compared to those of both gain and lost region (**Fig. 68**).

This suggested that LSD1 binding to promoter regions is highly stable and unaffected by LSD1i treatment.

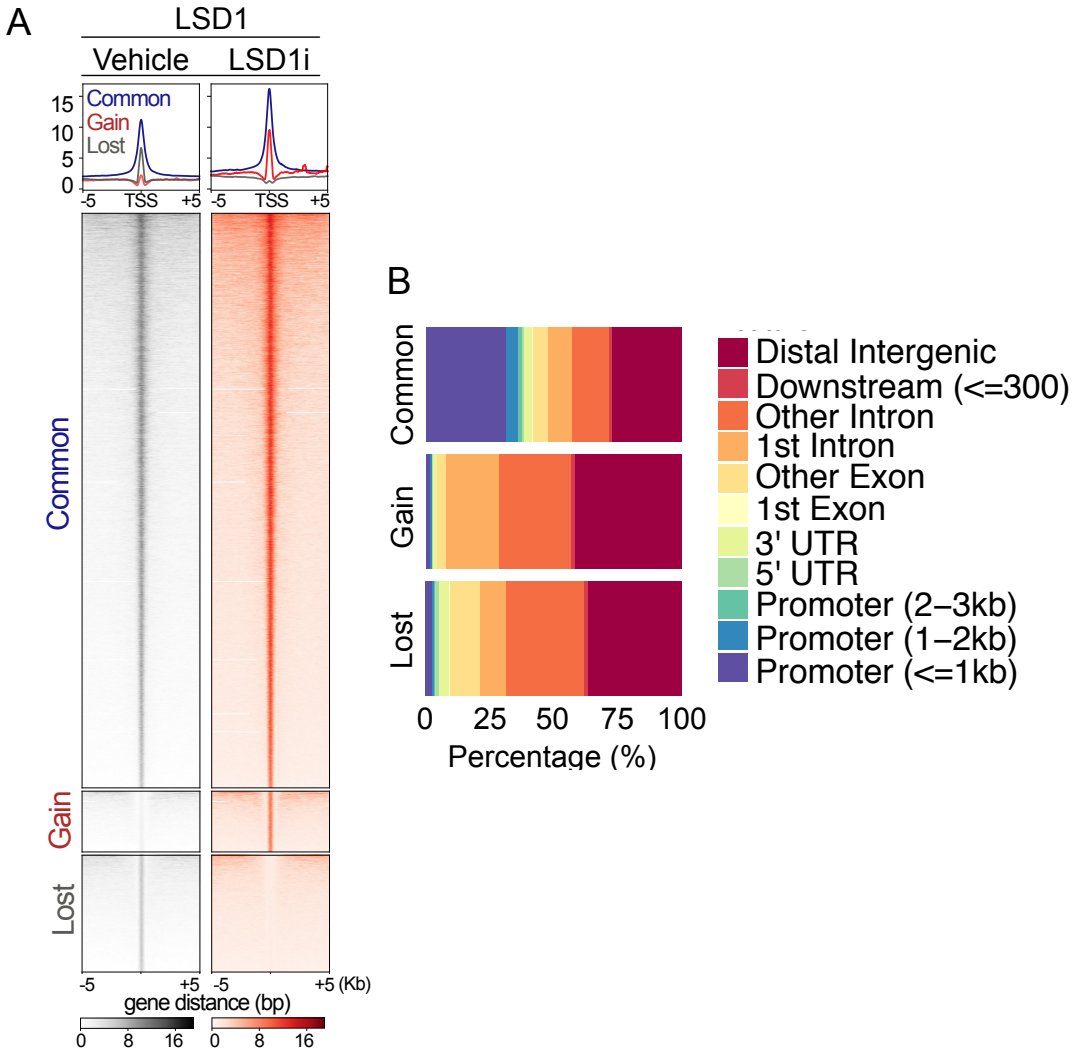

Figure 67. Characterization of LSD1 displacement or recruitment upon its pharmacological inhibition. (A-B) Heatmap (A) and genomic annotation (B) of LSD1 binding sites in LSD1i- or vehicle-treated GBM#22 TICs. Common: LSD1-binding sites present in both LSD1i- and vehicle-treated cells. Gain: LSD1 -binding sites present only in LSD1i-treated cells. Lost: LSD1-binding sites present only in vehicle-treated cells. LSD1i was administered 2.5uM for 24 hours.

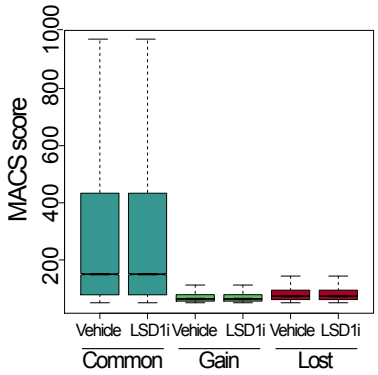

Figure 68. MACS score of LSD1 peaks upon its pharmacological inhibition. MACS score of LSD1 binding sites in LSD1i- or vehicle-treated GBM#22 TICs. Common: LSD1-binding sites present in both LSD1i- and vehicle-treated cells. Gain: LSD1 binding sites present only in LSD1i-treated cells. Lost: LSD1-binding sites present only in vehicle-treated cells. LSD1i was administered 2.5uM for 24 hours.

5.14 LSD1i does not displace LSD1 and ATF4 from LSD1 regulated genes

A site-specific analysis based on ChIP-seq data confirmed that LSD1 binding to the promoter region of its DEGs was not altered by LSD1i treatment. Indeed, LSD1 was not displaced by the 44 bound DEG. Likewise it was not recruited to the promoter of VCAM, ANXA1, FAT3 and SLC7A11, that were not bound by LSD1 in untreated cells (**Fig. 69**).

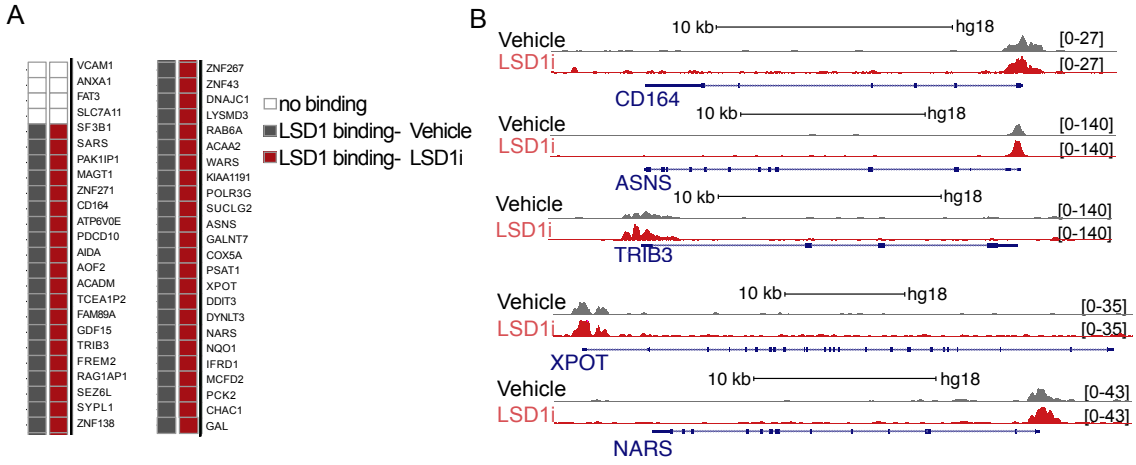

Figure 69. LSD1 binding to the promoter of its target genes upon LSD1 pharmacological inhibition. (A) List of the 48 DEGs identified in shLSD1 RNA-seq. Flags indicate presence or absence of LSD1 peaks at the promoter (+/- 2.5Kbp around TSS) of the corresponding genes. Black: LSD1-binding peak in vehicle-treated GBM#22 TICs; Red: LSD1-binding peak in LSD1i-treated GBM#22 TICs; White: no LSD1 binding. (B) ChIP-seq signal tracks showing LSD1-binding peaks (black bars) at the indicated genes in LSD1i- or vehicle-treated GBM#22 TICs. Tracks are visualized with University of California Santa Cruz Genome Browser. LSD1i was administered 2.5uM for 24 hours.

This result has been further confirmed through an independent LSD1 ChIP followed by q-PCR. Importantly, LSD1 binding to the promoter of ATF4, whose expression in turn

regulates the transcription of ISR downstream mediators, remained stable as well (**Fig. 70**).

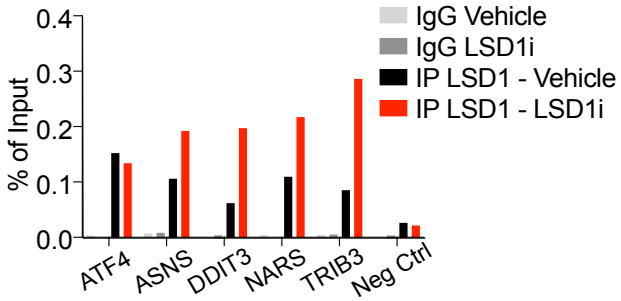

Figure 70. LSD1 binding to the promoter of its target genes upon LSD1 pharmacological inhibition (2). LSD1 ChIP-qPCR at the promoter of the indicated genes in LSD1i- and vehicle-treated GBM#22 TICs. IgG and a gene desert region on human chromosome 12 have been used as controls. LSD1 was administered 2.5uM for 24 hours.

Remarkably, neither ATF4 binding to the promoter of LSD1 target genes was modified by LSD1 pharmacological inhibition (**Fig. 71**).

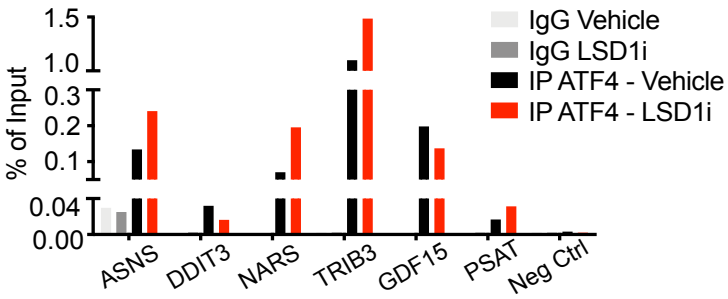

Figure 71. ATF4 binding to the promoter of LSD1 target genes upon LSD1 pharmacological inhibition. ATF4 ChIP-qPCR at the promoter of the indicated genes in LSD1i- and vehicle-treated GBM#22 TICs. IgG and a gene desert region on human chromosome 12 have been used as controls. LSD1 was administered 2.5uM.

5.15 LSD1 regulates its target genes in GBM TIC independently by its demethylase functions

Mechanistically, we verified whether LSD1 demethylase activity was required for the regulation of LSD1 target genes and to mediate its pro-oncogenic role in GBM TICs.

5.15.1 LSD1i-induced H3K4 methylation is not linked to gene expression changes in GBM TICs

ChIP-seq experiments demonstrated that LSD1i treatment significantly increased H3K4me2 levels and, to a lesser extent, H3K4me3 levels, in the "common" regions, while H3K4me1 levels were unchanged. H3K4 methylation levels in "gain" and "lost" regions were not modified by LSD1i (**Fig. 72**).

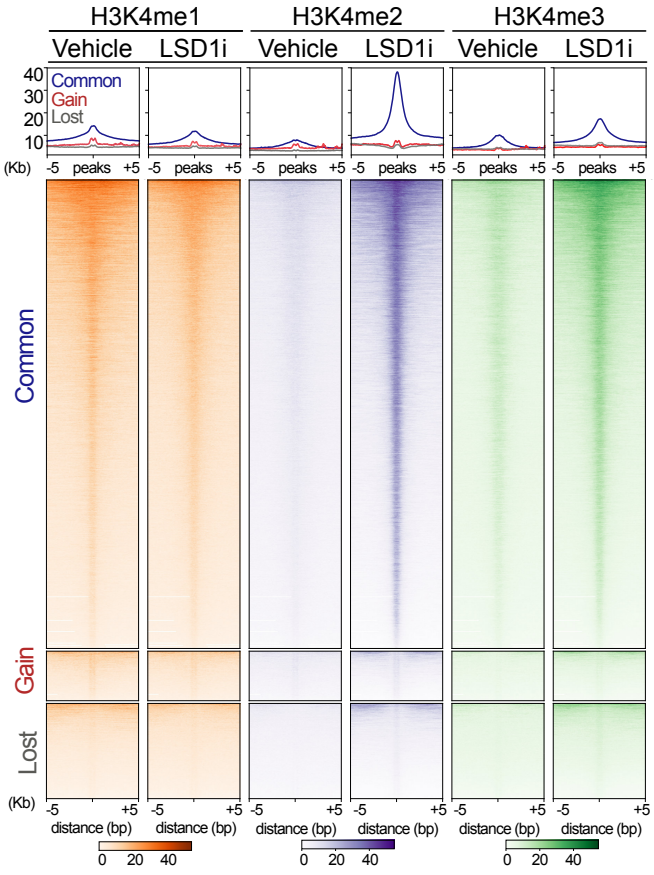

Figure 72. H3K4 methylation profile in GBM TICs upon LSD1 pharmacological inhibition. Heatmap showing ChIP-seq signals of H3K4me1, H3K4me2 and H4K4me3 in LSD1i- and vehicle-treated GBM#22 TICs. Common: LSD1-binding sites present in both LSD1i- and vehicle-treated cells. Gain: LSD1 binding sites present only in LSD1i-treated cells. Lost: LSD1-binding sites present only in vehicle-treated cells. LSD1i was administered 2.5uM for 24 hours.

In accordance, LSD1i significantly increased H3K4me2 levels at the promoters of LSD1-bound DEGs (**Fig. 73**). Coherently, no changes in H3K4me2 levels were observed at the promoter of the 4 unbound LSD1 regulated genes (VCAM, ANXA1, FAT3 and SLC7A11) (**Fig. 73**), confirming that the increased methylation of Lysine 4 on Histone H3 observed upon LSD1i treatment was specifically due to the inhibition of the catalytic activity of LSD1.

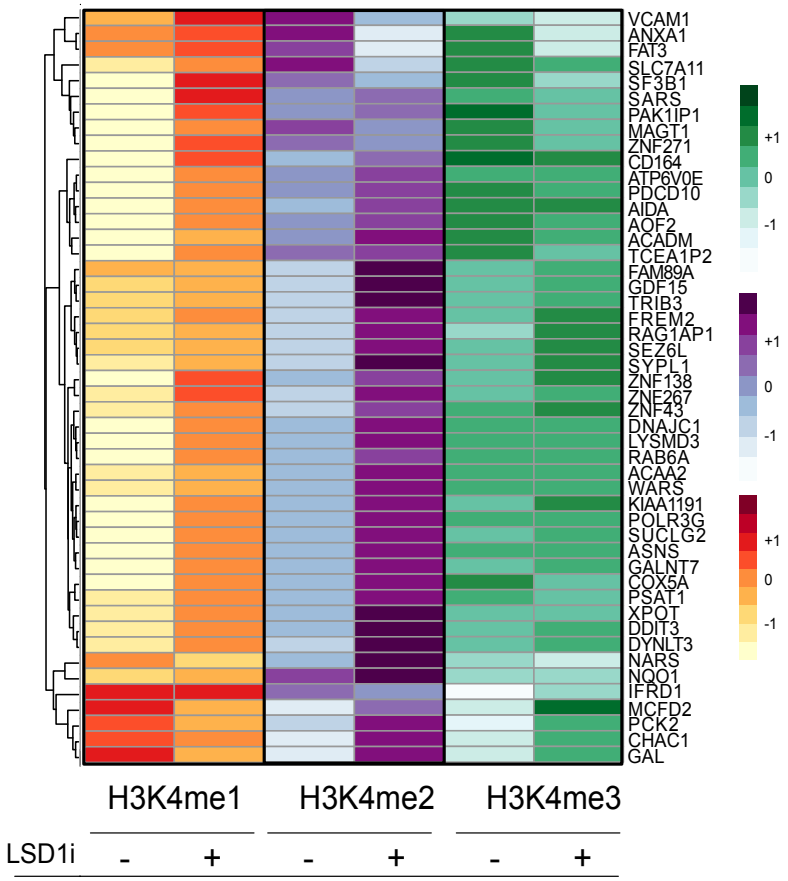

Figure 73. H3K4 methylation within the promoter of LSD1 target genes upon LSD1 pharmacological inhibition. Heatmap showing H3K4me1, H3K4me2 and H4K4me3 signals at the promoter of the 48 DEGs identified in shLSD1 RNA-seq, in vehicle- and LSD1i-treated GBM#22 TICs. LSD1i was administered 2.5uM for 24 hours.

Unexpectedly, the increased methylation of H3K4 was not directly associated with neither change in gene expression or chromatin accessibility.

Indeed, we profiled the transcriptomic changes induced by LSD1 pharmacological inhibition by RNA-seq. We compared the transcriptomic profile of control GBM#22 TICs with that of cells treated with LSD1i 2.5uM for 24 hours. Despite this treatment modality was sufficient to inhibit LSD1 catalytic activity (**Fig. 72-73**), no significant changes in gene expression were observed (**Fig. 74**).

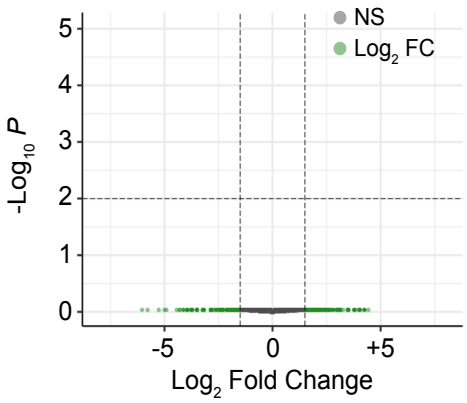

Figure 74. Differential gene expression in GBM TIC upon LSD1 pharmacological inhibition. Volcano plot representation of differential expression analysis of LSD1i- or vehicle-treated GBM#22 TICs, as assessed by RNA-seq. LSD1i was administered 2.5uM for 24 hours. DEGs have been defined according to these tresholds: |Log2FC|>1.2, FDR≤0.05. *The* x-axis shows log_2fold-changes in expression. The Y-axis show statistical significance (-log10 of the p-value). Green points mark the genes with increased or decreased expression respectively (|Log2FC|>1.2). Data from three biological replicates are shown.

Further, by performing Assay for Transposase Accessible Chromatin with high-throughput sequencing (ATAC-seq), we could not observe any changes in chromatin accessibility in LSD1i-treated cells compared to control cells (**Fig. 75**).

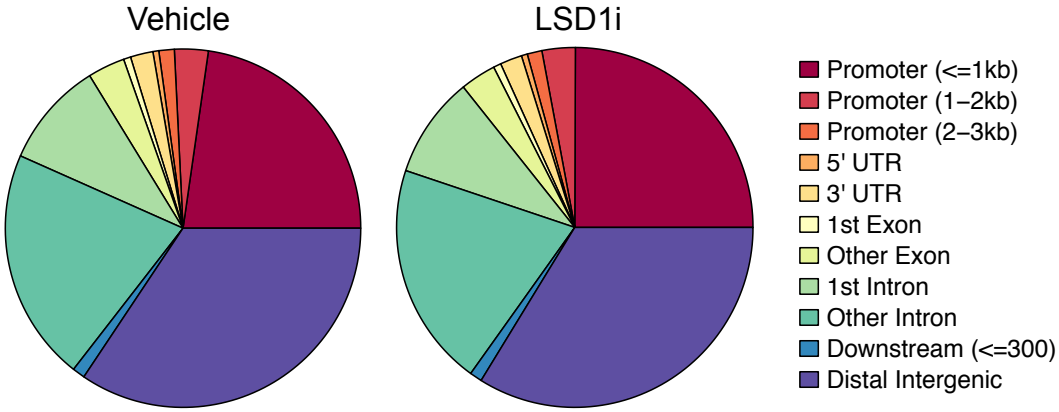

Figure 75. Chromatin accessibility upon LSD1 pharmacological inhibition. Genomic annotation of chromatin accessible regions on the genome of LSD1i- and vehicle-treated GBM#22 TICs, as assessed by ATAC-seq. LSD1i was administered 2.5uM for 24 hours. Two biological replicates have been performed.

Focusing our attention on the subset of LSD1 target genes, we confirmed that LSD1i administration does not alter neither their expression levels, neither the chromatin accessibility of their promoter regions (**Fig. 76**)

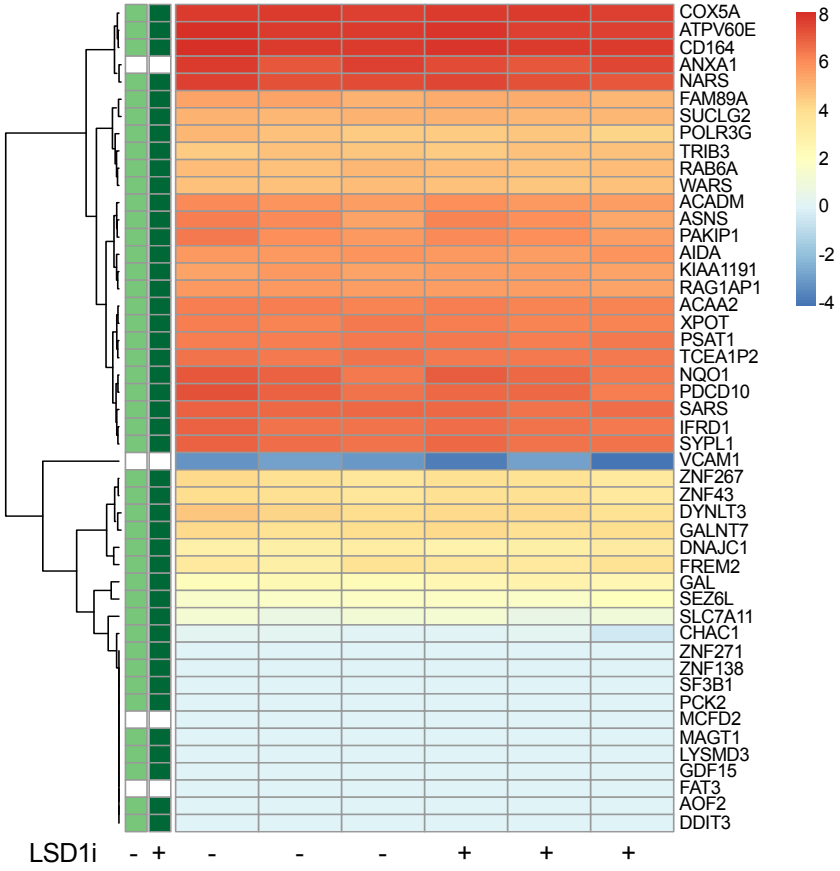

Figure 76. LSD1 target gene expression and accessibility upon LSD1 pharmacological inhibition. Heatmap showing the expression of the 48 LSD1 target genes in LSD1i- or vehicle-treated GBM#22 TICs, as assessed by RNA-seq. LSD1i was administered 2.5uM for 24 hours. Data from three biological replicates are shown. Flags on the left indicate the accessibility state of the chromatin, as assessed by ATAC-seq. Green: accessible chromatin; White: not accessible chromatin. Two biological replicates have been performed.

These results suggested us that, opposite to LSD1 genetic targeting, LSD1i treatment alone is not sufficient to alter the expression of LSD1 target genes in non-stressed cells. Although, we have previously shown that LSD1i impairs the activation of ISR upon the application of stressfull stimuli, like Thapsigargin or L-Histidinol treatment (**Fig. 56**), or nutrient deprivation (**Fig. 59**). This led us to hypothesize that, in response to stress, LSD1 regulates the expression of its target genes in GBM TIC through a mechanism that is independent from its catalytic activity, maybe relying on its scaffolding functions.

5.15.2 LSD1 catalytic activity is dispensable to rescue LSD1-dependent phenotype in GBM TICs

To further assess the role of LSD1 catalytic activity, we transduced LSD1-KO GBM TICs with either WT (ΔN-LSD1^{WT}) and catalytic mutant (ΔN-LSD1^{K661A}) LSD1 cDNA (**Fig. 77**).

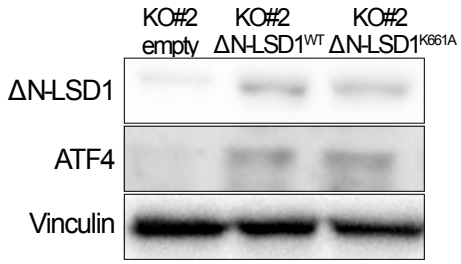

Figure 77. LSD1 and ATF4 expression upon LSD1 WT or catalytic mutant ectopic expression. LSD1 and ATF4 expression levels by western blot in LSD1-KO#2 GBM TICs overexpressing either ΔN-LSD1^{WT} (KO#2 ΔN-LSD1^{WT}) or ΔN-LSD1^{K661A} (KO#2 ΔN-LSD1^{K661A}). Mock-transduced LSD1-KO GBM TICs (KO#2 empty) were used as a control. Vinculin was used as loading control.

By monitoring cell growth for up to 5 days, we demonstrated that the expression of both LSD1 WT and catalytic mutant were able to confer growth advantage to LSD1 KO#1 GBM TICs. LSD1-KO GBM TICs expressing ΔN-LSD1^{WT} grew 60% more than control cells, while the cell growth of ΔN-LSD1^{K661A} expressing cells was increased up to 148% (**Fig. 78**).

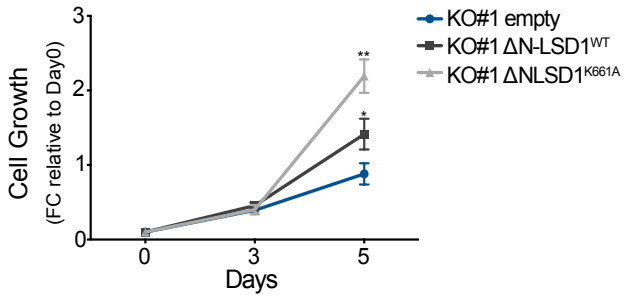

Figure 78. GBM TIC cell growth upon LSD1 WT or catalytic mutant ectopic expression. Growth of LSD1-KO#1 GBM TICs overexpressing either ΔN-LSD1^{WT} (KO#1 ΔN-LSD1^{WT}) or ΔN-LSD1^{K661A} (KO#1 ΔN-LSD1^{K661A}). Mock-transduced LSD1-KO GBM TICs (KO#1 empty) were used as a control. Viable cells have been manually counted at the indicated days. Results are the average of 3 technical replicates. Error bars represent mean +/− SD. p-values were calculated by a two-tailed Student's t-test. * indicates $p<0.05$. ** indicates $p<0.01$. *** indicates $p<0.001$.

Similarly, the self-renewal ability of GBM#22-KO#1 were equally increased by the exogenous expression of both ΔN-LSD1^{WT} and ΔN-LSD1^{K661A}. Indeed, ectopic expression

of WT or mutant LSD1 augmented the number of spheres formed by 50.6% and 48.9% respectively (**Fig. 79**).

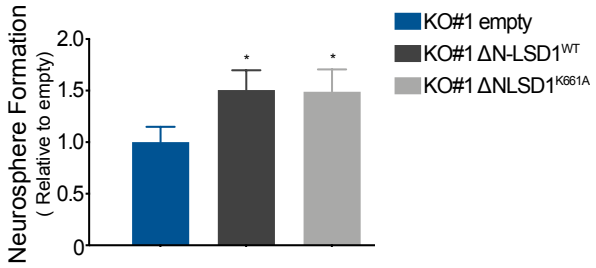

Figure 79. GBM TIC self-renewal upon LSD1 WT or catalytic mutant ectopic expression. Sphere formation of LSD1-KO#1 GBM TICs overexpressing either ΔN-LSD1^{WT} (KO#1 ΔN-LSD1^{WT}) or ΔN-LSD1^{K661A} (KO#1 ΔN-LSD1^{K661A}). Mock-transduced LSD1-KO GBM TICs (KO#1 empty) were used as a control. Sphere formation efficiency was evaluated after the first plating. Results are the average of 3 technical replicates. Error bars represent mean +/− SD. p-values were calculated by a two-tailed Student's t-test. * indicates p<0.05. ** indicates p<0.01. *** indicates p<0.001.

Importantly, they equally increased ATF4 mRNA (**Fig. 80**) and protein level (**Fig. 77**), as well as the mRNA levels of ASNS, a known ATF4 effector (**Fig. 80**).

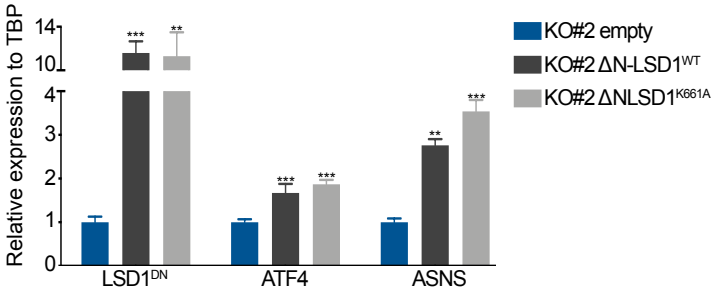

Figure 80. Target gene expression upon LSD1 WT or catalytic mutant ectopic expression. ATF4 target gene expression levels by qRT-PCR in LSD1-KO#2 GBM TICs overexpressing either ΔN-LSD1^{WT} (KO#2 ΔN-LSD1^{WT}) or ΔN-LSD1^{K661A} (KO#2 ΔN-LSD1^{K661A}). Mock-transduced LSD1-KO GBM TICs (KO#2 empty) were used as a control. Results are the average of 3 technical replicates. Error bars represent mean +/− SD. p-values were calculated by a two-tailed Student's t-test. * indicates p<0.05. ** indicates p<0.01. *** indicates p<0.001.

Hence, we have demonstrated that LSD1 demethylase activity was dispensable to rescue the phenotype induced by LSD1 depletion as well as to rescue the expression of its target genes, supporting the hypothesis that LSD1i treatment impairs LSD1 pro-tumorigenic properties through a mechanism that is independent by the loss of LSD1 catalytic activity.

Altogether, the results presented in this thesis demonstrate the effectiveness of the compound DDP_38003 for therapeutic intervention in human GBM, independently of the GBM molecular landscape, hence representing a strong rational for the rapid clinical translation of this approach. Additionally, we shed light on the pro-tumorigenic role played by LSD1 in the GBM TIC compartment and we unraveled the mechanism of action of the compound DDP_38003 in GBM TIC model, smoothing the way to develop new combinatorial treatment to defy this tremendous disease.

6. DISCUSSION

Numerous efforts have been undertaken to improve GBM patient prognosis in the last years: a multitude of alternative treatment modalities have been proposed, some of them entering in clinical trials, including anti-angiogenic therapies and immunotherapies[278]. However, GBM remains one of the tumors with higher mortality and no advancement in the standard of care have been reached since the introduction of the Stupp protocol, in 2005[63]. Currently, lack of biomarkers, high inter- and intra-tumoral GBM heterogeneity, at both cellular and molecular levels, and poor blood–brain barrier penetration by almost all drugs all impair target therapies efficacy and clearly highlight the urgent need for new targets and clinical treatments. Being at the apex of GBM hierarchy, TICs are responsible of either GBM onset, regrowth, and extensive heterogeneity. The direct consequence of GBM TIC persistence beyond any therapeutic approach is the inevitable and rapid relapse of this continuously evolving tumor, eventually culminating in patient death. Hence, novel therapeutic approaches directly targeting GBM TIC population are urgently needed.

6.1 LSD1 targeting in GBM

In order to acquire and/or maintain a stem-cell like phenotype, GBM TICs undergo a series of genetic and epigenetic alterations, such as DNA and histone modifications, that can distinguish them from the tumor bulk by controlling chromatin conformation and gene transcription[279]. In virtue of their reversible nature, epigenetic traits can be targeted to revoke the tumorigenic potential typical of this subpopulation[280,281].

The dysregulated expression of LSD1 and different others histone modifiers in cancer encouraged the testing of molecules targeting epigenetic traits in preclinical and clinical trials. Inhibitors of DNA demethylation and histone deacetylation have been the first approved epigenetic therapies for cancer[281,282], and many studies are focusing on their therapeutic potential in combination with other drugs. In GBM, histone deacetylase inhibitors showed efficacy against GBM TICs, reducing their proliferation and the expression of stemness markers[283]. Notably, their efficacy against GBM cells has been increased by LSD1 inhibition[204,229]. As far as LSD1, its role in normal and cancer stem cells and its tumor-promoting activity in different malignancies, have raised a great interest in the development of several LSD1 inhibitors. Remarkably, while few of them already

progressed to human clinical trials for the management of SMLC and AML[232,284], pre-clinical studies with GBM models are still at their infancy[204,228,285].

LSD1 enrichment in human GBM tissues as well as in GBM patient-derived TICs prompt us to test the efficacy of LSD1-directed therapy as a potential novel therapeutic strategy against GBM. In the present study we demonstrated that LSD1 is likely a therapeutically relevant target in human GBM by using both pharmacologic and genetic targeting. The novel, selective, irreversible, orally bioavailable and brain penetrant LSD1i DDP_38003 (here LSD1i) exerts anti-tumor effects *in vitro* and *in vivo* against GBM TICs, independently of their expression and mutational profile.

LSD1i affects GBM TIC viability, reduces their growth, and strongly decreases their stem cell-like traits, namely self-renewal ability and stem cell frequency. Exploiting orthotopic PDXs, we demonstrated that LSD1i treatment delays GBM onset and growth, thus prolonging mice survival. Remarkably, LSD1 silencing and knock-out in GBM TICs phenocopied LSD1i effects.

The marked decline of self-renewal potential measured in clonogenic assays and the reduction of stem cell frequency observed both *in vitro* and *in vivo,* are in line with the established role of LSD1 as a critical regulator of cancer stem cell maintenance. Hence, considering the fundamental endorsement furnished by GBM TICs during gliomagenesis, the exhaustion of this pool might seriously compromise GBM aggressiveness and explain how LSD1 targeting extends the survival of GBM bearing mice.

Ravasio and colleagues demonstrated that LSD1 pharmacological inhibition decreases the aggressiveness of APL and AML cells by inducing blast differentiation[221] and similar finding had been previously reported in AML models by employing a different LSD1 inhibitor[206]. Differently, we did not observe any change in GBM TIC morphology or in the expression of stem cell or differentiation markers, neither *in vitro* or *in vivo,* suggesting that GBM TIC exhaustion is not due to their differentiation. Rather, in our model, the depletion of the stem cell like cells could be attributed to the concomitant reduction of self-renewal and growth, accompanied by an increase in apoptotic cell death.

Our data are in accordance with the literature, which attributes a pro-survival role for LSD1 in GBM cells[204,225,229], but better clarify the specific effect of LSD1 inhibition on the GBM TIC compartment. Although other studies demonstrated LSD1 enrichment in GBM TICs

compared with normal progenitor cells, as well as the sensibility of GBM TICs toward different LSD1 inhibitors[204,228,285], the results of some of the pre-existent studies might be affected by the low selectivity of some LSD1 inhibitors. Indeed, due to the high structural homology of LSD1 with other members of the MAO family, some LSD1 inhibitors have been recognized as non-selective compounds that possibly induce substantial toxicity *in vitro* and *in vivo* and whose potential side effects make the interpretation of LSD1 role misleading[286]. Tranylcypromine and pargyline showed greater inhibition of mono-ammino oxidases and other FAD-dependent enzymes, while SP2509 showed effects even against LSD1-KO cells[236]. Compared to other available LSD1 inhibitors, our compound, used in the therapeutic dose-range, is highly selective for LSD1[240]. This, together with its ability to cross the brain blood barrier, pave the way for the development of new therapeutic strategies based on LSD1 inhibition. LSD1i ability to curtail GBM TIC compartment makes it an ideal candidate to be combined with more traditional drugs, such as Temozolomide, to simultaneously hit the tumor bulk and the GBM TIC pool, with the final aim to overcome GBM TIC therapy resistance and avoid the onset of relapses. This aspect is particularly relevant in GBM, in which recurrences occur in almost all of the cases, originating a new tumor that is not always resectable and often becomes resistant to standard treatments, finally leading to patient's death.

Of note, LSD1i treatment was tolerated, demonstrating the existence of a therapeutic window for its administration. A further support to LSD1i efficacy comes from its application in hematological malignancies, either alone[240] or in combination with retinoic acid[221].

6.2 LSD1 molecular players in GBM

The genes deregulated upon LSD1 silencing suggested an association with the ISR in GBM TICs. ISR is an adaptive pathway essential to cell survival in response to a plethora of stressful stimuli, such as nutrient deprivation, lack of amino-acids, unfolded protein accumulation and oxidative stress. The ISR mediates its effects by reducing global protein synthesis, while inducing ATF4 expression, which in turn coordinates the adaptive response in cells. Indeed, ATF4 effectors are involved in different processes including cell metabolism, amino acid synthesis and transport, resistance to oxidative stress, proliferation and survival, invasive tumor growth and angiogenesis[263]. Once the stress is

solved, ISR activation is finished off. On the contrary, in case of unabated activation, ISR behaves like a maladaptive response, triggering cell death. In particular, the intensity and the duration of the expression of some UPR-mediators, such as DDIT3, can be critical to switch cellular destiny in response to stress[276]. Xl765 (a dual PI3K/mTOR inhibitor[287] and NH125 (a high-powered ISR activator)[288] induce GBM cell apoptosis through the uncontrolled activation of the DDIT3/DR5 pathway.
Moreover, it is known that ATF4 can modulate different set of target genes, leading to different cellular behavior, depending on the epigenetic landscape of the cells[289].

Interestingly, ISR activation is also linked to stemness maintenance and differentiation. Hypoxia-induced ISR activation leads to preferential translation of "stemness" factors including NANOG, SNAIL and NODAL, favoring the acquisition of a stem-cell like phenotype in breast cancer cells[290]. Above this, the phosphorylation level of eIF2α is high in hESC and decreases during their differentiation[291], consistently with LSD1 expression trend[193].

Here, we show for the first time that LSD1 sustains the activation of the ISR pathway in GBM TICs. Indeed, we observed that LSD1 genetic targeting in non-stressed cells reduced the expression of ATF4 and some of its effector genes. Among these genes, some help cells to restore amino-acid homeostasis in case of nutrient deprivation and/or unfolded protein accumulation, while others are involved in apoptosis regulation. Moreover, LSD1 knock down/out prevents ATF4 up-regulation upon induction of either ER and nutrient stress.

Likewise, our findings suggest that LSD1 pharmacological inhibition impairs the ability of GBM TICs to promptly and properly activate the ISR, making GBM TICs unable to solve the stress and thus leading to cell death.
Indeed, LSD1i first limits ATF4 induction upon stress, and then prolongs its activation, as well as the activation of many ATF4-downstream effectors, leading to the death of cells experiencing stress. Coherently, LSD1i treatment sensitizes GBM TICs to stressful stimuli, reducing their growth rate. On the other hand, stressed cells are more sensitive to LSD1i treatment. This is strongly encouraging, since it suggests that, *in vivo,* LSD1i efficacy may be increased by stressful cues normally encountered by GBM cells in their hostile micro-environment. Indeed, given the high proliferation index, GBM cells are constantly

struggling with the challenge to survive and rapidly divide despite the lack of nutrients and oxygen, and the accumulation of unfolded proteins. On top of that, it should be also kept in consideration that GBM TICs have a different metabolic profile compared to more differentiated GBM cells, relying less on glucose availability, and depending more on amino-acids[292]. Thus, the employment of an epigenetic-based therapy -such as LSD1 inhibition- to impair the cellular ability to cope with amino-acid shortage may represent a powerful strategy to undermine GBM TIC tumorigenic potential.

Notably, the association between LSD1 and UPR, ER stress pathway and oxidative stress response in GBM TICs had been already reported in the study of Sareddy and colleagues. However, they showed that LSD1 inhibition, by means of NCD-38 and NCL-1, was *per se* sufficient to burst the expression of ATF4 and some UPR-related effectors to violently activate the UPR pathway also in non-stressed cells, concomitantly triggering differentiation and apoptosis[227]. These discrepancies may be at least partially explained by the fact that NCD-38 mechanism of action is different from that of our LSD1i. Indeed, the authors linked the induction of UPR mediators to the enrichment of H3K4me2 at the promoters of the UPR stress genes, implying that the phenotype that they had reported was due to the loss of LSD1 enzymatic activity.

6.3 LSD1 target gene regulation

Despite the aforementioned differences, the study of Sareddy and coworkers is consistent with our findings in suggesting that LSD1 can modulate ATF4-mediated stress response. ATF4 is highly expressed and sustains tumorigenicity in different cancers, including human fibrosarcoma and human colorectal adenocarcinoma[265], colon cancer[293], prostate cancer[294] and GBM[295]. Intriguingly, ATF4 overexpression associates with poorer patient overall survival, including that of GBM patient[295].

Different oncogenes sustains ATF4 expression and activation in malignant cells, such as KRAS in colon cancer[293], FLT3 tyrosine kinase receptor in AML[296], KDM4C in neuroblastoma[297] and BRAF in melanoma[298]. Although canonical ATF4 upregulation is post-transcriptionally driven by eIF2α phosphorylation[267], our results indicates that LSD1i limits ATF4 activation upon treatment with L-Histidinol and Thapsigargin without affecting

the phosphorylation of eIF2α. In spite of its peculiarity, this is not completely unexpected, since there are evidences that ATF4 can be also transcriptionally regulated[299]. We showed that LSD1 knock-down/out reduces the mRNA levels of ATF4 in GBM TICs. In line with this, we found that LSD1 binds ATF4 promoter and regulates its transcriptional activity, demonstrating that LSD1 is a novel transcriptional regulator of ATF4 expression.

Interestingly, since LSD1 and ATF4 share the same binding regions on the promoter of well-known ATF4 target genes, it is conceivable that LSD1 may cooperate with ATF4 to regulate the expression of their common target genes. On support of this hypothesis, LSD1 and ATF4 significantly overlap at the promoter of protein coding genes in K562 cells. Moreover, a cooperation between ATF4 and KDM4C, another member of KDM family, has been already documented in a cellular model of neuroblastoma. In this model, KDM4C controls ATF4 transcription by binding to ATF4 promoter, similarly to our results. In addition, KDM4C and ATF4 are reciprocally necessary to bind and regulate the promoter of effector genes involved in amino-acid metabolism to sustain cancer cell proliferation[297].

Collectively, these findings strengthen the link between LSD1 and ATF4 in supporting GBM formation likely through the tight coordination of the transcriptional response of GBM TICs to stress.

In agreement with this, the reconstitution of ATF4 expression in LSD1-KO GBM TICs was able to restore their growth and self-renewal ability, together with the expression of some of their common target genes.

6.4 LSD1i mechanism of action

In addition, we start to address the molecular mechanisms through which LSD1i regulates the expression of LSD1 target genes in GBM TICs. LSD1 is a component of different multi-protein complexes, and the mechanism mediating its tumor promoting activity might rely either on its enzymatic activity or on its scaffolding role. Recent evidences highlighted the involvement of the demethylase-independent function of LSD1 in cancer progression[206,220,221,223,224,300]. Here, the convergence of LSD1 genetic and pharmacological

targeting phenotypes supports the scaffolding function of LSD1, rather than its histone demethylase activity, in sustaining GBM TIC growth and survival through the ATF4-dependent ISR.

Coherently with the loss of LSD1 enzymatic activity, LSD1i administration increases the levels of H3K4me1 and H3K4me2 in correspondence of LSD1 binding sites, including the promoter of its target genes, but this is not accompanied by a concomitant change of target gene expression. In fact, LSD1i administration in non-stressed GBM TICs does not significantly alter either their gene expression profile, or their chromatin accessibility.

LSD1 genetic targeting, instead, yield a list of deregulated genes, mostly unexpectedly downregulated in LSD1 silenced/KO cells, further supporting the hypothesis that, in the GBM TIC context, LSD1 target gene regulation rely on its scaffolding functions rather than on the loss of its demethylase activity.

Moreover, the expression of either the wild-type or the enzymatic-deficient human mutant protein $LSD1^{K661A}$ in LSD1 KO GBM TIC equally rescued growth and stemness, and restored ATF4 expression. Notably, the catalytically inactive $LSD1^{K661A}$ does not exerts H3K4 demethylase activity on histone H3 peptide or protein substrates[166]. Albeit a residual H3K4 demethylase activity was measured on nucleosomes only recently[301], the efficiency of K661A mutation in impairing many LSD1 functions has been largely described[178,193,302–306]

We further showed that LSD1 inhibition does not displace LSD1, neither at a global level nor at the target genes promoters. Analogously, ATF4 binding to the promoter of its target genes remained stable upon LSD1i administration.

This sheds light on the peculiar mechanism of action exerted by our compound in GBM TICs. Oppositely, Sehrawat and Colleagues suggested that the reversible LSD1 inhibitor SP2509 partially displaces LSD1 from its binding site in a prostate cancer model[223]. Nevertheless, they show that SP2509 binding makes LSD1 instable and more prone to be degraded. Thus, LSD1 degradation might partially explain its minor recruitment to the genome. Beside this, SP2509 treatment did not increase H3K4me1 and H3K4me2 levels[223], contrary to what we have observed. In this regard, it should be kept in consideration that SP2509 is an allosteric, and not a catalytic inhibitor. Similarly, the studies of Ravasio and colleagues and Maiques-Diaz and her coworkers both reported

LSD1 displacement from the genome upon LSD1 inhibition, by, respectively, the compounds MC_2580 and OG86[206,221].

Despite the aforementioned differences, these studies agree with our in highlighting the importance of non-enzymatic functions of LSD1 in cancer.

Since we have demonstrated that LSD1i acts independently by loss of LSD1 catalytic activity and that neither LSD1 complex or ATF4 are displaced from their binding regions, we hypothesize that LSD1i may disrupt LSD1 protein-protein interaction with its molecular partners, thus changing LSD1-complex composition and function. We started to address this question in collaboration with Tiziana Bonaldi's Laboratory only recently (see. Future Perspective).

7. FUTURE PERSPECTIVES

7.1 LSD1 interactome assessment (In collaboration with Tiziana Bonaldi's Laboratory)

To verify the hypothesis that modification in the composition of LSD1 complexes may be responsible for the above described results, we first characterized the basal LSD1-interaction network in GBM TICs using mass spectrometry approach (MS/MS). The results obtained in Tiziana Bonaldi's Laboratory showed that LSD1 interactors were enriched in the best-known complexes CoREST, CtBP and BHC complexes. Interestingly, several complexes associated with histone H3 lysine 4 (H3K4) methyl-transferase activity, such as the MLL3, the MLL4 and the PTIP-HMT complexes were enriched as well. A further analysis revealed that the proteins co-immuno-precipitated with LSD1 were mostly involved in chromosome organization, histone PTM activity, regulation of transcription and DNA repair (data not shown).

Once defined the basal LSD1-interactors network, we started to unravel LSD1 interactors changes upon LSD1 inhibition. Overall, the majority of interactors remained stably associated with LSD1 upon inhibitor treatment, except for a few of them. Intriguingly, among the interactors in GBM TICs, LSD1 binds the histone acetyltransferase (HAT) CREB binding protein (CREBBP, or CBP), a known interactor of ATF4 (**Fig. 81A**). ATF4 contains a bZIP domain that directly interact with CBP and its homologous protein p300[307] leading to ATF4 acetylation[308]. Importantly, p300/CBP are required for stress-dependent ATF4 stabilization and transactivation[307], even if the importance of their HAT activity in this phenomenon is still under debate[308]. After having assured that CBP eviction was not due to a reduction of its expression in LSD1i treated cells (**Fig. 81B**), we validated for the first time a basal interaction between LSD1 and CBP in GBM TICs by exploiting a proximity ligation assay (PLA). (**Fig. 81C**).
Thus, LSD1i treatment may disrupt displaces CBP from LSD1 protein complex at the promoter of ATF4 and ATF4 target genes, thus likely inhibiting their transactivation under stress conditions (see: Summary of the Hypothesis Model and **Fig. 82**).

We are now planning to validate if LSD1 and CBP interaction if disrupted by LSD1i administration by employing either co-immunoprecipitation analysis or PLA.

Finally, we are going to exploit biologic assays to validate the role of CBP in GBM TICs. To this aim, we will target it by mean of RNA small interfering techniques, and we will evaluate how this affects the expression of LSD1 target genes and how it regulates ATF4-dependent ISR, alone or in combination with LSD1i.

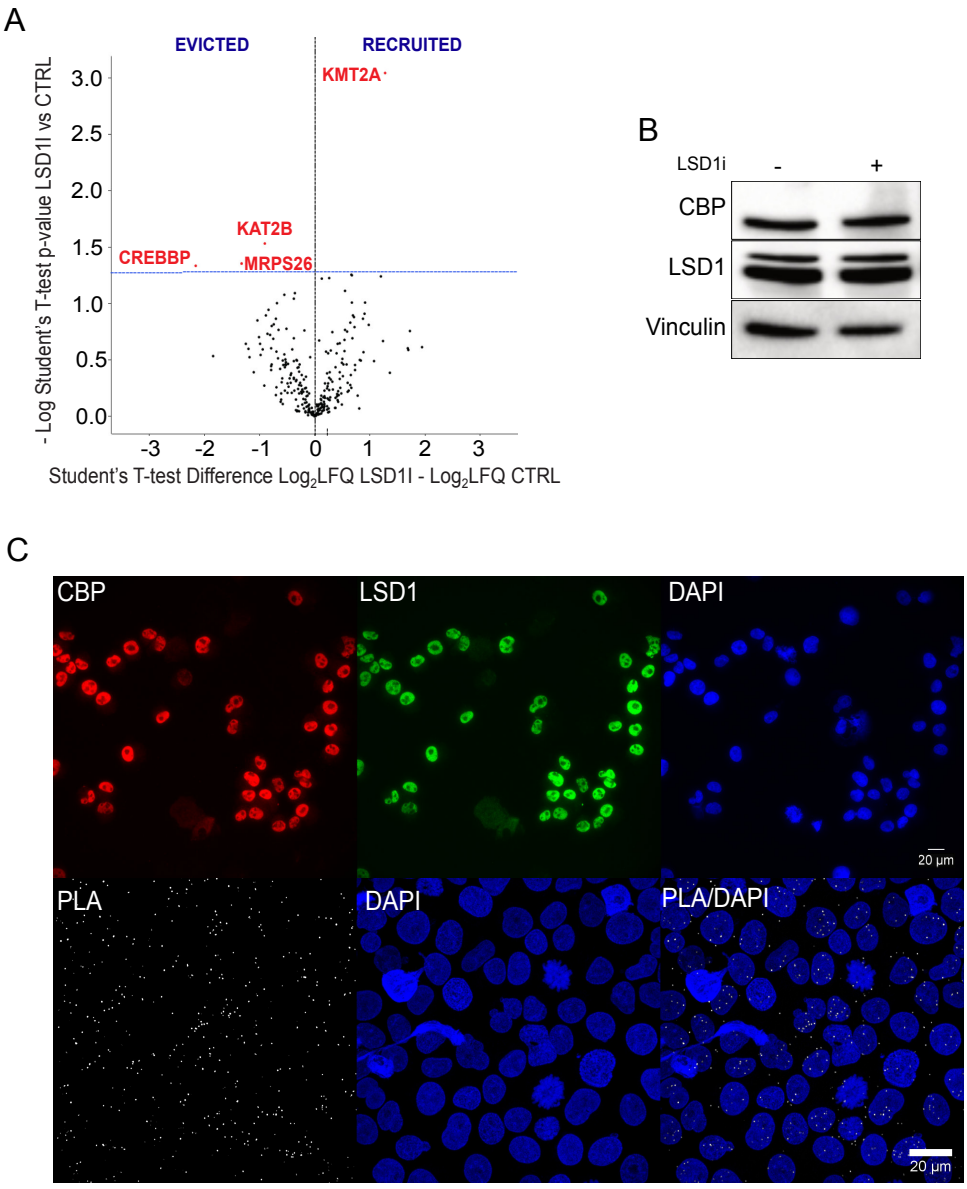

Figure 81. LSD1i effects of LSD1 complex. (A) MS assessment of LSD1 protein interactors changes upon LSD1i 2.5uM administration. (B) CBP expression in vehicle- or LSD1-treated GBM TICs. LSD1i was administered 2.5uM for 24 hours. (C) LSD1 and CBP interaction in GBM#22 TICs using IF-PLA confocal microscopy. Representative images of CBP (red), LSD1 (green), and nuclei (blue) have been employed to monitor localization (first row: widefield microscopy, pixel sixe 162 nm) and proximity (second row: Max Intensity Projection of a Confocal Z-Stack, pixel size 138 nm) by Proximity Ligation Analysis.

7.2 Therapeutic implications

We aim to assess the therapeutic potential of LSD1i in combination with drugs interfering with ISR. First, we will combine LSD1i with ISRIB, a molecule able to reverse the effects of the ISR activation, including ATF4 up-regulation[309]. ISRIB specifically blocks the PERK-branch of the UPR, and counteracts ATF4 induction upon ER stress without affecting neither PERK or EIF2α phosphorylation[309]. Similarly, it efficiently reverts ATF4 up-regulation in starved cells, without impeding GCN2 activation and its dependent eIF2α phosphorylation, indicating that this drug blocks signaling downstream of eIF2α phosphorylation[309]. Indeed, ISRIB rescues translation processes despite eIF2α phosphorylation, hence making cells insensitive to ISR activation signals[309].
ISRIB showed efficacy in a PDX model of prostate cancer[310] and it is able to cross the brain blood barrier[309]. Its use *in vivo* did not highlight important side effects, since it suppress the chronic activation of the ISR, without impeding an acute response to intense and abrupt stress, probably minimizing the impact on normal tissues, for which ISR is a vital adaptive pathway[311]. Finally, ISRIB administration reduced the acquisition of a stem-cell like phenotype in a breast cancer model[290], providing a further rationale to test ISRIB efficacy in the GBM TIC compartment.

An alternative approach may be the combination of LSD1i with a drug targeting the pathway downstream to ATF4. One of the main targets of ATF4 is Asparagine Synthetase (ASNS), whose upregulation promotes protein synthesis and cell proliferation through asparagine biosynthesis. L-Asparaginase catalyzes asparagine reduction to aspartic acid and glutamate and is a drug already used in clinical practice to successfully treat Acute Lymphoblastic Leukemia patients (Erwinase, Elspar)[312]. Consistently, L-Asparaginase reduced the growth of multiple GBM cell lines[313].

We hypothesize that the combination of LSD1 and ISR inhibitors, such as ISRIB, or drugs able to counteract the activation of ATF4 downstream effector, like L-Asparaginase, can contribute to GBM TIC exhaustion, thus effectively endangering GBM growth and aggressiveness.

To verify these hypotheses, we will treat GBM TICs with the individual agents and the combination treatments and we will evaluate the phenotype in term of *i)* viability ii) growth *iii)* sphere formation ability and *iv) in vivo* tumorigenic potential

8. SUMMARY OF THE HYPOTHESIS MODEL

Altogether, our results led us to build an hypothesis model in which LSD1 scaffolding function is crucial to positively control the transcription of both ATF4 and other ISR downstream mediators, and sustain their up-regulation in response to stressful stimuli that characterize the micro-environment of a rapidly proliferating tumor such as GBM. Thus, LSD1 behave like a stress-adaptor gene in GBM TICs, permitting them to mount an adaptive response to both amino-acid shortage and proteostasis perturbation, restoring cell homeostasis and allowing their growth and survival. In turn, by maintaining the GBM TIC population and preserving its stem-cell like features, LSD1 contributes to the tumor growth and relapse (**Fig. 82**).

LSD1i does not alter the recruitment of neither LSD1 or ATF4 to the promoter of ISR mediators. Instead, we can hypothesize that LSD1i treatment, by displacing the transactivator CBP from LSD1 protein complex, may interfere with the activation of ATF4, thus dysregulating both the intensity and the duration of the activation of the ISR pathway. The aberrant activation of this pathway prevents the stress resolution and determines a maladaptive cellular response to stress, triggering the apoptotic process and impairing GBM TIC maintenance and tumor growth (**Fig. 82**).

Although the regulation of the ISR pathway observed upon both LSD1 genetic and pharmacological targeting rely on LSD1 scaffolding function, the compound DDP_38003 is a catalytic inhibitor whose ability to reduce LSD1 demethylase activity in GBM TICs has been demonstrated by both hPTM (**Fig. 24**) and ChIP-sequencing analysis (**Fig. 72**). Hence, our results do not exclude that LSD1 demethylase activity can exert additional pro-tumorigenic roles in GBM TICs. In particular, the effects of this compound on the methylation and the function of LSD1 non-histone targets have still to be addressed. Of particular interest in GBM is the LSD1-dependent demethylation of p53, through which LSD1 protects GBM cells from apoptosis[225]. Therefore, the anti-tumorigenic potential exerted by this compound in GBM might be further enhanced by a concomitant effect on both LSD1 scaffolding and demethylase function.

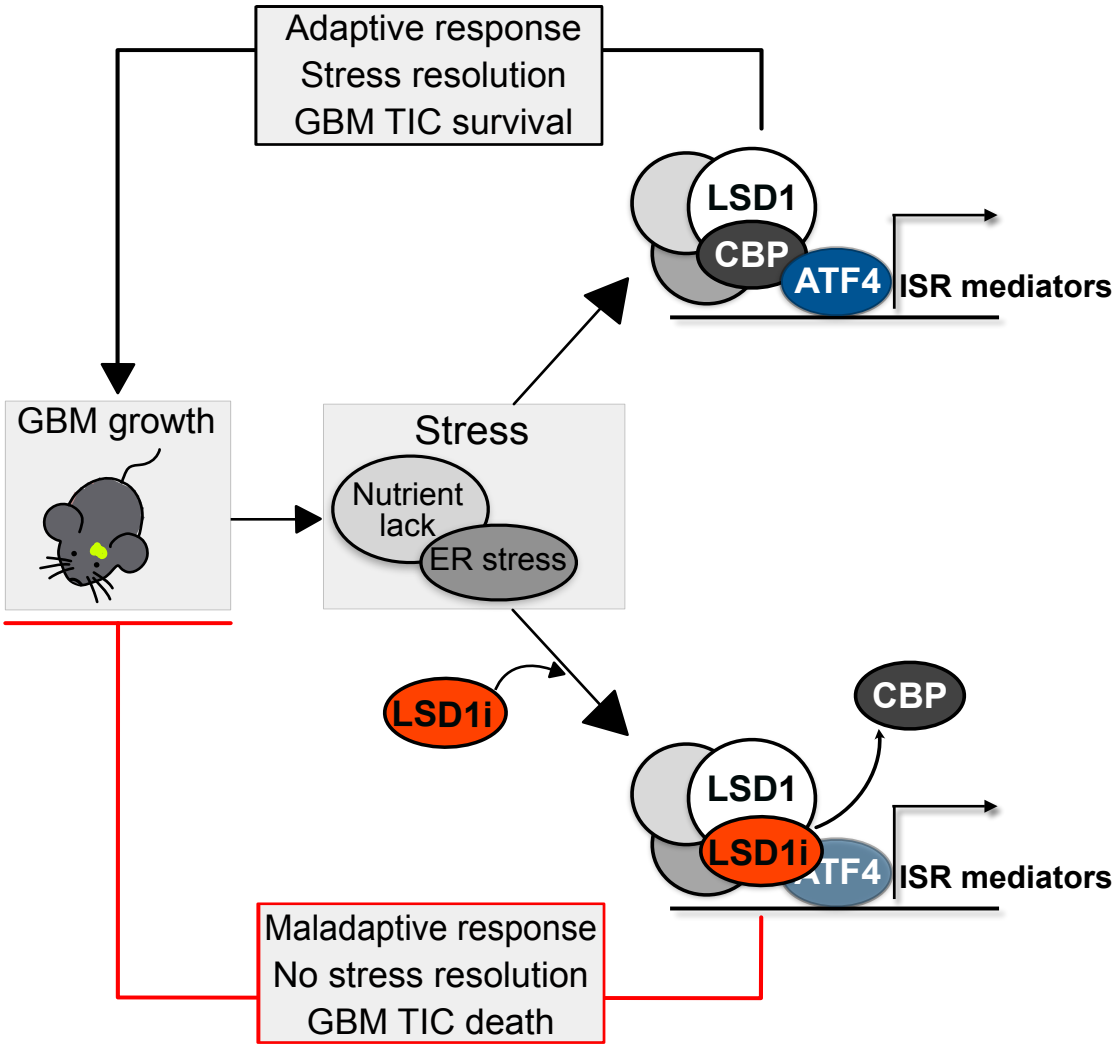

Figure 82. Hypothesis model of the molecular mechanisms regulating LSD1-targeting dependent phenotype in GBM TICs

9. LIST OF PUBLICATION DURING PHD

Published papers:

1. Osti, D., Del Bene, M., Rappa, G., Santos, M., Matafora, V., Richichi, C., **Faletti, S**., Beznoussenko, G. V., Mironov, A., Bachi, A., Fornasari, L., Bongetta, D., Gaetani, P., DiMeco, F., Lorico, A., & Pelicci, G. (2019). Clinical Significance of Extracellular Vesicles in Plasma from Glioblastoma Patients. *Clinical cancer research 25*(1), 266–276. *Impact factor: 8.9*

2. Famà, R., Borroni, E., Merlin, S., Airoldi, C., Pignani, S., Cucci, A., Corà, D., Bruscaggin, V., Scardellato, S., **Faletti, S**., Pelicci, G., Pinotti, M., Walker, G. E., & Follenzi, A. (2020). Deciphering the Ets-1/2-mediated transcriptional regulation of F8 gene identifies a minimal F8 promoter for hemophilia A gene therapy. *Haematologica*,2019.239202. Advance online publication.
   Impact factor: 7.1

Manuscript submitted:

Faletti, S[#]., Osti, D[#]., Ceccacci, E., Richichi, C., Costanza, B., Nicosia, L., Noberini, R., Marotta, G., Faretta, M., Brambillasca, S., Quarto, M., Bertero, L., Boldorini, R., Pollo, B., Gandini, S., Cora', D., Minucci, S., Mercurio, C., Varasi, M., Bonaldi, T., Pelicci, G.
LSD1-directed therapy affects glioblastoma tumorigenicity by deregulating the protective ATF4-dependent integrated stress response
[#] "These authors contributed equally"

10. REFERENCES

1. Louis, D. N. *et al.* The 2007 WHO classification of tumours of the central nervous system. *Acta Neuropathologica* **114**, 97–109 (2007).
2. Ostrom, Q. T. *et al.* CBTRUS Statistical Report: Primary brain and other central nervous system tumors diagnosed in the United States in 2010-2014. *Neuro. Oncol.* **19**, v1–v88 (2017).
3. Ostrom, Q. T. *et al.* The epidemiology of glioma in adults: A state of the science review. *Neuro-Oncology* **16**, 896–913 (2014).
4. Blakeley, J. & Grossman, S. Anaplastic oligodendroglioma. *Current Treatment Options in Neurology* **10**, 295–307 (2008).
5. Ohgaki, H. & Kleihues, P. Genetic pathways to primary and secondary glioblastoma. *American Journal of Pathology* **170**, 1445–1453 (2007).
6. Stupp, R., Hegi, M. E., Gilbert, M. R. & Chakravarti, A. Chemoradiotherapy in malignant glioma: Standard of care and future directions. *Journal of Clinical Oncology* **25**, 4127–4136 (2007).
7. McLendon, R. *et al.* Comprehensive genomic characterization defines human glioblastoma genes and core pathways. *Nature* **455**, 1061–1068 (2008).
8. Parsons, D. W. *et al.* An integrated genomic analysis of human glioblastoma multiforme. *Science (80-.).* **321**, 1807–1812 (2008).
9. Huse, J. T. & Holland, E. C. Genetically engineered mouse models of brain cancer and the promise of preclinical testing. in *Brain Pathology* **19**, 132–143 (John Wiley & Sons, Ltd, 2009).
10. Brennan, C. W. *et al.* The somatic genomic landscape of glioblastoma. *Cell* **155**, 462–77 (2013).
11. Sugawa, N., Ekstrand, A. J., James, C. D. & Collins, V. P. Identical splicing of aberrant epidermal growth factor receptor transcripts from amplified rearranged genes in human glioblastomas. *Proc. Natl. Acad. Sci. U. S. A.* **87**, 8602–8606 (1990).
12. Katanasaka, Y. *et al.* Epidermal growth factor receptor variant type III markedly accelerates angiogenesis and tumor growth via inducing c-myc mediated angiopoietin-like 4 expression in malignant glioma. *Mol. Cancer* **12**, 31 (2013).
13. Bonavia, R. *et al.* EGFRvIII promotes glioma angiogenesis and growth through the NF-B, interleukin-8 pathway. *Oncogene* **31**, 4054–4066 (2012).
14. Martinho, O. *et al.* Expression, mutation and copy number analysis of platelet-derived growth factor receptor A (PDGFRA) and its ligand PDGFA in gliomas. *Br. J. Cancer* **101**, 973–982 (2009).
15. Clarke, I. D. & Dirks, P. B. A human brain tumor-derived PDGFR-**α** deletion mutant is transforming. *Oncogene* **22**, 722–733 (2003).
16. Shih, A. H. *et al.* Dose-dependent effects of platelet-derived growth factor-B on glial tumorigenesis. *Cancer Res.* **64**, 4783–4789 (2004).
17. Abounader, R. & Laterra, J. Scatter factor/hepatocyte growth factor in brain tumor growth and angiogenesis. *Neuro-Oncology* **7**, 436–451 (2005).
18. Huang, M. *et al.* c-Met-mediated endothelial plasticity drives aberrant vascularization and chemoresistance in glioblastoma. *J. Clin. Invest.* **126**, 1801–1814 (2016).
19. Walter, K. A. *et al.* Scatter Factor/Hepatocyte Growth Factor Stimulation of Glioblastoma Cell Cycle Progression through G1 Is c-Myc Dependent and Independent of p27 Suppression, Cdk2 Activation, or E2F1-Dependent Transcription. *Mol. Cell. Biol.* **22**, 2703–2715 (2002).
20. De Bacco, F. *et al.* MET inhibition overcomes radiation resistance of glioblastoma stem-like cells . *EMBO Mol. Med.* **8**, 550–568 (2016).
21. Soroceanu, L. *et al.* Identification of IGF2 signaling through phosphoinositide-3-kinase regulatory subunit 3 as a growth-promoting axis in glioblastoma. *Proc. Natl. Acad. Sci. U. S. A.* **104**, 3466–3471 (2007).
22. Cantley, L. C. The phosphoinositide 3-kinase pathway. *Science* **296**, 1655–1657 (2002).
23. Dhillon, A. S., Hagan, S., Rath, O. & Kolch, W. MAP kinase signalling pathways in cancer. *Oncogene* **26**, 3279–3290 (2007).
24. Hartmann, C., Bartels, G., Gehlhaar, C., Holtkamp, N. & von Deimling, A. PIK3CA mutations in glioblastoma multiforme. *Acta Neuropathol.* **109**, 639–642 (2005).
25. Weber, G. L., Parat, M. O., Binder, Z. A., Gallia, G. L. & Riggins, G. J. Abrogation of PIK3CA or PIK3R1 reduces proliferation, migration, and invasion in glioblastoma multiforme cells. *Oncotarget* **2**, 833–849 (2011).
26. Lam, P. Y. P. *et al.* Expression of p19(INK4d), CDK4, CDK6 in glioblastoma multiforme. *Br. J. Neurosurg.* **14**, 28–32 (2000).
27. Halatsch, M. E., Schmidt, U., Unterberg, A. & Vougioukas, V. I. Uniform MDM2 overexpression in a panel of glioblastoma multiforme cell lines with divergent EGFR and p53 expression status. *Anticancer Res.* **26**, 4191–4194 (2006).
28. Kraus, J. A. *et al.* Molecular analysis of the PTEN, TP53 and CDKN2A tumor suppressor genes in long-term survivors of glioblastoma multiforme. *J. Neurooncol.* **48**, 89–94 (2000).
29. Yan, H. *et al.* IDH1 and IDH2 mutations in gliomas. *N. Engl. J. Med.* **360**, 765–773 (2009).
30. Noushmehr, H. *et al.* Identification of a CpG Island Methylator Phenotype that Defines a Distinct Subgroup of Glioma. *Cancer Cell* **17**, 510–522 (2010).
31. Turcan, S. *et al.* IDH1 mutation is sufficient to establish the glioma hypermethylator phenotype. *Nature* **483**, 479–483 (2012).
32. Nakamura, M. *et al. Loss of heterozygosity on chromosome 19 in secondary glioblastomas. Journal of Neuropathology and Experimental Neurology* **59**, (2000).
33. Erridge, S. C. *et al.* Trends in classification, referral and treatment and the effect on outcome of patients with glioma: A 20 year cohort. *J. Neurooncol.* **104**, 789–800 (2011).
34. Pollo, B. Neuropathological diagnosis of brain tumours. *Neurol. Sci.* **32 Suppl 2**, 209–211 (2011).
35. Louis, D. N. *et al.* The 2016 World Health Organization Classification of Tumors of the Central Nervous System: a summary. *Acta Neuropathol.* **131**, 803–820 (2016).
36. Nutt, C. L. *et al.* Gene expression-based classification of malignant gliomas correlates better with survival than histological classification. *Cancer Res.* **63**, 1602–1607 (2003).
37. Kurian, K. M., Haynes, H. R., Crosby, C., Hopkins, K. & Williams, M. IDH mutation analysis in gliomas as a diagnostic and prognostic biomarker. *Br. J. Neurosurg.* **27**, 442–445 (2013).
38. Weller, M. *et al.* Molecular neuro-oncology in clinical practice: A new horizon. *The Lancet Oncology* **14**, e370-9 (2013).
39. Boots-Sprenger, S. H. E. *et al.* Significance of complete 1p/19q co-deletion, IDH1 mutation and

MGMT promoter methylation in gliomas: Use with caution. *Mod. Pathol.* **26**, 922–929 (2013).
40. Leu, S. *et al.* IDH/MGMT-driven molecular classification of low-grade glioma is a strong predictor for long-term survival. *Neuro. Oncol.* **15**, 469–479 (2013).
41. Hegi, M. E. *et al.* MGMT gene silencing and benefit from temozolomide in glioblastoma. *N. Engl. J. Med.* **352**, 997–1003 (2005).
42. Shirahata, M. *et al.* Gene expression-based molecular diagnostic system for malignant gliomas is superior to histological diagnosis. *Clin. Cancer Res.* **13**, 7341–7356 (2007).
43. Shai, R. *et al.* Gene expression profiling identifies molecular subtypes of gliomas. *Oncogene* **22**, 4918–4923 (2003).
44. Tso, C. L. *et al.* Distinct transcription profiles of primary and secondary glioblastoma subgroups. *Cancer Res.* **66**, 159–167 (2006).
45. Faury, D. *et al.* Molecular profiling identifies prognostic subgroups of pediatric glioblastoma and shows increased YB-1 expression in tumors. *J. Clin. Oncol.* **25**, 1196–1208 (2007).
46. Freije, W. A. *et al.* Gene expression profiling of gliomas strongly predicts survival. *Cancer Res.* **64**, 6503–6510 (2004).
47. Nigro, J. M. *et al.* Integrated array-comparative genomic hybridization and expression array profiles identify clinically relevant molecular subtypes of glioblastoma. *Cancer Res.* **65**, 1678–1686 (2005).
48. Verhaak, R. G. W. *et al.* Integrated Genomic Analysis Identifies Clinically Relevant Subtypes of Glioblastoma Characterized by Abnormalities in PDGFRA, IDH1, EGFR, and NF1. *Cancer Cell* **17**, 98–110 (2010).
49. Vital, A. L. *et al.* Gene expression profiles of human glioblastomas are associated with both tumor cytogenetics and histopathology. *Neuro-Oncology* **12**, 991–1003 (2010).
50. Phillips, H. S. *et al.* Molecular subclasses of high-grade glioma predict prognosis, delineate a pattern of disease progression, and resemble stages in neurogenesis. *Cancer Cell* **9**, 157–173 (2006).
51. Carro, M. S. *et al.* The transcriptional network for mesenchymal transformation of brain tumours. *Nature* **463**, 318–325 (2010).
52. Bartek, J. *et al.* Key concepts in glioblastoma therapy. *J. Neurol. Neurosurg. Psychiatry* **83**, 753–760 (2012).
53. Madhavan, S. *et al.* Rembrandt: Helping personalized medicine become a reality through integrative translational research. *Mol. Cancer Res.* **7**, 157–167 (2009).
54. Brennan, C. *et al.* Glioblastoma subclasses can be defined by activity among signal transduction pathways and associated genomic alterations. *PLoS One* **4**, e7752 (2009).
55. Colman, H. *et al.* A multigene predictor of outcome in glioblastoma. *Neuro. Oncol.* **12**, 49–57 (2010).
56. Van Tellingen, O. *et al.* Overcoming the blood-brain tumor barrier for effective glioblastoma treatment. *Drug Resistance Updates* **19**, 1–12 (2015).
57. Bao, S. *et al.* Glioma stem cells promote radioresistance by preferential activation of the DNA damage response. *Nature* **444**, 756–760 (2006).
58. De Bonis, P. *et al.* The influence of surgery on recurrence pattern of glioblastoma. *Clin. Neurol. Neurosurg.* **115**, 37–43 (2013).
59. Hadjipanayis, C. G. & Stummer, W. 5-ALA and FDA approval for glioma surgery. *Journal of Neuro-Oncology* **141**, 479–486 (2019).
60. Greene-Schloesser, D. *et al.* Radiation-induced brain injury: A review. *Frontiers in Oncology* **2 JUL**, 73 (2012).
61. Reithmeier, T. *et al.* BCNU for recurrent glioblastoma multiforme: Efficacy, toxicity and prognostic factors. *BMC Cancer* **10**, 30 (2010).
62. Schmidt, F. *et al.* PCV chemotherapy for recurrent glioblastoma. *Neurology* **66**, 587–589 (2006).
63. Stupp, R. *et al.* Radiotherapy plus concomitant and adjuvant temozolomide for glioblastoma. *N. Engl. J. Med.* **352**, 987–996 (2005).
64. Giladi, M. *et al.* Mitotic Spindle Disruption by Alternating Electric Fields Leads to Improper Chromosome Segregation and Mitotic Catastrophe in Cancer Cells. *Sci. Rep.* **5**, 18046 (2015).
65. Stupp, R. *et al.* Effect of tumor-treating fields plus maintenance temozolomide vs maintenance temozolomide alone on survival in patients with glioblastoma a randomized clinical trial. *JAMA - J. Am. Med. Assoc.* **318**, 2306–2316 (2017).
66. Dong, Q., He, L., Chen, L. & Deng, Q. Opening the Blood-Brain Barrier and Improving the Efficacy of Temozolomide Treatments of Glioblastoma Using Pulsed, Focused Ultrasound with a Microbubble Contrast Agent. *Biomed Res. Int.* **2018**, 6501508 (2018).
67. Castillo, L. *et al.* Pharmacological background of EGFR targeting. *Annals of Oncology* **15**, 1007–1012 (2004).
68. Rich, J. N. *et al.* Phase II trial of gefitinib in recurrent glioblastoma. *J. Clin. Oncol.* **22**, 133–142 (2004).
69. Chakravarti, A. *et al.* RTOG 0211: A phase 1/2 study of radiation therapy with concurrent gefitinib for newly diagnosed glioblastoma patients. *Int. J. Radiat. Oncol. Biol. Phys.* **85**, 1206–1211 (2013).
70. Prados, M. D. *et al.* Phase II study of erlotinib plus temozolomide during and after radiation therapy in patients with newly diagnosed glioblastoma multiforme or gliosarcoma. *J. Clin. Oncol.* **27**, 579–584 (2009).
71. Van Den Bent, M. J. *et al.* Randomized phase II trial of erlotinib versus temozolomide or carmustine in recurrent glioblastoma: EORTC brain tumor group study 26034. *J. Clin. Oncol.* **27**, 1268–1274 (2009).
72. Sathornsumetee, S. *et al.* Phase II trial of bevacizumab and erlotinib in patients with recurrent malignant glioma. *Neuro. Oncol.* **12**, 1300–1310 (2010).
73. Reardon, D. A. *et al.* Phase I/randomized phase II study of afatinib, an irreversible ErbB family blocker, with or without protracted temozolomide in adults with recurrent glioblastoma. *Neuro. Oncol.* **17**, 430–439 (2015).
74. Liu, X. *et al.* The third-generation EGFR inhibitor AZD9291 overcomes primary resistance by continuously blocking ERK signaling in glioblastoma. *J. Exp. Clin. Cancer Res.* **38**, 219 (2019).
75. Neyns, B. *et al.* Stratified phase II trial of cetuximab in patients with recurrent high-grade glioma. *Ann. Oncol.* **20**, 1596–1603 (2009).
76. Choi, B. D. *et al.* EGFRvIII-targeted vaccination therapy of malignant glioma. in *Brain Pathology* **19**, 713–723 (NIH Public Access, 2009).
77. Platten, M. EGFRvIII vaccine in glioblastoma-InACT-IVe or not ReACTive enough? *Neuro-Oncology* **19**, 1425–1426 (2017).
78. Dresemann, G. *et al.* Imatinib in combination with hydroxyurea versus hydroxyurea alone as oral therapy in patients with progressive pretreated glioblastoma resistant to standard dose temozolomide. *J. Neurooncol.* **96**, 393–402 (2010).
79. Kalpathy-Cramer, J. *et al.* Phase II study of tivozanib, an oral VEGFR inhibitor, in patients with recurrent

glioblastoma. *J. Neurooncol.* **131**, 603–610 (2017).
80. Iwamoto, F. M. *et al.* Phase II trial of pazopanib (GW786034), an oral multi-targeted angiogenesis inhibitor, for adults with recurrent glioblastoma (North American Brain Tumor Consortium Study 06-02). *Neuro. Oncol.* **12**, 855–861 (2010).
81. Vredenburgh, J. J. *et al.* Phase II trial of bevacizumab and irinotecan in recurrent malignant glioma. *Clin. Cancer Res.* **13**, 1253–1259 (2007).
82. Cohen, M. H., Shen, Y. L., Keegan, P. & Pazdur, R. FDA Drug Approval Summary: Bevacizumab (Avastin®) as Treatment of Recurrent Glioblastoma Multiforme. *Oncologist* **14**, 1131–1138 (2009).
83. Yang, S. B., Gao, K. Di, Jiang, T., Cheng, S. J. & Li, W. Bin. Bevacizumab combined with chemotherapy for glioblastoma: A meta-analysis of randomized controlled trials. *Oncotarget* **8**, 57337–57344 (2017).
84. De Groot, J. F. *et al.* Phase II study of aflibercept in recurrent malignant glioma: A North American brain tumor consortium study. *J. Clin. Oncol.* **29**, 2689–2695 (2011).
85. Di Tomaso, E. *et al.* Glioblastoma recurrence after cediranib therapy in patients: Lack of 'rebound' revascularization as mode of escape. *Cancer Res.* **71**, 19–28 (2011).
86. Zustovich, F. *et al.* Sorafenib plus daily low-dose temozolomide for relapsed glioblastoma: A phase ii study. *Anticancer Res.* **33**, 3487–3494 (2013).
87. Grisanti, S. *et al.* Second line treatment of recurrent glioblastoma with sunitinib: Results of a phase IIstudy and systematic review of literature. *Journal of Neurosurgical Sciences* **63**, 458–467 (2019).
88. Lee, E. Q. *et al.* A multicenter, phase II, randomized, noncomparative clinical trial of radiation and temozolomide with or without vandetanib in newly diagnosed glioblastoma patients. *Clin. Cancer Res.* **21**, 3610–3618 (2015).
89. Fidler, I. J. & Hart, I. R. Biological diversity in metastatic neoplasms: Origins and implications. *Science* **217**, 998–1003 (1982).
90. McGranahan, T., Elizabeth Therkelsen, K., Ahmad, S. & Nagpal, S. Current State of Immunotherapy for Treatment of Glioblastoma. *Options in Oncol* **20**, 24 (2019).
91. Qazi, M. A. *et al.* Intratumoral heterogeneity: Pathways to treatment resistance and relapse in human glioblastoma. *Ann. Oncol.* **28**, 1448–1456 (2017).
92. Shi, X., Chakraborty, P. & Chaudhuri, A. Unmasking tumor heterogeneity and clonal evolution by single-cell analysis. *J. Cancer Metastasis Treat.* **4**, 47 (2018).
93. Patel, A. P. *et al.* Single-cell RNA-seq highlights intratumoral heterogeneity in primary glioblastoma. *Science (80-.).* **344**, 1396–1401 (2014).
94. Couturier, C. P. *et al.* Single-cell RNA-seq reveals that glioblastoma recapitulates a normal neurodevelopmental hierarchy. *Nat. Commun.* **11**, 3406 (2020).
95. Nowell, P. C. The clonal evolution of tumor cell populations. *Science (80-.).* **194**, 23–28 (1976).
96. Campbell, L. L. & Polyak, K. Breast tumor heterogeneity: Cancer stem cells or clonal evolution? *Cell Cycle* **6**, 2332–2338 (2007).
97. Bonnet, D. & Dick, J. E. Human acute myeloid leukemia is organized as a hierarchy that originates from a primitive hematopoietic cell. *Nat. Med.* **3**, 730–737 (1997).
98. Reya, T., Morrison, S. J., Clarke, M. F. & Weissman, I. L. Stem cells, cancer, and cancer stem cells. *Nature* **414**, 105–111 (2001).
99. Shackleton, M., Quintana, E., Fearon, E. R. & Morrison, S. J. Heterogeneity in Cancer: Cancer Stem Cells versus Clonal Evolution. *Cell* **138**, 822–829 (2009).
100. Meacham, C. E. & Morrison, S. J. Tumour heterogeneity and cancer cell plasticity. *Nature* **501**, 328–337 (2013).
101. Soto, C. *et al.* **β**-sheet breaker peptides inhibit fibrillogenesis in a rat brain model of amyloidosis: Implications for Alzheimer's therapy. *Nat. Med.* **4**, 822–826 (1998).
102. Hemmati, H. D. *et al.* Cancerous stem cells can arise from pediatric brain tumors. *Proc. Natl. Acad. Sci. U. S. A.* **100**, 15178–15183 (2003).
103. Singh, S. K. *et al.* Identification of human brain tumour initiating cells. *Nature* **432**, 396–401 (2004).
104. Al-Hajj, M., Wicha, M. S., Benito-Hernandez, A., Morrison, S. J. & Clarke, M. F. Prospective identification of tumorigenic breast cancer cells. *Proc. Natl. Acad. Sci. U. S. A.* **100**, 3983–3988 (2003).
105. O'Brien, C. A., Pollett, A., Gallinger, S. & Dick, J. E. A human colon cancer cell capable of initiating tumour growth in immunodeficient mice. *Nature* **445**, 106–110 (2007).
106. Li, C. *et al.* Identification of pancreatic cancer stem cells. *Cancer Res.* **67**, 1030–1037 (2007).
107. Garcia-Mayea, Y., Mir, C., Masson, F., Paciucci, R. & LLeonart, M. E. Insights into new mechanisms and models of cancer stem cell multidrug resistance. *Semin. Cancer Biol.* **60**, 166–180 (2020).
108. Liu, G. *et al.* Analysis of gene expression and chemoresistance of CD133+ cancer stem cells in glioblastoma. *Mol. Cancer* **5**, 1–12 (2006).
109. Chen, J. *et al.* A restricted cell population propagates glioblastoma growth after chemotherapy. *Nature* **488**, 522–526 (2012).
110. Bao, S. *et al.* Stem cell-like glioma cells promote tumor angiogenesis through vascular endothelial growth factor. *Cancer Res.* **66**, 7843–7848 (2006).
111. Thomas, D. *et al.* Increased cancer stem cell invasion is mediated by myosin IIB and nuclear translocation. *Oncotarget* **7**, 47586–47592 (2016).
112. Yang, J. & Weinberg, R. A. Epithelial-Mesenchymal Transition: At the Crossroads of Development and Tumor Metastasis. *Developmental Cell* **14**, 818–829 (2008).
113. Rich, J. N. Cancer stem cells: Understanding tumor hierarchy and heterogeneity. *Medicine (United States)* **95**, S2–S7 (2016).
114. Barabé, F., Kennedy, J. A., Hope, K. J. & Dick, J. E. Modeling the initiation and progression of human acute leukemia in mice. *Science (80-.).* **316**, 600–604 (2007).
115. Cabrera, M. C. Cancer stem cell plasticity and tumor hierarchy. *World J. Stem Cells* **7**, 27 (2015).
116. Laks, D. R., Visnyei, K. & Kornblum, H. I. Brain tumor stem cells as therapeutic targets in models of glioma. *Yonsei Medical Journal* **51**, 633–640 (2010).
117. Gimple, R. C., Bhargava, S., Dixit, D. & Rich, J. N. Glioblastoma stem cells: Lessons from the tumor hierarchy in a lethal cancer. *Genes and Development* **33**, 591–609 (2019).
118. Holland, E. C. Glioblastoma multiforme: The terminator. *Proc. Natl. Acad. Sci. U. S. A.* **97**, 6242–6244 (2000).
119. Uhrbom, L. *et al.* Ink4a-Arf loss cooperates with KRas activation in astrocytes and neural progenitors to generate glioblastomas of various morphologies depending on activated Akt. *Cancer Res.* **62**, 5551–5558 (2002).
120. Bachoo, R. M. *et al.* Epidermal growth factor receptor and Ink4a/Arf: Convergent mechanisms governing terminal differentiation and transformation along the neural stem cell to astrocyte axis. *Cancer*

Cell **1**, 269–277 (2002).
121. Stiles, C. D. & Rowitch, D. H. Glioma Stem Cells: A Midterm Exam. *Neuron* **58**, 832–846 (2008).
122. Hanahan, D. & Weinberg, R. A. The hallmarks of cancer. *Cell* **100**, 57–70 (2000).
123. Calabrese, C. *et al.* A Perivascular Niche for Brain Tumor Stem Cells. *Cancer Cell* **11**, 69–82 (2007).
124. Ignatova, T. N. *et al.* Human cortical glial tumors contain neural stem-like cells expressing astroglial and neuronal markers in vitro. *Glia* **39**, 193–206 (2002).
125. Galli, R. *et al. Isolation and Characterization of Tumorigenic, Stem-like Neural Precursors from Human Glioblastoma. CANCER RESEARCH* **64**, (2004).
126. Wang, J. *et al.* CD133 negative glioma cells form tumors in nude rats and give rise to CD133 positive cells. *Int. J. Cancer* **122**, 761–768 (2008).
127. Richichi, C., Brescia, P., Alberizzi, V., Fornasari, L. & Pelicci, G. Marker-independent method for isolating slow-dividing cancer stem cells in human glioblastoma. *Neoplasia (United States)* **15**, 840–847 (2013).
128. Brescia, P., Richichi, C. & Pelicci, G. Current Strategies for Identification of Glioma Stem Cells: Adequate or Unsatisfactory? *J. Oncol.* **2012**, 1–10 (2012).
129. Gilbertson, R. J. & Rich, J. N. Making a tumour's bed: Glioblastoma stem cells and the vascular niche. *Nature Reviews Cancer* **7**, 733–736 (2007).
130. Vescovi, A. L., Galli, R. & Reynolds, B. A. Brain tumour stem cells. *Nature Reviews Cancer* **6**, 425–436 (2006).
131. Vik-Mo, E. O. *et al.* Brain tumor stem cells maintain overall phenotype and tumorigenicity after in vitro culturing in serum-free conditions. *Neuro. Oncol.* **12**, 1220–1230 (2010).
132. Suslov, O. N., Kukekov, V. G., Ignatova, T. N. & Steindler, D. A. Neural stem cell heterogeneity demonstrated by molecular phenotyping of clonal neurospheres. *Proc. Natl. Acad. Sci. U. S. A.* **99**, 14506–14511 (2002).
133. Richichi, C. *et al.* Tumor-initiating cell frequency is relevant for glioblastoma aggressiveness. *Oncotarget* **7**, (2016).
134. Nakai, E. *et al.* Enhanced mdr1 expression and chemoresistance of cancer stem cells derived from glioblastoma. *Cancer Invest.* **27**, 901–908 (2009).
135. Eramo, A. *et al.* Chemotherapy resistance of glioblastoma stem cells [2]. *Cell Death and Differentiation* **13**, 1238–1241 (2006).
136. Piccirillo, S. G. & Vescovi, A. L. Bone morphogenetic proteins regulate tumorigenicity in human glioblastoma stem cells. *Ernst Schering Foundation symposium proceedings* **5**, 59–81 (2006).
137. Ricci-Vitiani, L. *et al.* Tumour vascularization via endothelial differentiation of glioblastoma stem-like cells. *Nature* **468**, 824–830 (2010).
138. Prager, B. C., Bhargava, S., Mahadev, V., Hubert, C. G. & Rich, J. N. Glioblastoma Stem Cells: Driving Resilience through Chaos. *Trends in Cancer* **6**, 223–235 (2020).
139. Rheinbay, E. *et al.* An Aberrant Transcription Factor Network Essential for Wnt Signaling and Stem Cell Maintenance in Glioblastoma. *Cell Rep.* **3**, 1567–1579 (2013).
140. Scadden, D. T. The stem-cell niche as an entity of action. *Nature* **441**, 1075–1079 (2006).
141. Dirkse, A. *et al.* Stem cell-associated heterogeneity in Glioblastoma results from intrinsic tumor plasticity shaped by the microenvironment. *Nat. Commun.* **10**, 1787 (2019).
142. Zhu, T. S. *et al.* Endothelial cells create a stem cell niche in glioblastoma by providing NOTCH ligands that nurture self-renewal of cancer stem-like cells. *Cancer Res.* **71**, 6061–6072 (2011).
143. Rao, S. *et al.* CXCL12 mediates trophic interactions between endothelial and tumor cells in glioblastoma. *PLoS One* **7**, (2012).
144. Jain, R. K. *et al.* Angiogenesis in brain tumours. *Nat. Rev. Neurosci.* **8**, 610–622 (2007).
145. Brooks, M. D., Sengupta, R., Snyder, S. C. & Rubin, J. B. Hitting Them Where They Live: Targeting the Glioblastoma Perivascular Stem Cell Niche. *Curr. Pathobiol. Rep.* **1**, 101–110 (2013).
146. Hardee, M. E. *et al.* Resistance of glioblastoma-initiating cells to radiation mediated by the tumor microenvironment can be abolished by inhibiting transforming growth factor-**β**. *Cancer Res.* **72**, 4119–4129 (2012).
147. Semenza, G. L. HIF-1 mediates metabolic responses to intratumoral hypoxia and oncogenic mutations. *Journal of Clinical Investigation* **123**, 3664–3671 (2013).
148. Covello, K. L. *et al.* HIF-2**α** regulates Oct-4: Effects of hypoxia on stem cell function, embryonic development, and tumor growth. *Genes Dev.* **20**, 557–570 (2006).
149. Cheng, L. *et al.* Elevated invasive potential of glioblastoma stem cells. *Biochem. Biophys. Res. Commun.* **406**, 643–648 (2011).
150. Velpula, K. K. *et al.* Glioma stem cell invasion through regulation of the interconnected ERK, integrin **α**6 and N-cadherin signaling pathway. *Cell. Signal.* **24**, 2076–2084 (2012).
151. Reik, W. Stability and flexibility of epigenetic gene regulation in mammalian development. *Nature* **447**, 425–432 (2007).
152. Hoffmeyer, K. *et al.* Wnt/**β**-catenin signaling regulates telomerase in stem cells and cancer cells. *Science (80-.).* **336**, 1549–1554 (2012).
153. Klarmann, G. J., Decker, A. & Farrar, W. L. Epigenetic gene silencing in the Wnt pathway in breast cancer. *Epigenetics* **3**, 59–63 (2008).
154. Canettieri, G. *et al.* Histone deacetylase and Cullin3-REN KCTD11 ubiquitin ligase interplay regulates Hedgehog signalling through Gli acetylation. *Nat. Cell Biol.* **12**, 132–142 (2010).
155. Duan, Z. H. *et al.* Cooperatively transcriptional and epigenetic regulation of sonic hedgehog overexpression drives malignant potential of breast cancer. *Cancer Sci.* **106**, 1084–1091 (2015).
156. Ghoshal, P. *et al.* Loss of the SMRT/NCoR2 corepressor correlates with JAG2 overexpression in multiple myeloma. *Cancer Res.* **69**, 4380–4387 (2009).
157. Jin, L., Vu, T., Yuan, G. & Datta, P. K. STRAP promotes stemness of human colorectal cancer via epigenetic regulation of the NOTCH pathwaya. *Cancer Res.* **77**, 5464–5478 (2017).
158. Zhou, D. *et al.* Distinctive epigenomes characterize glioma stem cells and their response to differentiation cues. *Genome Biol.* **19**, (2018).
159. Pangeni, R. P. *et al.* Genome-wide methylomic and transcriptomic analyses identify subtype-specific epigenetic signatures commonly dysregulated in glioma stem cells and glioblastoma. *Epigenetics* **13**, 432–448 (2018).
160. Strahl, B. D. & Allis, C. D. The language of covalent histone modifications. *Nature* **403**, 41–45 (2000).
161. Martin, C. & Zhang, Y. The diverse functions of histone lysine methylation. *Nature Reviews Molecular Cell Biology* **6**, 838–849 (2005).
162. Hou, H. & Yu, H. Structural insights into histone lysine

demethylation. *Current Opinion in Structural Biology* **20**, 739–748 (2010).
163. Shi, Y. *et al. Histone Demethylation Mediated by the Nuclear Amine Oxidase Homolog LSD1 instance, histone H3 K9 (H3-K9) methylation is associ-ated with heterochromatin formation (Nakayama et al and also. The Sidney Kimmel Comprehensive Cancer Center* **119**, (2004).
164. Forneris, F., Binda, C., Vanoni, M. A., Mattevi, A. & Battaglioli, E. Histone demethylation catalysed by LSD1 is a flavin-dependent oxidative process. *FEBS Lett.* **579**, 2203–2207 (2005).
165. Chen, Y. *et al.* Crystal structure of human histone lysine-specific demethlase 1 (LSD1). *Proc. Natl. Acad. Sci. U. S. A.* **103**, 13956–13961 (2006).
166. Stavropoulos, P., Blobel, G. & Hoelz, A. Crystal structure and mechanism of human lysine-specific demethylase-1. *Nat. Struct. Mol. Biol.* **13**, 626–632 (2006).
167. Wang, Y. *et al.* LSD1 Is a Subunit of the NuRD Complex and Targets the Metastasis Programs in Breast Cancer. *Cell* **138**, 660–672 (2009).
168. Shi, Y. J. *et al.* Regulation of LSD1 histone demethylase activity by its associated factors. *Mol. Cell* **19**, 857–864 (2005).
169. Metzger, E. *et al.* LSD1 demethylates repressive histone marks to promote androgen-receptor-dependent transcription. (2005). doi:10.1038/nature04020
170. Lee, M. G., Wynder, C., Cooch, N. & Shiekhattar, R. An essential role for CoREST in nucleosomal histone 3 lysine 4 demethylation. *Nature* (2005). doi:10.1038/nature04021
171. Ballas, N., Grunseich, C., Lu, D. D., Speh, J. C. & Mandel, G. REST and its corepressors mediate plasticity of neuronal gene chromatin throughout neurogenesis. *Cell* **121**, 645–657 (2005).
172. Lan, F. *et al.* Recognition of unmethylated histone H3 lysine 4 links BHC80 to LSD1-mediated gene repression. *Nature* **448**, 718–722 (2007).
173. Lin, Y. *et al.* The SNAG domain of snail1 functions as a molecular hook for recruiting lysine-specific demethylase 1. *EMBO J.* **29**, 1803–1816 (2010).
174. Saleque, S., Kim, J., Rooke, H. M. & Orkin, S. H. Epigenetic Regulation of Hematopoietic Differentiation by Gfi-1 and Gfi-1b Is Mediated by the Cofactors CoREST and LSD1. *Mol. Cell* **27**, 562–572 (2007).
175. Patel, D., Shimomura, A., Majumdar, S., Holley, M. C. & Hashino, E. The histone demethylase LSD1 regulates inner ear progenitor differentiation through interactions with Pax2 and the NuRD repressor complex. *PLoS One* **13**, e0191689 (2018).
176. Ouyang, H., Qin, Y., Liu, Y., Xie, Y. & Liu, J. Prox1 Directly Interacts with LSD1 and Recruits the LSD1/NuRD Complex to Epigenetically Co-Repress CYP7A1 Transcription. *PLoS One* **8**, (2013).
177. Basta, J. & Rauchman, M. The nucleosome remodeling deacetylase (NuRD) complex in Development and Disease. *Transl. Res.* **165**, 36–47 (2009).
178. Whyte, W. A. *et al.* Enhancer decommissioning by LSD1 during embryonic stem cell differentiation. *Nature* **482**, 221–225 (2012).
179. Sankar, S. *et al.* Mechanism and relevance of EWS/FLI-mediated transcriptional repression in Ewing sarcoma. *Oncogene* **32**, 5089–5100 (2013).
180. Yokoyama, A., Takezawa, S., Schüle, R., Kitagawa, H. & Kato, S. Transrepressive Function of TLX Requires the Histone Demethylase LSD1. *Mol. Cell. Biol.* **28**, 3995–4003 (2008).
181. Metzger, E. *et al.* Phosphorylation of histone H3T6 by PKC**B** i controls demethylation at histone H3K4. *Nature* **464**, 792–796 (2010).
182. Nair, S. S. *et al.* PELP1 is a reader of histone H3 methylation that facilitates oestrogen receptor-**α** target gene activation by regulating lysine demethylase 1 specificity. *EMBO Rep.* **11**, 438–444 (2010).
183. Laurent, B. *et al.* A Specific LSD1/KDM1A Isoform Regulates Neuronal Differentiation through H3K9 Demethylation. *Mol. Cell* **57**, 957–970 (2015).
184. Wang, J. *et al.* LSD1n is an H4K20 demethylase regulating memory formation via transcriptional elongation control. *Nat. Neurosci.* **18**, 1256–1264 (2015).
185. Magliulo, D., Bernardi, R. & Messina, S. Lysine-specific demethylase 1A as a promising target in acute myeloid leukemia. *Frontiers in Oncology* **8**, 255 (2018).
186. Huang, J. *et al.* p53 is regulated by the lysine demethylase LSD1. *Nature* **449**, 105–108 (2007).
187. Kontaki, H. & Talianidis, I. Lysine Methylation Regulates E2F1-Induced Cell Death. *Mol. Cell* **39**, 152–160 (2010).
188. Cho, H. S. *et al.* Demethylation of RB regulator MYPT1 by histone demethylase LSD1 promotes cell cycle progression in cancer cells. *Cancer Res.* **71**, 655–660 (2011).
189. Bao, L. *et al.* Methylation of hypoxia-inducible factor (HIF)-1**α** by G9a/GLP inhibits HIF-1 transcriptional activity and cell migration. *Nucleic Acids Res.* **46**, 6576–6591 (2018).
190. Sheng, W. *et al.* LSD1 Ablation Stimulates Anti-tumor Immunity and Enables Checkpoint Blockade. *Cell* **174**, 549-563.e19 (2018).
191. Qin, Y. *et al.* Inhibition of histone lysine-specific demethylase 1 elicits breast tumor immunity and enhances antitumor efficacy of immune checkpoint blockade. *Oncogene* **38**, 390–405 (2019).
192. Wang, J. *et al.* Opposing LSD1 complexes function in developmental gene activation and repression programmes. *Nature* (2007). doi:10.1038/nature05671
193. Adamo, A. *et al.* LSD1 regulates the balance between self-renewal and differentiation in human embryonic stem cells. *Nat. Cell Biol.* **13**, 652–661 (2011).
194. Thambyrajah, R. *et al.* GFI1 proteins orchestrate the emergence of haematopoietic stem cells through recruitment of LSD1. *Nat. Cell Biol.* **18**, 21–32 (2016).
195. Schenk, T. *et al.* Inhibition of the LSD1 (KDM1A) demethylase reactivates the all-trans-retinoic acid differentiation pathway in acute myeloid leukemia. *Nat. Med.* **18**, 605–611 (2012).
196. Mosammaparast, N. *et al.* The histone demethylase LSD1/KDM1A promotes the DNA damage response. *J. Cell Biol.* **203**, 457–470 (2013).
197. Nam, H. J. *et al.* Phosphorylation of LSD1 by PKC**α** Is Crucial for Circadian Rhythmicity and Phase Resetting. *Mol. Cell* **53**, 791–805 (2014).
198. Sakamoto, A. *et al.* Lysine demethylase LSD1 coordinates glycolytic and mitochondrial metabolism in hepatocellular carcinoma cells. *Cancer Res.* **75**, 1445–1456 (2015).
199. Schulte, J. H. *et al.* Lysine-Specific Demethylase 1 Is Strongly Expressed in Poorly Differentiated Neuroblastoma: Implications for Therapy. *Cancer Res* **69**, 2065–71 (2009).
200. Hosseini, A. & Minucci, S. A comprehensive review of lysine-specific demethylase 1 and its roles in cancer. *Epigenomics* **9**, 1123–1142 (2017).
201. Hayami, S. *et al.* Overexpression of LSD1 contributes to human carcinogenesis through chromatin

regulation in various cancers. *Int. J. Cancer* **128**, 574–586 (2011).
202. Lim, S. *et al.* Lysine-specific demethylase 1 (LSD1) is highly expressed in ER-negative breast cancers and a biomarker predicting aggressive biology. *Carcinogenesis* **31**, 512–520 (2010).
203. Schulte, J. H. *et al.* Lysine-specific demethylase 1 is strongly expressed in poorly differentiated neuroblastoma: Implications for therapy. *Cancer Res.* **69**, 2065–2071 (2009).
204. Singh, M. M. *et al.* Inhibition of LSD1 sensitizes glioblastoma cells to histone deacetylase inhibitors. *Neuro. Oncol.* **13**, 894–903 (2011).
205. Lv, T. *et al.* Over-expression of LSD1 promotes proliferation, migration and invasion in non-small cell lung cancer. *PLoS One* **7**, e35065 (2012).
206. Maiques-Diaz, A. *et al.* Enhancer Activation by Pharmacologic Displacement of LSD1 from GFI1 Induces Differentiation in Acute Myeloid Leukemia. *Cell Rep.* **22**, 3641–3659 (2018).
207. Ambrosio, S. *et al.* LSD1 mediates MYCN control of epithelial-mesenchymal transition through silencing of metastatic suppressor NDRG1 gene. *Oncotarget* **8**, 3854–3869 (2017).
208. Mohammad, H. P. *et al.* A DNA Hypomethylation Signature Predicts Antitumor Activity of LSD1 Inhibitors in SCLC. *Cancer Cell* **28**, 57–69 (2015).
209. Serce, N. *et al.* Elevated expression of LSD1 (Lysine-specific demethylase 1) during tumour progression from pre-invasive to invasive ductal carcinoma of the breast. *BMC Clin. Pathol.* **12**, 13 (2012).
210. Pollock, J. A., Larrea, M. D., Jasper, J. S., McDonnell, D. P. & McCafferty, D. G. Lysine-specific histone demethylase 1 inhibitors control breast cancer proliferation in ER**α**-dependent and -independent manners. *ACS Chem. Biol.* **7**, 1221–1231 (2012).
211. Bai, J. W. *et al.* The zinc-finger transcriptional factor Slug transcriptionally downregulates ER**α** by recruiting lysine-specific demethylase 1 in human breast cancer. *Oncogenesis* **6**, e330–e330 (2017).
212. Maier, S. *et al.* SOX2 amplification is a common event in squamous cell carcinomas of different organ sites. *Hum. Pathol.* **42**, 1078–1088 (2011).
213. Leis, O. *et al.* Sox2 expression in breast tumours and activation in breast cancer stem cells. *Oncogene* **31**, 1354–1365 (2012).
214. Zhang, X. *et al.* Pluripotent Stem Cell Protein Sox2 Confers Sensitivity to LSD1 Inhibition in Cancer Cells. *Cell Rep.* **5**, 445–457 (2013).
215. Jie, D. *et al.* Positive expression of LSD1 and negative expression of E-cadherin correlate with metastasis and poor prognosis of colon cancer. *Dig. Dis. Sci.* **58**, 1581–1589 (2013).
216. Chen, J. *et al.* Identification of downstream metastasis-associated target genes regulated by LSD1 in colon cancer cells. *Oncotarget* **8**, 19609–19630 (2017).
217. Huang, Z. *et al.* Lysine-Specific Demethylase 1 (LSD1/KDM1A) Contributes to Colorectal Tumorigenesis via Activation of the Wnt/**B**-Catenin Pathway by Down-Regulating Dickkopf-1 (DKK1). *PLoS One* **8**, e70077 (2013).
218. Harris, W. J. *et al.* The Histone Demethylase KDM1A Sustains the Oncogenic Potential of MLL-AF9 Leukemia Stem Cells. *Cancer Cell* **21**, 473–487 (2012).
219. Maiques-Diaz, A., Lynch, J. T., Spencer, G. J. & Somervaille, T. C. P. LSD1 inhibitors disrupt the GFI1 transcription repressor complex. *Mol. Cell. Oncol.* **5**, e1481813 (2018).
220. Ishikawa, Y. *et al.* A Novel LSD1 Inhibitor T-3775440 Disrupts GFI1B-Containing Complex Leading to Transdifferentiation and Impaired Growth of AML Cells. *Mol. Cancer Ther.* **16**, 273–284 (2016).
221. Ravasio, R. *et al.* Targeting the scaffolding role of LSD1 (KDM1A) poises acute myeloid leukemia cells for retinoic acid-induced differentiation. *Sci. Adv.* **6**, (2020).
222. Lee, C. *et al.* Lsd1 as a therapeutic target in Gfi1-activated medulloblastoma. *Nat. Commun.* **10**, 332 (2019).
223. Sehrawat, A. *et al.* LSD1 activates a lethal prostate cancer gene network independently of its demethylase function. *Proc. Natl. Acad. Sci. U. S. A.* **115**, E4179–E4188 (2018).
224. Takagi, S. *et al.* LSD1 inhibitor T-3775440 inhibits SCLC cell proliferation by disrupting LSD1 interactions with SNAG domain proteins INSM1 and GFI1B. *Cancer Res.* **77**, 4652–4662 (2017).
225. Sareddy, G. R. *et al.* KDM1 is a novel therapeutic target for the treatment of gliomas. *Oncotarget* **4**, 18–28 (2013).
226. Saccà, C. D. *et al.* Inhibition of lysine-specific demethylase LSD1 induces senescence in Glioblastoma cells through a HIF-1**α**-dependent pathway. *Biochim. Biophys. Acta - Gene Regul. Mech.* **1862**, 535–546 (2019).
227. Sareddy, G. R. *et al.* Novel KDM1A inhibitors induce differentiation and apoptosis of glioma stem cells via unfolded protein response pathway. *Oncogene* **36**, 2423–2434 (2017).
228. Kozono, D. *et al.* Dynamic epigenetic regulation of glioblastoma tumorigenicity through LSD1 modulation of MYC expression. *Proc. Natl. Acad. Sci.* **112**, E4055–E4064 (2015).
229. Singh, M. M. *et al.* Preclinical activity of combined HDAC and KDM1A inhibition in glioblastoma. *Neuro. Oncol.* **17**, 1463–1473 (2015).
230. Engel, M. *et al.* Novel dual-action prodrug triggers apoptosis in glioblastoma cells by releasing a glutathione quencher and lysine-specific histone demethylase 1A inhibitor. *J. Neurochem.* **149**, 535–550 (2019).
231. Yang, M. *et al.* Structural basis for the inhibition of the LSD1 histone demethylase by the antidepressant trans-2-phenylcyclopropylamine. *Biochemistry* **46**, 8058–8065 (2007).
232. Fang, Y., Liao, G. & Yu, B. LSD1/KDM1A inhibitors in clinical trials: Advances and prospects. *Journal of Hematology and Oncology* **12**, 129 (2019).
233. Mould, D. P., McGonagle, A. E., Wiseman, D. H., Williams, E. L. & Jordan, A. M. Reversible inhibitors of LSD1 as therapeutic agents in acute myeloid leukemia: Clinical significance and progress to date. *Med. Res. Rev.* **35**, 586–618 (2015).
234. McGrath, J. P. *et al.* Pharmacological inhibition of the histone lysine demethylase KDM1A suppresses the growth of multiple acute myeloid leukemia subtypes. *Cancer Res.* **76**, 1975–1988 (2016).
235. Haydn, T., Metzger, E., Schuele, R. & Fulda, S. Concomitant epigenetic targeting of LSD1 and HDAC synergistically induces mitochondrial apoptosis in rhabdomyosarcoma cells. *Cell Death Dis.* **8**, e2879–e2879 (2017).
236. Sonnemann, J. *et al.* LSD1 (KDM1A)-independent effects of the LSD1 inhibitor SP2509 in cancer cells. *Br. J. Haematol.* **183**, 494–497 (2018).
237. Li, Z. *et al.* Development of the triazole-fused pyrimidine derivatives as highly potent and reversible inhibitors of histone lysine specific demethylase 1 (LSD1/KDM1A). *Acta Pharm. Sin. B* **9**, 794–808 (2019).
238. Li, L., Li, R. & Wang, Y. Identification of selective and reversible LSD1 inhibitors with anti-metastasis activity

by high-throughput docking. *Bioorganic Med. Chem. Lett.* **29**, 544–548 (2019).
239. Xi, J. *et al.* Design, synthesis and biological activity of 4-(4-benzyloxy)phenoxypiperidines as selective and reversible LSD1 inhibitors. *Bioorg. Chem.* **78**, 7–16 (2018).
240. Vianello, P. *et al.* Discovery of a Novel Inhibitor of Histone Lysine-Specific Demethylase 1A (KDM1A/LSD1) as Orally Active Antitumor Agent. *J. Med. Chem.* **59**, 1501–1517 (2016).
241. Ortensi, B. *et al.* Rai is a new regulator of neural progenitor migration and glioblastoma invasion. *Stem Cells* **30**, 817–832 (2012).
242. Hu, Y. & Smyth, G. K. ELDA: Extreme limiting dilution analysis for comparing depleted and enriched populations in stem cell and other assays. *J. Immunol. Methods* **347**, 70–78 (2009).
243. Baumann, B. C., Dorsey, J. F., Benci, J. L., Joh, D. Y. & Kao, G. D. Stereotactic intracranial implantation and in vivo bioluminescent imaging of tumor xenografts in a mouse model system of glioblastoma multiforme. *J. Vis. Exp.* (2012). doi:10.3791/4089
244. Dobin, A. *et al.* Sequence analysis STAR: ultrafast universal RNA-seq aligner. **29**, 15–21 (2013).
245. Liao, Y., Smyth, G. K. & Shi, W. FeatureCounts: An efficient general purpose program for assigning sequence reads to genomic features. *Bioinformatics* **30**, 923–930 (2014).
246. Robinson, M. D., McCarthy, D. J. & Smyth, G. K. edgeR: A Bioconductor package for differential expression analysis of digital gene expression data. *Bioinformatics* **26**, 139–140 (2009).
247. Blecher-Gonen, R. *et al.* High-throughput chromatin immunoprecipitation for genome-wide mapping of in vivo protein-DNA interactions and epigenomic states. *Nat. Protoc.* **8**, (2013).
248. Langmead, B., Trapnell, C., Pop, M. & Salzberg, S. L. Ultrafast and memory-efficient alignment of short DNA sequences to the human genome. *Genome Biol.* **10**, 25 (2009).
249. Zhang, Y. *et al.* Model-based Analysis of ChIP-Seq (MACS). (2008). doi:10.1186/gb-2008-9-9-r137
250. Gerstein, M. B. *et al.* Architecture of the human regulatory network derived from ENCODE data. *Nature* **489**, 91–100 (2012).
251. Zerbino, D. R. *et al.* Ensembl 2018. *Nucleic Acids Res.* **46**, D754–D761 (2018).
252. Quinlan, A. R. & Hall, I. M. BEDTools: A flexible suite of utilities for comparing genomic features. *Bioinformatics* **26**, 841–842 (2010).
253. Khan, A. *et al.* JASPAR 2018: Update of the open-access database of transcription factor binding profiles and its web framework. *Nucleic Acids Research* **46**, D1284 (2018).
254. Picelli, S. *et al.* Tn5 transposase and tagmentation procedures for massively scaled sequencing projects. *Genome Res.* **24**, 2033–2040 (2014).
255. Noberini, R., Restellini, C., Savoia, E. O. & Bonaldi, T. Enrichment of histones from patient samples for mass spectrometry-based analysis of post-translational modifications. *Methods* (2019). doi:10.1016/j.ymeth.2019.10.001
256. Noberini, R. & Bonaldi, T. A Super-SILAC Strategy for the Accurate and Multiplexed Profiling of Histone Posttranslational Modifications. *Methods Enzymol.* **586**, 311–332 (2017).
257. Noberini, R. *et al.* Extensive and systematic rewiring of histone post-translational modifications in cancer model systems. *Nucleic Acids Res.* **46**, 3817 (2018).
258. Ding, J. *et al.* LSD1-mediated epigenetic modification contributes to proliferation and metastasis of colon cancer. (2013). doi:10.1038/bjc.2013.364
259. Son, M. J., Woolard, K., Nam, D. H., Lee, J. & Fine, H. A. SSEA-1 Is an Enrichment Marker for Tumor-Initiating Cells in Human Glioblastoma. *Cell Stem Cell* **4**, 440–452 (2009).
260. Lathia, J. D. *et al.* Integrin Alpha 6 regulates glioblastoma stem cells. *Cell Stem Cell* **6**, 421–432 (2010).
261. Lesch, B. J. & Page, D. C. Poised chromatin in the mammalian germ line. *Development* **141**, 3619 (2014).
262. Yan, H. J. *et al.* The effects of LSD1 inhibition on self-renewal and differentiation of human induced pluripotent stem cells. *Exp. Cell Res.* **340**, 227–237 (2016).
263. Harding, H. P. *et al.* An integrated stress response regulates amino acid metabolism and resistance to oxidative stress. *Mol. Cell* **11**, 619–633 (2003).
264. Ma, Y. & Hendershot, L. M. The role of the unfolded protein response in tumour development: friend or foe? *Nat. Rev. Cancer* **4**, 966–977 (2004).
265. Ye, J. *et al.* The GCN2-ATF4 pathway is critical for tumour cell survival and proliferation in response to nutrient deprivation. *EMBO J.* **29**, 2082–2096 (2010).
266. Kilberg, M. S., Shan, J. & Su, N. ATF4-dependent transcription mediates signaling of amino acid limitation. *Trends in Endocrinology and Metabolism* **20**, 436–443 (2009).
267. Wek, R. C., Jiang, H.-Y. & Anthony, T. G. Coping with stress: eIF2 kinases and translational control. *Biochem. Soc. Trans.* **34**, 7–11 (2006).
268. Ohoka, N., Yoshii, S., Hattori, T., Onozaki, K. & Hayashi, H. TRB3, a novel ER stress-inducible gene, is induced via ATF4-CHOP pathway and is involved in cell death. *EMBO J.* **24**, 1243–1255 (2005).
269. Jousse, C. *et al.* TRB3 inhibits the transcriptional activation of stress-regulated genes by a negative feedback on the ATF4 pathway. *J. Biol. Chem.* **282**, 15851–15861 (2007).
270. Van Galen, P. *et al.* The unfolded protein response governs integrity of the haematopoietic stem-cell pool during stress. *Nature* **510**, 268–272 (2014).
271. Rogers, T. B., Inesi, G., Wade, R. & Lederer, W. J. Use of thapsigargin to study Ca2+ homeostasis in cardiac cells. *Bioscience Reports* **15**, 341–349 (1995).
272. Zhang, P. *et al.* The GCN2 eIF2**α** Kinase Is Required for Adaptation to Amino Acid Deprivation in Mice. *Mol. Cell. Biol.* **22**, 6681–6688 (2002).
273. Pakos-zebrucka, K. *et al.* The integrated stress response. **17**, 1374–1395 (2016).
274. Balasubramanian, M. N., Butterworth, E. A. & Kilberg, M. S. Asparagine synthetase: regulation by cell stress and involvement in tumor biology. *Am. J. Physiol. Metab.* **304**, E789–E799 (2013).
275. Kalhan, S. C. & Hanson, R. W. Resurgence of serine: An often neglected but indispensable amino acid. *J. Biol. Chem.* **287**, 19786–19791 (2012).
276. Rozpedek, W., Pytel, D. & Mucha, B. The Role of the PERK/eIF2**α**/ATF4/CHOP Signaling Pathway in Tumor Progression During Endoplasmic Reticulum Stress. *Curr. Mol. Med* **16**, 533–544 (2016).
277. Mungrue, I. N., Pagnon, J., Kohannim, O., Gargalovic, P. S. & Lusis, A. J. NIH Public Access Author Manuscript J Immunol. Author manuscript; available in PMC 2010 March 29. Published in final edited form as: J Immunol. 2009 January 1; 182(1): 466–476. CHAC1/MGC4504 Is a Novel Proapoptotic Component of the Unfolded Protein Respon. *J. Immunol.* **182**, 466–476 (2009).
278. Geraldo, L. H. M. *et al.* Glioblastoma Therapy in the Age of Molecular Medicine. *Trends in Cancer* **5**, 46–65 (2019).

279. Huang, H., Sabari, B. R., Garcia, B. A., Allis, C. D. & Zhao, Y. SnapShot: histone modifications. *Cell* **159**, 458-458.e1 (2014).
280. Ahuja, N., Sharma, A. R. & Baylin, S. B. Epigenetic Therapeutics: A New Weapon in the War Against Cancer. *Annu. Rev. Med.* **67**, 73–89 (2016).
281. Tsai, H.-C. *et al.* Transient low doses of DNA-demethylating agents exert durable antitumor effects on hematological and epithelial tumor cells. *Cancer Cell* **21**, 430–46 (2012).
282. Kaminskas, E., Farrell, A. T., Wang, Y.-C., Sridhara, R. & Pazdur, R. FDA drug approval summary: azacitidine (5-azacytidine, Vidaza) for injectable suspension. *Oncologist* **10**, 176–82 (2005).
283. Alvarez, A. A., Field, M., Bushnev, S., Longo, M. S. & Sugaya, K. The Effects of Histone Deacetylase Inhibitors on Glioblastoma-Derived Stem Cells. *J. Mol. Neurosci.* **55**, 7–20 (2014).
284. Bauer, T. M. *et al.* Phase I, Open-Label, Dose-Escalation Study of the Safety, Pharmacokinetics, Pharmacodynamics, and Efficacy of GSK2879552 in Relapsed/Refractory SCLC. *J. Thorac. Oncol.* **14**, 1828–1838 (2019).
285. Suvà, M. L. *et al.* Reconstructing and reprogramming the tumor-propagating potential of glioblastoma stem-like cells. *Cell* **157**, 580–94 (2014).
286. Wang, J. *et al.* Novel histone demethylase LSD1 inhibitors selectively target cancer cells with pluripotent stem cell properties. *Cancer Res.* **71**, 7238–7249 (2011).
287. Zhao, H., Chen, G. & Liang, H. Dual PI3K/mTOR Inhibitor, XL765, suppresses glioblastoma growth by inducing ER stress-dependent apoptosis. *Onco. Targets. Ther.* **Volume 12**, 5415–5424 (2019).
288. Sheikh, S. *et al.* An Integrated Stress Response Agent that Modulates DR5-Dependent TRAIL Synergy Reduces Patient-Derived Glioma Stem Cell Viability. *Mol. Cancer Res.* **17**, 1102–1114 (2019).
289. Wortel, I. M. N., van der Meer, L. T., Kilberg, M. S. & van Leeuwen, F. N. Surviving Stress: Modulation of ATF4-Mediated Stress Responses in Normal and Malignant Cells. *Trends Endocrinol. Metab.* **28**, 794–806 (2017).
290. Jewer, M. *et al.* Translational control of breast cancer plasticity. *bioRxiv* 596544 (2019). doi:10.1101/596544
291. Friend, K., Brooks, H. A., Propson, N. E., Thomson, J. A. & Kimble, J. Embryonic Stem Cell Growth Factors Regulate eIF2α Phosphorylation. *PLoS One* **10**, e0139076 (2015).
292. Hoang-Minh, L. B. *et al.* Infiltrative and drug-resistant slow-cycling cells support metabolic heterogeneity in glioblastoma. *EMBO J.* **37**, (2018).
293. Gwinn, D. M. *et al.* Oncogenic KRAS regulates amino acid homeostasis and asparagine biosynthesis via ATF4 and alters sensitivity to L-asparaginase HHS Public Access. *Cancer Cell* **33**, 91–107 (2018).
294. Pällmann, N. *et al.* Regulation of the unfolded protein response through ATF4 and FAM129A in prostate cancer. *Oncogene* **38**, 6301–6318 (2019).
295. Peñaranda-Fajardo, N. M. *et al.* ER stress and UPR activation in glioblastoma: identification of a noncanonical PERK mechanism regulating GBM stem cells through SOX2 modulation. *Cell Death Dis.* **10**, 690 (2019).
296. Heydt, Q. *et al.* Oncogenic FLT3-ITD supports autophagy via ATF4 in acute myeloid leukemia. *Oncogene* **37**, 787–797 (2018).
297. Zhao, E. *et al.* KDM4C and ATF4 Cooperate in Transcriptional Control of Amino Acid Metabolism. *Cell Rep.* **14**, 506–519 (2016).
298. Nagasawa, I. *et al.* Disrupting ATF4 Expression Mechanisms Provides an Effective Strategy for BRAF-Targeted Melanoma Therapy. *iScience* **23**, 101028 (2020).
299. Dey, S. *et al.* Both transcriptional regulation and translational control of ATF4 are central to the integrated stress response. *J. Biol. Chem.* **285**, 33165–33174 (2010).
300. Vinyard, M. E. *et al.* CRISPR-suppressor scanning reveals a nonenzymatic role of LSD1 in AML. *Nat. Chem. Biol.* **15**, 529–539 (2019).
301. Kim, S. A., Zhu, J., Yennawar, N., Eek, P. & Tan, S. Crystal Structure of the LSD1/CoREST Histone Demethylase Bound to Its Nucleosome Substrate. *Mol. Cell* **78**, 903-914.e4 (2020).
302. Chen, Y. *et al.* Histone Demethylase LSD1 Promotes Adipocyte Differentiation through Repressing Wnt Signaling. *Cell Chem. Biol.* **23**, 1228–1240 (2016).
303. Sun, H. *et al.* Lysine-specific histone demethylase 1 inhibition promotes reprogramming by facilitating the expression of exogenous transcriptional factors and metabolic switch OPEN. (2016). doi:10.1038/srep30903
304. Porro, A., Feuerhahn, S. & Lingner, J. TERRA-Reinforced Association of LSD1 with MRE11 Promotes Processing of Uncapped Telomeres. *Cell Rep.* **6**, 765–776 (2014).
305. Kim, Y. *et al.* Methylation-dependent regulation of HIF-1α stability restricts retinal and tumour angiogenesis. *Nat. Commun.* **7**, (2016).
306. Roth, M., Wang, Z. & Chen, W. Y. SIRT1 and LSD1 competitively regulate KU70 functions in DNA repair and mutation acquisition in cancer cells. *Oncotarget* **7**, 50195–50214 (2016).
307. Liang, G. & Hai, T. Characterization of human activating transcription factor 4, a transcriptional activator that interacts with multiple domains of cAMP- responsive element-binding protein (CREB)-binding protein (CBP). *J. Biol. Chem.* **272**, 24088–24095 (1997).
308. Gachon, F., Devaux, C. & Mesnard, J. M. Activation of HTLV-I transcription in the presence of Tax is independent of the acetylation of CREB-2 (ATF-4). *Virology* **299**, 271–278 (2002).
309. Sidrauski, C. *et al.* Pharmacological brake-release of mRNA translation enhances cognitive memory. *Elife* **2**, e00498 (2013).
310. Nguyen, H. G. *et al.* Development of a stress response therapy targeting aggressive prostate cancer. *Sci. Transl. Med.* **10**, eaar2036 (2018).
311. Rabouw, H. H. *et al.* Small molecule ISRIB suppresses the integrated stress response within a defined window of activation. *Proc. Natl. Acad. Sci. U. S. A.* **116**, 2097–2102 (2019).
312. Su, N. *et al.* Correlation between asparaginase sensitivity and asparagine synthetase protein content, but not mRNA, in acute lymphoblastic leukemia cell lines. *Pediatr. Blood Cancer* **50**, 274–279 (2008).
313. Panosyan, E. H. *et al.* Asparagine Depletion Potentiates the Cytotoxic Effect of Chemotherapy against Brain Tumors. *Mol. Cancer Res.* **12**, 694–702 (2014).

11. ACKNOWLEDGMENTS

I would like to sincerely thank my PhD supervisor, Prof. Giuliana Pelicci, for the opportunity to work on this research project and for her mentorship throughout my time in her laboratory. Thank you to all present and former members of Giuliana Pelicci's group. I am so pleased I had the opportunity to learn something from each of them and to grow with them, both personally and as a scientist. A special thanks to Daniela, who, with her guidance and precious advices, shared with me every aspect of this research project.

I would like to thank my Internal Advisor, Dr. Diego Pasini, for his suggestions and his critical support. I would also to thank my External Advisor, Prof. Simone Niclou, for her kind comments and for the time she dedicated to the evaluation of the progresses of my PhD project. I am very grateful to my PhD examiners, Prof. Saverio Minucci and Dr. Maria Stella Carro, for their availability to revise and ameliorate this work and to evaluate my PhD thesis defense. Thanks are due to Prof. Saverio Minucci and his group, with whom we are collaborating, for their help and the constructive discussions.

I would like to thank Elena Ceccacci and Davide Corà for the bioinformatic analyses, Tiziana Bonaldi's laboratory for proteomic studies, Ludovico Rizzuti for his help with ATAC-seq experiments, and Laura Furia and Mario Faretta for their contribution to PLA assays. Additionally, I thank the members of the qPCR service (Cogentech, IFOM) and of the Genomic Unit (IEO) for their kind and constant support.

I would say thank you to my colleagues and friends at the IEO for being wonderful travel companions and invaluable confidant and advisers.

Finally, I must thank my friends, my family, and specially Simone, for their never-ending encouragement and their unshakable trust in me.